FRA-77-20
REPORT NO. FRA/ORD-77/50

FRACTURE RESISTANCE AND FATIGUE CRACK GROWTH CHARACTERISTICS OF RAILROAD WHEELS AND AXLES

C. S. Carter
R. G. Caton
J. L. Guthrie

Boeing Commercial Airplane Company
P.O. Box 3707
Seattle WA 98124

NOVEMBER 1977

FINAL REPORT

DOCUMENT IS AVAILABLE TO THE U.S. PUBLIC THROUGH THE NATIONAL TECHNICAL INFORMATION SERVICE, SPRINGFIELD, VIRGINIA 22161

Prepared for

U.S. DEPARTMENT OF TRANSPORTATION
FEDERAL RAILROAD ADMINISTRATION
Office of Research and Development
Washington DC 20590

Technical Report Documentation Page

1. Report No.	2. Government Accession No.	3. Recipient's Catalog No.
FRA/ORD-77/50		

4. Title and Subtitle	5. Report Date
FRACTURE RESISTANCE AND FATIGUE CRACK GROWTH CHARACTERISTICS OF RAILROAD WHEELS AND AXLES	November 1977
	6. Performing Organization Code
7. Author(s)	8. Performing Organization Report No.
C.S. Carter, R.G. Caton, and J.L. Guthrie	DOT-TSC-FRA-77-20
9. Performing Organization Name and Address Boeing Commercial Airplane Company* P.O. Box 3707 Seattle WA 98124	10. Work Unit No. (TRAIS) RR728/R8309
	11. Contract or Grant No. DOT-TSC-617
12. Sponsoring Agency Name and Address U.S. Department of Transportation Federal Railroad Administration Office of Research and Development Washington DC 20590	13. Type of Report and Period Covered Final Report 5-13-74 to 8-15-75
	14. Sponsoring Agency Code

15. Supplementary Notes

*Under contract to: U.S. Department of Transportation
Transportation Systems Center
Kendall Square
Cambridge MA 02142

16. Abstract

The effects of chemical composition, temperature and loading rates on the plane strain fracture toughness K_{Ic} of railroad wheels have been determined. Similarly, the effects of these variables were determined for grade U and F railroads axles. The carbon content was determined to be the principal factor controlling K_{Ic}. Sensitivity to loading rate (K_{Id}) was seen to be a function of the microstructure. Estimates have been made of the minimum size of crack, which could result in the failure of wheels and axles under adverse service conditions. Also investigated were the effects of chemical composition, heat treatment, temperature, stress ratio (R), environment and peak loads on the fatigue crack growth characteristics of wheels and axles. It was seen that the effects of R could be predicted by the Forman equation and that crack growth rates were predominantly affected by R. Otherwise, all values fell within the same scatterband. Predictions of crack growth to criticality as a function of cycles were made for wheels and axles. Bssed on these calculations, it was concluded that detection of subcritical flaws with a good degree of confidence would only be possible for the classes A and sub A wheels and the grades U and F axles.

17. Key Words	18. Distribution Statement
Railroad Wheels Railroad Axles Carbon Steels Fracture Toughness Fatigue Crack Growth Rates	DOCUMENT IS AVAILABLE TO THE U.S. PUBLIC THROUGH THE NATIONAL TECHNICAL INFORMATION SERVICE, SPRINGFIELD, VIRGINIA 22161

19. Security Classif. (of this report)	20. Security Classif. (of this page)	21. No. of Pages	22. Price
Unclassified	Unclassified	138	

Form DOT F 1700.7 (8-72) Reproduction of completed page authorized

PREFACE

The authors are grateful to the following individuals who contributed to this program: Mr. D. G. Sill (Boeing), who performed the metallographic studies Mr. T. S. DeSisto (U.S. Army Materials and Mechanics Research Center), who conducted the dynamic fracture toughness tests; and Mr. Rene Gauthier (National Railroad Passenger Corporation), who kindly made available the Class Sub A wheel. The authors would also like to acknowledge the encouragement and interest shown by the late Mr. J. W. Lyons, without whose support this program would have been measurably more difficult.

METRIC CONVERSION FACTORS

Approximate Conversions to Metric Measures

Symbol	When You Know	Multiply by	To Find	Symbol
		LENGTH		
in	inches	2.5	centimeters	cm
ft	feet	30	centimeters	cm
yd	yards	0.9	meters	m
mi	miles	1.6	kilometers	km
		AREA		
in^2	square inches	6.5	square centimeters	cm^2
ft^2	square feet	0.09	square meters	m^2
yd^2	square yards	0.8	square meters	m^2
mi^2	square miles	2.6	square kilometers	km^2
	acres	0.4	hectares	ha
		MASS (weight)		
oz	ounces	28	grams	g
lb	pounds	0.45	kilograms	kg
	short tons (2000 lb)	0.9	tonnes	t
		VOLUME		
tsp	teaspoons	5	milliliters	ml
Tbsp	tablespoons	15	milliliters	ml
fl oz	fluid ounces	30	milliliters	ml
c	cups	0.24	liters	l
pt	pints	0.47	liters	l
qt	quarts	0.95	liters	l
gal	gallons	3.8	liters	l
ft^3	cubic feet	0.03	cubic meters	m^3
yd^3	cubic yards	0.76	cubic meters	m^3
		TEMPERATURE (exact)		
°F	Fahrenheit temperature	5/9 (after subtracting 32)	Celsius temperature	°C

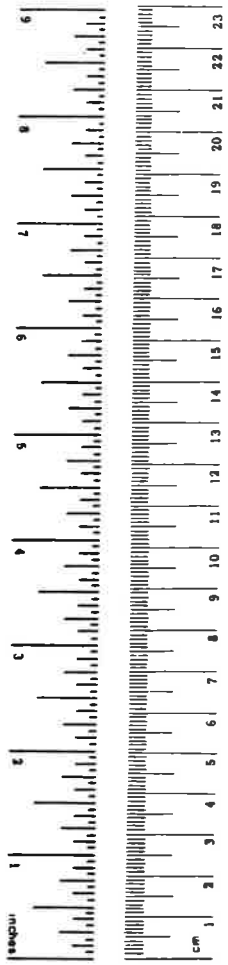

Approximate Conversions from Metric Measures

Symbol	When You Know	Multiply by	To Find	Symbol
		LENGTH		
mm	millimeters	0.04	inches	in
cm	centimeters	0.4	inches	in
m	meters	3.3	feet	ft
m	meters	1.1	yards	yd
km	kilometers	0.6	miles	mi
		AREA		
cm^2	square centimeters	0.16	square inches	in^2
m^2	square meters	1.2	square yards	yd^2
km^2	square kilometers	0.4	square miles	mi^2
ha	hectares (10,000 m^2)	2.5	acres	
		MASS (weight)		
g	grams	0.035	ounces	oz
kg	kilograms	2.2	pounds	lb
t	tonnes (1000 kg)	1.1	short tons	
		VOLUME		
ml	milliliters	0.03	fluid ounces	fl oz
l	liters	2.1	pints	pt
l	liters	1.06	quarts	qt
l	liters	0.26	gallons	gal
m^3	cubic meters	35	cubic feet	ft^3
m^3	cubic meters	1.3	cubic yards	yd^3
		TEMPERATURE (exact)		
°C	Celsius temperature	9/5 (then add 32)	Fahrenheit temperature	°F

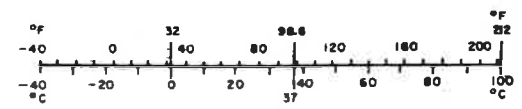

CONTENTS

FIGURES

FIGURES–(Continued)

FIGURES–(Concluded)

LIST OF TABLES

ABBREVIATIONS AND SYMBOLS

AAR	Association of American Railroads
BHN	Brinell hardness number
C_L	Centerline
cpm	Cycles per minute
da/dN	Crack growth rate
DCB	Double cantilever beam
dia	Diameter
Elong.	Elongation
fps	Feet per second
ft-lb	Foot-pound
in.	Inch
K	Stress intensity factor
K_{Ic}	Plane strain fracture toughness
K_{Id}	Dynamic fracture toughness
K_Q	Conditonal plane-strain fracture toughness value (see ASTM E 399-72 for complete definition)
ksi	Kips per square inch
mph	Miles per hour
P_{max}	Maximum load in fracture toughness test
P_Q	Conditional load in pounds to calculate K_Q (see ASTM E 399-72 for complete definition)
psi	Pounds per square inch
R	Stress ratio
RA	Reduction of area
RH	Relative humidity
RT	Room temperature
SEM	Scanning electron microscope
TUS, UTS	Tensile ultimate strength, ultimate tensile strength
TYS	Tensile yield strength
ΔK	Algebraic difference between maximum stress intensity (K_{max}) and minimum stress intensity (K_{min})

EXECUTIVE SUMMARY

Because broken wheels represent one of the major causes of reported train accidents attributable to defective vehicle components and axle failures have remained a persistent though variable cause of reported train accidents, tests to determine the fracture toughness and fatigue crack growth behavior of wheel and axle steels have been run. A previous (interim) report issued under this contract recorded the toughness characteristics of the following types of wheels:

U, cast

C, cast

U, wrought (new and used)

A, wrought

C, wrought

CE, wrought

In addition, a review of actual wheel service failure behavior was accomplished and the service conditions contributing to service failure were elucidated.

The work described in this report has carried this investigation further to define the crack growth behavior of the following types of axles and wheels:

Axles: U, non heat treated

F, double normalized and tempered

Wheels: U, cast and wrought*

C, cast and wrought

A, wrought

B, wrought

Sub A, wrought

*new and used

In addition to the fatigue crack growth behaviors, the dynamic and static toughnesses of the axle steels were determined. The effects of metallurgical structure size on toughness was noted. Fractographic examination was made of the fracture surfaces of test specimens and the contribution of cleavage to the fracture process ascertained.

The crack growth behavior was found to be adequately described by a Forman type equation. This equation was integrated and used in conjunction with estimates of service loadings to calculate approximate lifetimes after crack initiation for wheels and axles for some expected service conditions. The results have shown that reliable estimates of crack growth interval from initiation to fracture requires a detailed knowledge of thermal and mechanical loading history for each wheel. The same caveat applies to mechanical loading history for axles. Thus, the use of the information conveyed herein to estimate inspection interval or limit 'load' cycling will only be possible when better knowledge of 'load' spectra becomes available.

Critical flaw sizes were found to be below the detection thresholds for class U, B, and C wheels suggesting that inspection for subcritical cracks in these wheels will not be possible using current 'state-of-the-art'

technology. However, suitable inspection techniques are possible for class A and sub A wheels and for grade U and F axles. Thus, the maximum defect sizes can by established for inspection of class A and sub A wheels and grade U and F axles once the service 'load' spectra is known.

What is needed now is an effort to merge the results of this work with those from wheel stress analysis, load spectra studies, and train operation analyses to establish what are the conditions most likely to lead to wheel (and axle) failure and the time required to achieve these conditions in service. Until this is done, the maximum inspection interval which should be utilized to assure that wheels do not fail between inspection, and the definition of limits on mechanical loading and brake application practices (rim heating), cannot be established. This information would prove useful in promulgating more effective vehicle regulations.

1.0 INTRODUCTION

One major cause of train derailments has been the failure of wheels. These derailments often result in costly damage to equipment and pose serious threats to life, as in the case of freight trains. For example, a broken wheel derailed a freight train in Laurel, Mississippi in 1969 (ref 1). In the consist were tank cars carrying liquified petroleum gas. Most of these cars exploded following the derailment, igniting dwellings and buildings as well as inflicting mechanical damage. Several fatalities and over $3-million damage resulted. With the current trends in greater vehicle capacity and higher speeds, the incidence of wheel failure may further increase unless remedial action is taken.

Primary causes of wheel failures are the development of thermal cracks in the wheel rim and the growth of fatigue cracks in the wheel plate. If incipient cracking is not detected during prescribed inspection intervals and the conditions corrected, the cracks will eventually propagate, resulting in a compete brittle fracture of the wheel.

Axles generally fail either by overheating in the journals or by fatigue-initiated fracture. For the purpose of this investigation, failures resulting from overheating are not relevant. The primary failures to which this report will address itself will be those occurring cold as a result of a fatigue-initiated crack. Axle failures and their principal location within the axle for the years 1969–1971 are summarized in table 1 (ref 2). These failures resulted in derailment.

The data available for the year 1973 (ref 3) show that 10 fractures occurred between the journals, 16 in the journal, and 3 in the wheel seat, these again being cold breaks. However, these failures reported in the 1973 statistics did not necessarily involve a derailment.

TABLE 1.—INCIDENCE OF AXLE FAILURES, OTHER THAN OVERHEATING, LEADING TO DERAILMENT FOR THE TIME PERIOD 1969-1971 (REF. 2)

Location of failure	Number reported in		
	1969	1970	1971
Between journals	41	15	20
In journal	65	25	17
Other	2	7	13

Since very little had been reported on the resistance to crack extension and critical crack size in railroad materials, this investigation was initiated to provide data on the fracture toughness characteristics of these critical truck components and the inspection procedures necessary to detect cracks before they have grown to a critical size.

To meet these objectives, the program was divided into Phase I and Phase II. The results of Phase I are described in an earlier report (ref 4). Phase I was concerned with establishing the fracture toughness properties of wheels and assessing the significance of the results with respect to the service performance. Phase II, the results of which are described in this report, was directed towards establishing the fracture toughness properties of axles and two additional wheels, the fatigue crack growth characteristics of axles and wheel plate sections, and the significance of the results in terms of service performance.

The specific tasks conducted in Phase II were:

- Investigate the fracture toughness, K_{Ic}, and fatigue crack growth rate characteristics of Grade U and F axles (AAR specification M101-72), and establish their mechanical, and metallurgical properties.

- Obtain fracture toughness and fatigue crack growth data for a Class A wheel with a carbon content at the low end of the specified range, and a Class B wheel.

- Determine the fatigue crack growth characteristics of plate sections from the seven wheels evaluated during Phase I.

- Evaluate the influence of materials and test variables on fracture toughness and fatigue crack propagation for both wheels and axles.

- Determine the critical crack size which will cause axle and wheelset fracture for different stress levels, and assess the significance of the results on axle and wheelset service performance.

2.0 TEST PROCEDURES

2.1 MATERIALS EVALUATED

2.1.1 Axle Materials

Railroad axles are manufactured by forging directly from ingots or from blooms. AAR Specification M101-72 provides coverage for four different grades of axles (Grades U, F, G, and H) that are used according to the service requirements. Grade F, G, and H axles are heat-treated and are generally used for heavy-duty service on locomotives and cars. The non-heat-treated Grade U axles receive no heat treatment following slow cooling after forging. The specified heat treatments for the four axle grades are as follows:

Axle grade	Heat treatment
U	Non-Heat-Treated
F	Double Normalized and tempered
G	Quenched and Tempered
H	Normalized, Quenched and Tempered

Material from a Grade U axle and from two Grade F axles was evaluated. Table 2 lists the identification markings stamped on the ends of the axles. The three axles evaluated were standard 6- by 11-in. journal bearing design railway axles procured to AAR Specification M101-72.

TABLE 2.–AXLE IDENTIFICATION MARKINGS

Axle grade	I.D. markings	Description
U	SF 9 74 45834 UT	Black as forged, nonheat treated
F (F1)	SF 9 74 34457 FT	Black as forged, double normalized and tempered
F (F2)	SF 3 74 B396 TE71964	Machined, double normalized and tempered

Originally, U, F, and H axles were to have been evaluated. However, the purchased Grade H axle had a microstructure typical of a normalized axle and strength properties less than the properties required by AAR Specification M101-72 for a Grade H axle. Because of these latter inconsistencies, the supplier was asked to verify the axle grade. After checking, the supplier discovered the Grade H axle was in actuality a Grade F axle. This discovery was made after evaluation of the axle had already been completed.

The chemical compositions of the axles as determined by analysis at Boeing are given in table 3. The 0.44% carbon content of the Grade F axle designated F2 was less than the specified minimum of 0.45%, and the 0.46% carbon content of the grade F axle designated F1 was on the low side of the specified carbon range. The amount of silicon in the Grade U axle was low, but within the specified check analysis limits of ±0.02%.

TABLE 3.—CHEMICAL COMPOSITION OF AXLE MATERIALS

Axle grade	Source	Elements										
		C	P	S	Mn	Ni	Cr	Mo	Si	Cu	Co	Fe
U	Boeing analysis	0.47	0.008	0.022	0.65	0.25	0.20	0.11	0.13	0.05	0.05	Rem
	AAR specification M101-72[a]	0.40 to 0.55	0.045 max	0.050 max	0.60 to 0.90				0.15 min			
F (F1)	Boeing analysis	0.46	0.005	0.029	0.88	0.27	0.10	0.13	0.15	0.11	0.05	Rem
	AAR specification M101-72[a]	0.45 to 0.59	0.045 max	0.050 max	0.60 to 0.90				0.15 min			
F (F2)	Boeing analysis	0.44	0.007	0.27	0.75	0.28	0.15	0.11	0.22	0.15	0.05	Rem
	AAR specification M101-72[a]	0.45 to 0.59	0.045 max	0.050 max	0.60 to 0.90				0.15 min			

[a]Blank indicates no specification requirement.

2.1.2 Wheel Materials

Railroad wheels are manufactured by either rolling of forged preforms or by casting. The AAR specifications M107 and M208 cover wrought and cast wheels, respectively. They provide for four different classes of wheels–U, A, B, and C–to be selected according to the loads and braking anticipated in service. The four classes differ in specified carbon content and hardness, Class A, B, and C wheels must be austenitized, rim quenched, and tempered. This treatment also results in normalizing and tempering of the unquenched plate and hub regions. Specification M107 allows entire wheel quenching and tempering of wrought wheels to Classes A, B, and C which are designated AE, BE, and CE, respectively. Cast wheels are not fully quenched. While specification M208 allows the use of high carbon Class U1 material, wheels of this class are no longer manufactured because of their susceptibility to thermal cracking.

The wheel classes, manufacturer's identification markings, and heat treatments of the nine wheels evaluated are given in table 4. All the wheels were the AAR R33 design (Multiwear), except the Class Sub A wheel which was the R30 design. For the purpose of identification, each wheel was assigned an identifying number as shown by table 4. Wheels 1 through 7 were evaluated during Phase I, while wheels 8 and 9 had not been previously evaluated. An earlier report (ref 4) describes the results of the Phase I evaluation of wheels 1 through 7. The Phase I investigation included fracture toughness testing, chemical analysis, hardness determinations, and metallurgical evaluation. The Phase II testing of wheels 1 through 7 was limited to evaluating the fatigue crack growth characteristics.

TABLE 4.—WHEEL IDENTIFICATION MARKINGS AND HEAT TREATMENTS

Wheel		Manufacturer's I.D.	Heat treatment details[a]
No.	Class		
1	U, cast	3-73 GS 49506 CR 33	Normalized at 1700° F for 45 min.—programmed cool to avoid residual stresses
2	C, cast	12-72 GS 09171 C CR 33	Normalized at 1700° F for 45 min.—rim quenched to provide Brinell hardness in tread of 321-363; tempered at 900° F for 2 hr; controlled temperature gradients to minimize residual stresses
3	U, wrought	12-71 G 54761 R33	Untreated
4	A, wrought	4-69 E 36384 A R33	No details supplied
5	C, wrought	2-73 G 53307 C R33	Rim toughened
6	U, wrought (used)	2 28 56 ⏚ S ⏚ 277 Z 4464 AAR 1W	Untreated
7	CE, wrought	7-73 ⏚ S ⏚ 7646 CE R33	No details supplied
8	Sub A, wrought	4-73 E 68884 A 8189	No details supplied
9	B, wrought	11 70 G 59375 R33	Rim toughened

[a]Reported by manufacturer

Except for the Class A wheel (wheel 4), the carbon contents of wheels 1 through 7 were within a range of 0.70 to 0.75%. The carbon content of the Class A wheel (wheel 4 was 0.53%. To obtain additional fracture toughness data in the 0.57-0.67% carbon range, a Class B wheel (wheel 9) was selected for the Phase II evaluation. In addition, a Class Sub A wheel (wheel 8), with a carbon content at the lower end of the range used by the manufacturer, was selected for evaluation. The Class Sub A wheel contains less carbon than the Class A wheel, and is used to combat the thermal cracking of wheels on the metroliner.

Brinell hardness measurement results from wheels 8 and 9 at the rim location specified by AAR M107 were as follows:

Wheel number	Class	Measured BHN	Specified BHN
8	Sub A	229	248-262
9	B	285	277-341

Table 5 gives the chemical composition of wheels 1 through 9. The usual carbon content of the Class Sub A wheel is 0.38-0.42%, with a rim hardness requirement of 248 to 262 BHN. Because the carbon content was less than the usual range, the low rim hardness was expected. For future production of Class Sub A wheels,consideration is being given to specifying a 229 minimum Brinell hardness (ref 5).

TABLE 5.—CHEMICAL COMPOSITION OF WHEELS

Wheel		Source	Elements										
No.	Class		C	P	S	Mn	Ni	Cr	Mo	Si	Cu	Co	Fe
1	U, cast	Boeing analysis	0.70	0.020	0.038	0.62				0.23			Rem
		AAR M208-71[a]	0.65 to 0.80	0.05 max	0.05 max	0.60 to 0.85				0.15 min			Rem
2	C, cast	Boeing analysis	0.71	0.012	0.031	0.62				0.21			Rem
		AAR M208-71[a]	0.67 to 0.77	0.05 max	0.05 max	0.60 to 0.85				0.15 min			Rem
3	U, wrought	Boeing analysis	0.71	0.014	0.012	0.70				0.14			Rem
		AAR M107-71[a]	0.65 to 0.80	0.05 max	0.05 max	0.60 to 0.85				0.15 min			Rem
4	A, wrought	Boeing analysis	0.53	0.010	0.026	0.60				0.13			Rem
		AAR M107-71[a]	0.57 max	0.05 max	0.05 max	0.60 to 0.85				0.15 min			Rem
5	C, wrought	Boeing analysis	0.70	0.006	0.020	0.64				0.11			Rem
		AAR M107-71[a]	0.67 to 0.77	0.05 max	0.05 max	0.60 to 0.85				0.15 min			Rem
6	U, wrought (used)	Boeing analysis	0.73	0.032	0.040	0.61				0.16			Rem
		AAR M107-71[a]	0.65 to 0.80	0.05 max	0.05 max	0.60 to 0.85				0.15 min			Rem
7	CE, wrought	Boeing analysis	0.75	0.021	0.050	0.67				0.23			Rem
		AAR M107-71[a]	0.67 to 0.77		0.05 max	0.60 to 0.85				0.15 min			Rem
8	Sub A, wrought	Boeing analysis	0.35	0.011	0.022	0.65				0.23			Rem
		AAR M107-71[a]	0.57 to max	0.05 max	0.05 max	0.60 to 0.85	0.26	0.09	0.10	0.15 min	0.18	0.05	Rem
9	B, wrought	Boeing analysis	0.58	0.017	0.015	0.70	0.17	0.04	0.007	0.06	0.02	0.05	Rem
		Supplier analysis	0.60	0.020	0.015	0.72				0.23			Rem
		AAR M107-71[a]	0.57 to 0.67	0.05 max	0.05 max	0.60 to 0.85				0.15 min			Rem

[a]Blank indicates no specification requirement.

2.2 SPECIMEN LOCATIONS

2.2.1 Axle Specimen Locations

Fracture toughness, tensile, and fatigue specimens were removed from the axles at the locations shown in figure 1. The number of specimens fabricated from each of the three axles is given in table 6. The orientation of the specimens was such that direction of loading was parallel to the axis of the axles. The cracks in the fracture toughness and fatigue specimens were in a radially directed plane normal to the direction of loading.

TABLE 6.—TEST SPECIMENS FABRICATED FROM AXLE MATERIALS

Axle		Axle specimens			
			Fracture toughness		
I.D. code	Grade	Tensile	K_{Ic}	K_{Id}	Fatigue
U	U	2	5	6	2
F1	F	2	5	6	2
F2	F	2	5	6	2

The specimen numbering system used to identify the axle specimens was as follows:

XX X - X

- Specimen type (see fig. 1)
- Axle section letter (see fig. 1)
- Axle identification marking:

UU – U Grade axle
FF – F Grade axle designated F1 (see table 3)
HH – F Grade axle designated F2 (see table 3)

2.2.2 Wheel Specimen Locations

Test specimens were removed from the wheels at the locations shown in figure 2. Test specimens were removed from wheels 8 and 9 according to the schedule given by table 7. Fatigue specimens were removed from wheels 1 through 7, which were evaluated during the Phase I investigation (ref 4), as shown by table 8. The crack orientations with

TABLE 7.—NUMBER OF SPECIMENS REMOVED FROM WHEELS 8 AND 9

Specimen type	Wheel 8		Wheel 9	
	Rim	Plate	Rim	Plate
K_{Ic} fracture toughness	7	5	7	5
K_{Id} fracture toughness		5		5
Charpy impact	2		2	
Tensile	1	1	1	1
Fatigue		1		

TABLE 8.—FATIGUE SPECIMENS REMOVED FROM WHEELS 1 THROUGH 7

Wheel		Plate fatigue specimens
No.	Class	
1	U, cast	1
2	C, cast	1
3	U, wrought	1
4	A, wrought	5
5	C, wrought	2
6	U, wrought (used)	1
7	CE, wrought	1

respect to the wheel were radial for the rim specimens and tangential for the plate specimens, as shown in figure 3. These orientations corresponded to the direction of brittle crack propagation experienced in service. Other investigators (ref 6) have found that differences in crack orientation do not have any effect on the fracture toughness of wheels.

Each specimen removed from the wheels was marked with an identifying specimen number so that the specimen location could be determined. The following illustrates the specimen numbering scheme:

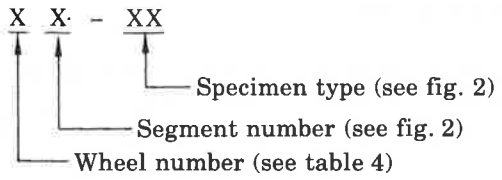

2.3 TEST METHODS

2.3.1 Tensile Testing

Tensile testing was conducted with the 0.250-in.-dia specimen shown in figure 4 in a 20-kip capacity Instron tensile machine. Testing was performed at room temperature to determine the ultimate strength, yield strength (0.2% offset), percent elongation in 1-in. gage length, and percent reduction of area. Specimens were tested at a strain rate of 0.005 in. per in. through yield and then at a rate of 0.1 in. per in. per minute.

2.3.2 Charpy Impact Testing

Standard Charpy V-notched specimens were tested in a Wiedemann-Baldwin impact machine. Figure 5 shows the specimen configuration. All impact testing was performed at room temperature according to the requirements of ASTM E23-66.

2.3.3 K_{Ic} Testing

Fracture toughness testing of the wheels was conducted with the three-point notch-bend specimen shown in figure 6. The dimensions of specimens were varied to accommodate the differences of wheel geometry. Actual notch-bend specimen dimensions are listed with the results (see table 11, section 3.3). A 2.50-in.-thick compact tension specimen of the configuration shown in figure 7 was used to test the axle materials. All specimens were precracked and tested in accordance with the requirements of ASTM E399-72 (Standard Method of Test for Plane-Strain Fracture Toughness of Metallic Materials).

In essence, the fracture toughness tests conducted to ASTM E399-72 consist of loading a precracked specimen to failure. The specimen is instrumented to obtain a curve of load versus crack-opening displacement at the mouth of the notch. After completion of the test, a 5% offset secant line is constructed on the load displacement curve and the load corresponding to the point of intersection of the secant line with the curve (which represents a 2% crack extension) is designated P_Q. If the following criteria are fulfilled, then K_Q is equal to the plane strain fracture toughness K_{Ic}:

1)	Specimen thickness (B)	$>2.5\ (K_Q/TYS)^2$
2)	Crack length (a)	$> 2.5\ (K_Q/TYS)^2$
3)	P_{max}/P_Q	< 1.10

where P_{max} is the maximum load recorded in the test. Items 1 and 2 are required to ensure that plane strain conditions are operative at the crack tip. Item 3 was introduced as a result of experimental work which had shown that items 1 and 2 were insufficient to guarantee a valid K_{Ic} in some materials. Figure 8 shows the notch-bend specimen test set-up.

Test temperatures were −40° F, 0° F, 150° F, and 300° F. The elevated and cold temperatures were thermostatically maintained to ±5° F in a Develco Model TSC-12 environmental chamber. Prior to the start of testing, the specimens were held at temperature a minimum of 1/2 hour per in. of thickness.

2.3.4 K_{Id} Testing

Plane strain dynamic fracture toughness data (K_{Id}) were obtained by testing precracked, standard 0.394-in.-square Charpy V-notch specimens in a computerized impact testing system. Testing was conducted by the U.S. Army Materials and Mechanics Research Center. Data were obtained at a hammer velocity of 4 to 11 fps. Tests were conducted at -40° F, 32° F, 75° F, 150° F, and 300° F.

2.3.5 Fatigue Testing

A constant-deflection fatigue machine was used to cycle the Double Cantilever Beam (DCB) specimen shown in figure 9. Grooves were machined along the sides of the specimens to promote straight crack growth. A view of the fatigue machine showing the specimen and grip arrangement is shown in figure 10. The number of cycles was counted with a digital counter. The deflection applied to the specimen was set with an adjustable cam and was measured with a dial indicator to ±0.0002 in. Crack length was measured with a machinist scale to the nearest 0.01 in. along the sides of the specimen with the aid of a 30X binocular microscope. To facilitate observation of the crack tip, the specimen side grooves were hand-polished to a 16 micron finish. All specimens were cycled at a rate of 300 cycles per minute (based on the cyclic rate seen by a 33-in.-dia wheel traveling at 30 mph).

Stress intensity at the tip of the crack was calculated using the following equation (refs 7 and 8):

$$K = \frac{VEh\left[3h\,(a + 0.6h)^2 + h^3\right]^{1/2}}{4\left[(a + 0.6h)^3 + h^2a\right]}\left[\frac{b}{b_n}\right]^{1/2}$$

V = total deflection of the two arms of the DCB specimen at the load point

E = modulus of elasticity (29×10^6 psi for steels)

h = 1/2 specimen height (1.00 in.)

a = crack length measured from load point

b = specimen thickness

b_n = specimen thickness between side grooves

Crack growth rates were determined as a function of ΔK and the stress ratio (R), which were defined as follows:

$$\Delta K = K_{max} - K_{min}$$

$$R = K_{min}/K_{max}$$

K_{min} and K_{max} were calculated from the minimum and maximum deflections.

Room temperature testing was conducted in 100% humidity room-temperature air or in the presence of an aqueous solution of 3½% NaCl. The 100% humidity environment was achieved by sealing the specimen in a plastic bag containing water and allowing the environment in the bag to stabilize. Testing of the 3½% NaCl solution was accomplished by periodically squirting the crack tip with a salt water solution. The −40° F testing was performed in a box that was placed around the specimen and cooled with liquid nitrogen vapor. A thermocouple attached to the specimen was used to monitor temperature.

2.3.6 Metallographic Analysis and Hardness Traverses

Two grain flow specimens were taken from each of two wheels and one grain flow specimen was taken from each of the three axles. Figures 1 and 2 show the locations of the grain flow specimens. The specimens were polished and then etched in a 50% aqueous solution of hydrocloric acid at approximately 180° F. The etched grain flow specimens were then photographed to document the results. After the sections had been photographed, hardness measurements were made at intervals of 0.25 in. along the traverse lines shown on figures 11 and 12. The hardness traverses were performed at the two locations identified as GF2 and GF5 (fig. 2).

Metallographic sections were prepared from the wheels and axles at the locations shown in figures 11 and 12. Three microsections were prepared from each of the wheels and two microsections were prepared from each of the axles. Inclusion ratings were made on each of the unetched microsections in accordance with ASTM E45-63, Method A. After the inclusion ratings were made, the microsections were then etched with 2% Nital and examined by means of a metallurgical microscope. Photographs were taken of typical microstructures seen in each alloy.

An assessment of both the percentage of ferrite and the pearlite colony size was made. The percentage of ferrite in the microstructure was determined by a point-counting technique (ref 9). A grid was superimposed on a projection of the microstructure and a count was made of the ferrite grains falling at grid intersections. This count was then divided by the total number of grid points to determine the percentage ferrite. The average pearlite colony size was determined by measuring the colony widths along a linear projection. A total of 80 colony widths were measured per microsection.

3.0 RESULTS

3.1 TENSILE PROPERTIES

The results of the tensile testing are given in table 9. The yield and tensile strengths of the rims were higher than in the plate as a result of rim quenching. The strength properties of the two Grade F axles met the tensile requirements specified in AAR Specification M101-72. The fractured specimens from the two Grade F axles and the Class Sub A wheel displayed typical cup-cone ductile fractures. The fracture faces of the specimens from the Class B wheel were a mixture of 50% fibrous and 50% cleavage, the fibrous portion of the fracture occurring in the center of the section. The specimens from the Grade U axle displayed 100% cleavage.

TABLE 9.—ROOM TEMPERATURE TENSILE TEST RESULTS

Material	Specimen		UTS (ksi)	TYS[a] (ksi)	Elong. %	RA (%)
	No.	Location				
Class sub A wheel, wheel no. 8	86-T1	Rim	100.8	63.2	20	43
	86-T2	Plate	82.2	50.3	27	48
Class B wheel, wheel no. 9	96-T1	Rim	135.6	82.9	16	35
	96-T2	Plate	115.2	58.4	16	30
Grade F axle, F1	FFD-T1	Midradius	93.5	53.6	28	50
	FFD-T2	Midradius	93.4	50.1	27	47
Grade F axle, F2	HHD-T1	Midradius	92.9	50.6	27	48
	HHD-T2	Midradius	92.1	55.4	26	46
Grade U axle	UUD-T1	Midradius	102.4	51.6	13	27
	UUD-T2	Midradius	102.7	50.9	17	24

[a]Tensile yield strength—0.2% offset.

3.2 CHARPY IMPACT

Table 10 gives the results of room temperature Charpy impact testing of the wheel rim materials. The 9 to 15 ft-lb impact strength of the Class Sub A wheel was significantly higher than the 1 to 6.5 ft-lb impact strengths previously reported (ref 4). Even though the Class Sub A Charpy fracture energies were significantly higher than those of the Class B, this difference was not readily apparent in the fracture topographies. The Class Sub A fractures exhibited no lateral contraction and more than 95% cleavage. The Class B Charpy fractures showed no lateral contraction and were 100% cleavage.

TABLE 10.—ROOM TEMPERATURE CHARPY IMPACT TEST RESULTS

Material	Specimen		Impact value (ft–lb)	Cleavage (%)
	No.	Location		
Class sub A wheel, wheel no. 8	86-C1	Rim	15.1	95
	86-C2	Rim	9.0	95
Class B wheel, wheel no. 9	96-C1	Rim	5.0	100
	96-C2	Rim	4.8	100

3.3 FRACTURE TOUGHNESS, K_{Ic}

Results of the fracture toughness tests conducted during this Phase II investigation are listed in tables 11 and 12. None of the tests performed on the axles and only three of the tests performed on the wheels fulfilled the above requirements for a valid K_{Ic} test, for the reasons indicated in the table. Figures 13 and 14 are plots of the fracture toughness results for the Class Sub A and Class B wheels as a function of test temperature. Figures 15 and 16 are plots of the fracture toughness test results from the axles, also as a function of temperature. Examination of the data from the Class Sub A wheel reveals no discernible trends between the fracture toughness of the rim and plate. However, the Class B wheel test data indicated that the rim is indeed tougher at the higher (>150° F) test temperature. These data are of interest, but no correlation with other wheels is possible since no plate testing was previously conducted above 70° F. However, it does show a beneficial effect at elevated temperature of the rim quenching (rim toughening) process for the Class B wheel.

TABLE II.—RESULTS OF FRACTURE TOUGHNESS (K_{Ic}) TESTING FOR AXLES

Axle		Specimen no.	Test temp. (°F)	Specimen dimensions (in.)[a]			Load, P_Q (lb)	K_Q (ksi $in^{1/2}$)	$\frac{P_{max}}{P_Q}$	$2.5\left(\frac{K_Q}{TUS}\right)^2$ (in)	Conform to ASTM E-399-72 B and a
No.	Class			Thick (B)	Width (W)	Crack Length (a)					
U	U	UUEKC4	-40	2.510	5.00	1.96	43 000	55.1	1.00	2.88	No
		UUFKC5	-40	2.51	5.00	2.23	36 300	53.3	1.005	2.70	No
		UUDKC3	0	2.51	4.995	2.32	48 800	75.6	1.00	5.43	No
		UUBKC2	72	2.410	5.00	2.64	48 800	94.8	1.00	8.54	No
		UUGKC1	72	2.510	5.00	2.09	63 000	86.2	1.19	7.06	No
F1	F	FFEKC4	-40	2.515	4.995	2.24	45 200	66.8	1.00	4.16	No
		FFEKC5	-40	2.510	4.995	2.24	44 200	69.4	1.004	4.49	No
		FFDKC3	0	2.510	4.998	2.28	50 600	76.6	1.14	5.47	No
		FFBKC2	72	2.515	5.004	2.33	74 100	114.6	1.25	12.24	No
		FFGKC1	72	2.515	4.995	2.29	77 300	117.1	1.24	12.78	No
F2	F	HHEKC4	-40	2.510	4.999	2.23	49 600	72.9	1.00	4.73	No
		HAFKC5	-40	2.515	4.996	2.30	46 500	70.8	1.004	4.46	No
		HHDKC3	0	2.510	4.995	2.28	50 600	76.7	1.12	5.24	No
		HHBKC2	72	2.510	4.999	2.32	67 900	104.8	1.28	9.77	No
		HHGKC1	72	2.510	4.995	2.28	69 200	104.5	1.43	9.72	No

[a]Specimen dimensions identified according to ASTM E399-72.

TABLE 12.—RESULTS OF FRACTURE TOUGHNESS (K_{Ic}) TESTING FOR WHEELS

Wheel		Specimen		Test temp. (° F)	Specimen dimensions (in.)[a]			Load, P_Q (lb)	K_Q (ksi $in^{1/2}$)	$\frac{P_{max}}{P_Q}$	$2.5\left(\frac{K_Q}{\overline{TUS}}\right)^2$ (in)	Conform to ASTM E-399-72 B and a	Remarks
No.	Class	Location	No.		Thick (B)	Width (W)	Crack Length (a)						
8	Sub A, wrought		86-K7	-40	0.99	2.00	0.98	7320	53.7	1.001	1.80	No	
		Rim	83-K1A	-40	0.69	1.69	0.84	4460	52.8	1.41	1.74	No	
			81-K3A	0	0.69	1.70	0.86	3650	44.3	1.65	1.23	No	
			81-K4	72	0.99	2.00	0.95	6900	48.5	1.64	1.47	No	
			87-K6	72	1.00	2.00	1.05	5680	46.7	1.58	1.36	No	
			83-K2A	150	0.75	1.70	0.83	3950	41.5	1.90	1.08	No	
			88-K5	300	1.00	2.00	1.00	5750	43.1	1.80	1.16	No	
		Plate	83-KP1	-40	0.73	2.00	1.00	4340	44.8	1.18	1.98	No	
			87-KP4	0	0.71	2.00	1.01	3390	36.6	1.61	1.32	No	
			81-KP2	72	0.75	2.00	0.98	4020	39.1	1.97	1.51	No	
			86-KP5	150	0.75	2.00	0.98	3570	34.7	2.01	1.19	No	
			88-KP3	300	0.75	2.00	1.01	5200	53.1	1.56	2.79	No	
9	B, wrought	Rim	91-K3	-40	1.00	2.01	1.01	4460	33.6	1.08	0.41	Yes	$K_Q = K_{Ic}$
			93-K1A	-40	0.70	1.70	0.90	4040	51.7	1.00	0.97	No	
			91-K4A	0	0.74	1.70	0.87	3470	39.8	1.08	0.58	Yes	$K_Q = K_{Ic}$
			93-K2	72	1.00	2.00	1.03	5980	47.3	1.04	0.81	Yes	$K_Q = K_{Ic}$
			97-K6	150	1.00	2.00	1.00	8570	65.6	1.00	1.56	No	
			96-K7	300	1.00	2.00	1.06	7740	64.4	1.53	1.51	No	
			95-K5	300	1.00	2.00	1.00	7730	58.2	1.71	1.23	No	
		Plate	93-KP1	-40	0.75	2.00	0.97	3190	30.4	1.19	0.67	No	
			91-KP2	0	0.75	2.00	1.01	4590	39.8	1.10	1.16	No	Inadvertently Loaded-No curve
			96-KP5	72	0.75	2.00	-	-	-	-	-	-	
			97-KP4	150	0.75	2.00	1.01	4580	46.3	1.54	1.57	No	
			98-KP3	300	0.75	2.00	0.99	3380	33.2	2.10	0.81	No	

[a]Specimen dimensions identified according to ASTM E-399-72.

It is considered that no significant differences due to test temperature existed for all the classes of wheels tested. Comparison of the values obtained for the Grade U axle and the Grade F axles at fixed temperatures showed no significant differences. It must be pointed out that the values plotted in figures 15 and 16 are K_Q values and that deviation from the requirements of ASTM 399-72 for validity became more pronounced at higher temperature. Thus the trends in toughness seen as a function of temperature may not be valid for the axles tested.

3.4 K_{Id} DYNAMIC FRACTURE TOUGHNESS

Values of K_{Id} were calculated from a load/deflection curve in a similar manner to K_{Ic}. However, since there is no specification to control specimen geometries, testing procedures, etc., the degree of control obtained in K_{Ic} testing by ASTM E-399 is not available. For example hammer impact velocities varied between tests in the range of 4 to 11 ft per second. The values obtained are given in table 13, and the results are plotted in figure 17. It can be seen that the results obtained show similar trends to the K_{Ic} data, toughness increasing with increasing temperature.

TABLE 13.—DYNAMIC FRACTURE TOUGHNESS (K_{Id}) VALUES)

Wheel		K_{Id} (ksi $in^{1/2}$)[a]				
No.	Class	-40° F	32° F	75° F	150° F	300° F
8	Sub A	34.1 (82 KD1)	[b]44.9 (82 KD2)	48.5 (82 KD3)	[b]57.1 (82 KD4)	52.4 (82 KD5)
9	B	35.1 (92 KD1)	44.5 (92 KD2)	38.1 (92 KD3)	39.0 (92 KD4)	61.1 (92 KD5)
Axle						
No.	Grade					
U	U	49.3 (UUD KD1)	64.8 (UUD KD3)	60.5 (UUD KD5)	–	–
		38.4 (UUD KD2)	60.5 (UUD KD4)	61.7 (UUD KD6)	–	–
F1	F	47.1 (FFD KD1)	59.9 (FFD KD3)	56.6 (FFD KD5)	–	–
		48.1 (FFD KD2)	59.2 (FFD KD4)	52.4 (FFD KD6)	–	–
F2	F	46.8 (HHD KD1)	52.2 (HHD KD3)	– (HHD KD5)	–	–
		34.1 (HHD KD2)	54.5 (HHD KD4)	59.6 (HHD KD6)	–	–

[a]Specimen numbers in parenthesis

[b]Notch parallel to wheel thickness

3.5 FATIGUE PROPERTIES

The fatigue machine was set to obtain a predetermined value of ΔK and R. The specimen was then cycled to allow crack growth. The crack growth rate (da/dN) was determined by dividing the change of crack length by the number of cycles taken to grow this crack increment. Crack increments for determining crack growth rates were not standard and were dependent on the growth rates, environment, etc. For example at slow growth rates, smaller crack increments were utilized in order to expedite testing. Actual data are given in Appendix A. The ΔK value for the calculated rate of crack growth was taken as the average of ΔK between the start and end of each increment of crack growth. Figures 18 through 30 show the results of the fatigue crack growth rate testing. A detailed tabulation of the fatigue crack growth data is given in Appendix A. The major portion of the testing was performed in 100% relative humidity, room temperature air. Light corrosion products formed on the outside of the specimens tested in the 100% relative humidity environment and inspection of the cracks at up to 30X magnifications often revealed water droplets being squeezed from the crack tip. Choice of a 100% RH environment was based on a need to standardize this condition. Experience has shown that crack tips once wetted remain so for long periods of time without additional moisture. Thus it was considered a practical standard environment for the purposes of investigation.

Because the crack length could be measured only to the nearest 0.01 in. data points were plotted for a 0.04-in. minimum change of crack length or for a minimum of 200 000 cycles. For the baseline testing, small R values greater than zero were selected to avoid compressive loading of the specimen, although the constant-deflection type fatigue machine did not allow the deliberate use of negative stress ratios. The threshold levels below which essentially no crack growth occurs were not established because of the relatively slow (300 cpm) rate of cycling, and hence the long testing times which would be necessary to establish thresholds.

Examination of figure 18 revealed no distinct difference between the Grade U and grade F axles. During testing, straight crack growth was generally observed. Comparison of the limited -40° F results with the 100% relative humidity room temperature results, figures 19 and 23, showed no adverse effect due to the lower test temperature. Although it is recognized that axles generally experience a stress ratio of R = -1, selection of other positive stress ratios was necessitated by the availability of test equipment. Adjustment of these data to R = -1 was attempted by use of the Eisenstadt and Rajan relationship (ref 20).

Figures 21 and 24 show that increasing the stress ratio from R = 0.07 to R = 0.5 tended to increase the rate of crack growth for ΔK values from 12 to 25 ksi $in^{1/2}$. Cycling in the presence of 3-½% NaCl aqueous solution tended to retard crack growth, at the lower crack growth rates, as shown by figures 20 and 25. Applying ten cycles at 1.5 ΔK prior to cycling at ΔK tended to decrease the rate of crack growth within the scatter band for ΔK values of 21 ksi $in^{1/2}$, as illustrated by figure 26. Cycling ten times at ΔK = 24 ksi $in^{1/2}$prior to cycling at ΔK = 16 ksi $in^{1/2}$had no effect on the crack growth rate.

Figure 27 shows that the crack growth data from the Class Sub A wheel was within the scatter band of the Class A wheel test results. Figure 28 shows the results from the cast, wrought, and used Class U wheels. Figures 29 and 30 show the results from the Class C and CE wheels.

3.6 HARDNESS

The results of the Brinell hardness tests on the wheel treads are given in the wheel material section (2.1.2). Figures 31 and 32 show the results of the hardness traverses across the wheel sections. Since these hardness numbers are converted from a Rockwell number, direct comparison of the values obtained with an actual Brinell may be misleading. In any event, the values obtained do not satisfy the specification requirement since per the specification hardness must be taken on the wheel surface. The measurement methodology does provide a quantitative evaluation of differences existing within the wheel.

As indicated by the tensile results, the plate hardness was measurably lower than in the rim. The Class Sub A wheel was reasonably uniform and comparable in hardness properties between the two sections evaluated. The Class B wheel, however, showed a significant difference in hardness between the sections, more extensive than that seen in either the used, wrought Class U or the Class CE wheel evaluated in Phase I.

The results of the hardness traverses across the axle sections are shown in figures 33, 34, and 35. Measurements were reported as Rockwell B and, since no requirements are specified for axles, no reason was seen in converting these numbers to Brinell. The values again give a quantitative assessment of the properties across the section.

It can be seen from the Grade U axle results that the hardnesses in two orthogonal directions are remarkably consistent, with some softening being observed in the center. The Grade F axles showed a similar degree of consistency, both between the two traverses on each axle and comparing both axles together. The F1 axle did show a greater degree of softening in the center than did the F2 axle.

3.7 METALLOGRAPHY

Macrosections were taken from the Class Sub A wheel in the GF2 location and from the Class B wheel in the GF5 location. These are shown in Figures 36 and 37. Grain flow lines were visible in the plate sections of both wheels and to a lesser extent in the rim of the Class Sub A wheel. The rim of the Class B wheel did not exhibit any grain flow lines.

The macrosections taken from the wheel seat of each axle are shown in figures 38 through 40. The Grade U axle showed a center core which resulted from some prior forging operation and probably is representative of the shape forged at that time. Both Grade F axles displayed some coarsening in the center, but any effect was less pronounced than for the Grade U. This is probably because the Grade U axle did not have the benefit of a heat treatment, as did the Grade F axles.

Microsections taken from the X, Y, and Z locations of both the Class Sub A and Class B wheels were examined for inclusion content. Similarly, microsections taken from near surface and mid-radius of the Grade U and Grade F axles (F1 and F2) were examined for their inclusion content. These were estimated per ASTM E45, Method A, and the results given in Table 14. Inclusions were all of the Class D type, that is, globular oxides with both heavy and light ratings. The Class B wheel was slightly cleaner than the Class Sub A wheel, but this was not significant. The Grade U Axle had a higher inclusion rating than either of the Grade F axles.

TABLE 14.—INCLUSION RATINGS PER ASTM E45, METHOD A

Truck component	Class or grade	Inclusion rating[a]
Wheel 8	Sub A	D2L, D2H
Wheel 9	B	D2L, D1H
Axle U	U	D3L, D2H
Axle F1	F	D2L, D1H
Axle F2	F	D2L, D1H

[a]H indicates heavy; L indicates light

Typical microstructures for the rim and the plate of both wheels are shown in figures 41 and 42. The Class Sub A wheel exhibited a high percentage of ferrite. As would be expected from a 0.35 weight percent carbon steel, the slower cooled plate contained approximately 54% compared to the rim, which contained approximately 41% ferrite. This is because slower cooling more nearly approaches the equilibrium structure predicted by the Fe-Fe_3C phase diagram. The Class B wheel was predominantly pearlite, the relative proportions of ferrite in the rim and plate being approximately 6% and 8%, respectively (table 15). The percentage ferrite in the Class B wheel plate was not as high as might be expected based on the chemistry and processing. The pearlite colony sizes for both Class Sub A and Class B wheels (table 16) were significantly smaller in the tread and rim center than reported for the wheels examined in Phase I. Examination of the plate showed that the pearlite colony sizes for the Class Sub A and Class B wheels were also much lower than reported previously. There is no apparent reason why such a variation in pearlite colony sizes was observed. It may be appropriate to note that this variation had no apparent effect in fatigue crack growth rates.

TABLE 15.–PERCENTAGE FERRITE MEASURED IN LOCATIONS MICROSECTIONED FOR EACH WHEEL

Wheel		Percentage ferrite		
No.	Class	Tread (X)	Center (Y)	Plate (Z)
8	Sub A	30.9	41.1	54.1
9	B	4.1	6.1	8.0

TABLE 16.–PEARLITE COLONY SIZES AND PRIOR AUSTENITE GRAIN SIZES DETERMINED FOR RIM AND PLATE LOCATIONS OF WHEELS

Wheel		Rim				Plate	
		Pearlite colony size (in. x 10^{-3})		Prior Austenite grain size ASTM		Pearlite colony size (in. x 10^{-3})	Prior Austenite grain size ASTM
No.	Class	Tread	Center	Tread	Center		
8	Sub A	0.58	0.58	7	6	0.74	6
9	B	0.50	0.77	6	6	1.00	6

The results of the examination of the wheel sections for prior austenite grain size are given in table 16. Interestingly, the prior austenite grain size for the Class Sub A wheel is much larger than that measured for the Class A wheel reported in Phase I (ASTM 6 compared to ASTM 8). The Class B wheel compared to the wrought Class C wheel reported previously, both having an ASTM grain size of 6 in all locations. A similar study was performed on the axles. The typical microstructures for near surface and mid-radius are shown in figures 43, 44, and 45.

The non-heat-treated Grade U axle exhibited a much coarser microstructure than either of the Grade F axles. At the near surface locations of all axles, the percentage ferrite was approximately the same for all axles (table 17). However, at the mid-radius, whereas the heat treated Grade F axles had ferrite contents much the same as at the near surface location, the Grade U axle exhibited a sharply lower ferrite content. This is again a function of the original slow cool of the Grade U axle allowing structures nearer equilibrium to exist in the interior.

TABLE 17.–PERCENTAGE FERRITE MEASURED IN LOCATIONS MICROSECTIONED FOR EACH AXLE

Axle		Percentage ferrite	
No.	Class	Near-surface	Midradius
U	U	28.6	16.2
F1	F	24.2	27.0
F2	F	26.5	29.6

As can be seen from the photomicrographs (fig. 43), the pearlite colony sizes for the Grade U axle are significantly larger than either the Grade F axles. Table 18 shows the Grade U pearlite colony sizes compared to the Grade F colony sizes. The colony sizes measured in the Grade U axle were approximately three times larger at the mid-radius and about five times larger at the near surface. The colony sizes being a function of cooling rate, among other mechanical and thermal treatments, it would be expected that variation between axles would be less in the interior. The prior austenite grain size was slightly larger in the Grade U axle compared to both Grade F axles; however, both prior austenite grain sizes were relatively fine.

TABLE 18.–PEARLITE COLONY SIZES AND PRIOR AUSTENITE GRAIN SIZES DETERMINED IN LOCATIONS MICROSECTIONED FOR EACH AXLE

Axle		Property			
		Pearlite colony size (in. x 10^{-3})		Prior Austenite grain size ASTM	
No.	Grade	Midradius	Surface	Midradius	Surface
U	U	1.72	2.95	7	7
F1	F	0.46	0.58	8	8
F2	F	0.59	0.52	8	8

3.8 FRACTOGRAPHY

3.8.1 Wheels

Examination of the fractures obtained from the K_{Ic} specimens both optically and at low power was performed to document the fracture morphology at the various test temperatures (table 19). The rim specimens taken from the Class Sub A wheel showed that below 0° F the fracture was totally cleavage. Beginning at room temperature, about 5% fibrosity appeared and at 150° F and above the fracture was totally fibrous and ductile. The Class B wheel rim specimens began showing slight fibrosity at 70° F, but fracture did not become totally fibrous until between 150° to 300° F.

TABLE 19.–ESTIMATE OF RELATIVE PERCENTAGES OF CLEAVAGE AND FIBROUS FRACTURE MODES EXHIBITED BY K_{Ic} FRACTURES–WHEELS

Wheel		Relative percent cleavage/fibrous of fracture face[a]									
		Rim					Plate				
No.	Class	-40° F	0° F	70° F	150° F	300° F	-40° F	0° F	70° F	150° F	300° F
8	Sub A	100C	100C	5F 95C	100F	100F	100C	100C	30F 70F	10C 90F	100F
9	Class B	100C	100C	<5F	<5F	100F	100C	100C	100C	5C 95F	100F

[a]C = cleavage; F = fibrous

As noted previously, the plate specimens were tested up to 300° F whereas in Phase I, the highest temperature testing of plate specimens was 70° F. As would be expected, both wheels showed a total cleavage mode of fracture at 0° F and below. The Class B wheel was also 100% cleavage at room temperature. The transition to mainly fibrous fracture occurred in the temperature range of 70° F, to 150° F and more sharply for the Class B wheel. At 300° F, both wheel plate specimens exhibited total fibrosity.

The effect of the temperature of testing on the fracture appearance for the rim and plate specimens is summarized in table 20. The fracture appearances as a function of test temperature are documented in figures 46 and 47.

TABLE 20.–ESTIMATE OF RELATIVE PERCENTAGE OF CLEAVAGE AND FIBROUS FRACTURE MODES EXHIBITED BY K_{Ic} FRACTURES–AXLES

Axle class	No.	Relative percent cleavage/fibrous of fracture face[a]					
		-40° F		0° F		70° F	
U	U	UUE KC4	100C	UUD KC3	100C	UUG KC1	100C
		UUF KC4	100C			UUB KC2	100C
F	F1	FFE KC4	100C	FFD KC3	100C	FFG KC1	40 F/60 C
		FFF KC5	100C			FFB KC2	60 F/40 C
	F2	HHH KC4	100C	HHD KC3	100C	HHB KC2	<5F
		HHF KC5	100C			HHG KC1	50 F/50 C

[a]C = cleavage; F = fibrous

3.8.2 Axles

A similar examination of the fractures from the axles was performed. The Class U exhibited 100% cleavage fractures at all temperatures tested (-40° F to 70° F). Figures 48 and 49 show the typical fracture seen for this grade at -40° F and 70° F. However, at 70° F fairly extensive fibrosity may be seen, the one exception being a specimen from the F2 axle. In this specimen, the fracture remained about 95% cleavage (table 20). Figures 50 and 51 show typical Grade F fracture appearances at -40° F and 70° F. Three of the room temperature tests performed on the Grade F axles exhibited a fracture that initially extended normal to the precrack direction before turning to become parallel to the precrack direction (fig. 52). The specimen mentioned above, showing 95% cleavage at room temperature, did not exhibit this fracture behavior. It would appear from these results that when the fracture mode is greater than about 40% fibrous, this type of fracture orientation would be expected.

3.8.3 Fractographic Analysis of Fatigue Specimens–Wheel and Axles

The fracture appearance of the fatigue specimens was typically smooth. The degree of smoothness varied as a function of ΔK; the smallerΔK, the finer the fracture

topography. Arrest marks corresponding to the changes in ΔK, and thus changes in growth rates, were readily apparent. Figures 53 through 56 show typical fatigue topographies, which in these materials contain substantial amounts of cleavage. Figure 53 is the fatigue fracture from specimen UUB-F1 taken from the U axle. Three zones may be discerned on the fracture. Extending approximately 0.44 in. from the top of the chevron crack starter is a relatively coarse zone of fatigue which corresponds to the average ΔK of 24 ksi $in^{1/2}$. The next 0.17-in. crack growth which is noticeably finer corresponds to an average ΔK of 17.5 ksi $in^{1/2}$.The final crack extension is by cleavage which occurred during breaking open of the specimen to examine the fracture. The difference between the growth rates at the ΔK of 24 ksi $in^{1/2}$ and 17.5 ksi $in^{1/2}$ is approximately a factor of 4.

Similarly by such an analysis, the zones shown on the fracture from specimen 43-F2 (Class A wheel) can be correlated with the change in ΔK (fig. 54). The fractures discussed above are for 100% relative humidity, $R = 0.06$. Of interest is the fracture shown in figure 55 (specimen 44-F3). Here, the first fatigue zone corresponds to the initial room temperature precrack at a $\Delta = 27$ ksi $in^{1/2}$. This can be seen to be much coarser than the second zone which was cracked at -40° F with a ΔK of approximately 26.7 ksi $in^{1/2}$. The other fatigue fracture examined in detail and shown in figure 56 is the 44-F4 specimen (Class A wheel) which was tested in 3-½% NaCl solution. Extensive corrosion can be seen which masked the basic fracture topography.

Examination of selected fractures using the scanning electron microscope (SEM) was made. The specimen UUB-F1 from the Grade U axle showed the typical fatigue fractography seen (fig. 57).

Examination of specimen 44-F4 (tested in 3-½% NaCl)confirmed that the fracture was extensively corroded and, thus, it was not possible to identify any fracture modes (fig. 58).

No differences in fractography were seen between specimens tested at an $R = 0.06$ and $R = 0.5$.

4.0 DISCUSSION

4.1 TENSILE PROPERTIES

The mechanical properties of the two wheels tested in this program are compared in table 21 with values reported by other investigators for the Class B wheels. The values obtained in this investigation were slightly lower in the rim but essentially the same in the plate compared to the values reported previously (ref 4). No data were found for the Class Sub A wheel, but the values obtained were lower than the Class A wheel data reported previously (ref 4). A similar comparison for the axles could not be made because these data were not obtained in the previous work.

TABLE 21.–COMPARISON OF WHEEL TENSILE PROPERTIES

Class	Location	Yield strength (ksi)	Tensile strength (ksi)	Reference
Sub A	Rim	63	101	
	Plate	50	82	
B	Rim	83	136	
		(85-88)	(144-145)	10 and 11
	Plate	58	115	
		(50)	(117)	11

( ) Referenced data.

The hardness of the Class B wheel met the specification requirements (AAR M 107). The hardness of the Class Sub A wheel was less than the minimum required for Class A wheels, but met the minimum hardness which probably will be specified in future procurement of Class Sub A wheels (ref 5).

By plotting a curve of ultimate tensile strength and carbon content (fig. 59) for rim toughened wheels, it can be seen that the Class Sub A falls on the curve. Class B values are higher and comparable to the higher carbon Class C. However, comparison of the percentage reduction of area shows the Class B wheel to be as ductile as the Class A previously reported, although not as ductile as the Class Sub A (table 22).

TABLE 22.—COMPARISON OF DUCTILITY OF HEAT-TREATED WROUGHT WHEELS

Wheel class	Reduction of area (%)	
	Rim	Plate
Sub A	43	48
A	38	35
B	35	30
C	33	21
CE	30	28

Tensile strength as a function of carbon content for the Grade U and both Grade F axles fitted the curve shown in figure 59, the data falling between the rim and plate curves of the wheels. The non-heat-treated axle had a higher tensile strength than the heat-treated grade of axle. However, the yield strengths were directly comparable. The ductility of the Grade U axle was significantly lower than either of the Grade F axles, by almost 50%.

4.2 FRACTURE TOUGHNESS

Fracture toughness of the Class Sub A wheel appeared unaffected by temperature in the range -40° F to 300° F (fig. 12), similar to the Class A wheel reported earlier in this work, although this is most probably a fictitious effect since valid K_{Ic} values were not measured. Fracture toughness of the Class B wheel showed some dependence on temperature, becoming tougher the higher the temperature. In this way, its behavior was comparable to the Class C wheels.

Comparison of the effect of carbon content on fracture toughness was not possible with the Class Sub A wheel because of the invalid K_{Ic} values. The class B wheel, however, compared well with previous data (fig. 60).

The lower carbon axles, which were tested in larger sections and whose K_Q approximated K_{Ic} to a higher degree, were also placed on the curve of fracture toughness versus carbon content shown in figure 60. If extrapolation of the trends shown previously are made, it is quite clear that a significant improvement in toughness occurs by reducing carbon content below 0.5%.

Comparing these observations on the strength and toughness with those reported previously (refs 4 and 12), the results for both classes of wheels tested agree generally with the published data. It is significant that the pearlite colony sizes for the Class Sub A wheel and Class B wheel are much finer than previously reported (ref 4). The percentage of free ferrite is much greater in the Class Sub A wheel compared to the Class A wheel, although the yield strengths are comparable. Looking at the data for axles, we see that again the pearlite colony sizes for the Grade F axles are appreciably finer than the non-heat-treated Grade U axle. The percentage of free ferrite is similar near the surface of both grades of axle. However, as the mid-radius location is reached, the double normalized and tempered Grade F axles show nearly 50% more ferrite than the slow cooled Grade U axle. Comparing these data with the mechanical properties obtained, we see that the yield strengths are comparable to the Class A and Sub A wheels with a significant increase in room temperature toughness (keeping in mind that the K_Q of the Class Sub A wheel is probably suppressed due to invalidity). Thus, the percentage increase in free ferrite lowers the yield strength and increases the toughness as found previously (ref 4).

Consideration of the data for the materials tested in this phase of the program confirms that at carbon levels of 0.5% and lower, the K_{Id} is significantly lower than K_{Ic}. Whereas for the Class B wheel (0.58% carbon) there is only a 19% reduction between K_{Ic} and K_{Id}, for the Grade F axle (0.45% carbon) there is a corresponding 48% reduction. This has been related to the percentage free ferrite in the microstructure, ferrite being strain rate sensitive (ref 4).

4.3 FATIGUE CRACK GROWTH

The general relationship between the stress intensity range, ΔK and fatigue crack growth rate da/dN is shown in figure 61. The fatigue crack growth rate curve can, in general, be separated into three regions (ref 13). The crack growth rate in Region I, at low ΔK values, is extremely stress intensity dependent and the curve becomes almost parallel to the crack growth rate axis. It is therefore possible to define a threshold stress intensity (ΔK_t) below which the crack growth rate becomes diminishingly small. In other words, this defines the stress intensity level below which a crack can be considered as nonpropagating.

In Region II, the functional relationship between crack growth and stress intensity range can be expressed as:

$$\frac{da}{dN} = C\Delta K^n$$

Where C and n are constants for a given material and fixed test conditions.

With increasing stress intensity range, a point is reached where there is a marked acceleration in fatigue crack growth. This region of accelerated growth is denoted as Region III in figure 61.

As previously noted in Section 3.5, threshold ΔK_t values were not definitely established in this study. Nevertheless, figures 18 and 28 show that at R = 0.06, the growth rate is less than 2×10^{-8} in./cycle at a stress intensity ΔK of 7 ksi $in^{1/2}$ in Grade U and F axles and Class U wheels. Beevers, et al. (ref 13) have reported a threshold (defined as a growth rate of less than 4×10^{-10} in./cycle) of 7 ksi $in^{1/2}$ at R = 0.05 for a 0.55C-0.66Mn steel.

Threshold values of 11 ksi $in^{1/2}$ have been reported (ref 14) for other medium carbon pearlitic steels, and it has been suggested (refs 14 and 15) that the value increases with yield strength at a given value of R. However, it can be seen from figure 30 that the threshold for the heat-treated Class CE wheel, which has a yield strength at least 30 ksi greater than the Class U wheels, and axle materials, does not exceed 7 ksi $in^{1/2}$.

Although not investigated in this study, the stress ratio R can have a significant effect on ΔK_t. The magnitude of this dependence appears to depend upon the material, and for pearlitic steels has been reported as (ref 14):

$$\Delta K_t = (1 - R)^{\gamma} \Delta K_{to}$$

Where ΔK_{to} is equal to ΔK_t at R = 0 and γ has been shown to equal 1.0 for pearlitic steels (ref 16).

The influence of negative R values has not been investigated for pearlitic steels, but data reported by Pook (ref 17) for mild steel indicates that ΔK_t at R = 0 and R = −1 are essentially equal when ΔK is calculated from the tensile portion of the load cycle.

All steels evaluated in this study exhibit Region II behavior at stress intensity levels above about 10 ksi $in^{1/2}$. There was no evidence of a Region III in any of the steels tested, probably because the ΔK values tested were not high enough.

A comparison of the test results of an R of 0.06 for the Class A (fig. 22), Class Sub A (fig. 27), cast and wrought Class U (fig. 28), cast and wrought Class C (fig. 29), and Class CE (fig. 30) wheel plates shows that all data points fall within the relatively narrow Region II scatter band constructed for the Class A wheel (fig. 22). Since these steels encompass the variations in carbon content, fabrication method, and heat treatment experienced in currently manufactured wheels, which in turn control the microstructural characteristics, mechanical properties, and fracture toughness, it can be said that none of these variables have any significant influence on the Region II fatigue crack growth properties. The relationship between the crack growth rate and stress intensity range for the lower bound of the scatter band can be expressed by:

$$\frac{da}{dN} = 4.318 \times 10^{-11} \Delta K^{3.53}$$

The exponent is in good agreement with the values of 3.2-4.2 reported for wheel and rail steels (refs 18 and 19).

Figure 24 shows that increasing the stress ratio R from 0.07 to 0.5 increases the fatigue crack growth rate. Similar results have been reported by Evans, et al. (ref 19) for a 0.56C-1.02Mn rail steel. These investigators further showed that the effect of R could be predicted by the relationship developed by Forman (ref 20):

$$\frac{da}{dN} = \frac{C\,\Delta K^m}{(1 - R)K_{Ic} - \Delta K}$$

The data obtained for the Class A wheel at R = 0.06 (fig. 22) was used to develop an equation of this type and the following relationship was obtained:

$$\frac{da}{dN} = \frac{5.638 \times 10^{-9}\,\Delta K^{2.99}}{(1 - R)50 - \Delta K}$$

where K_{Ic} was arbitrarily given the value of 50 ksi $in^{1/2}$ being considered a typical value that could be expected.

This expression was then used to predict the relationship between da/dN and ΔK for a stress ratio of 0.5. As shown in figure 62, there is good agreement between the prediction and the experimental data obtained at R = 0.5. The Forman relationship therefore appears to be directly applicable to wheel steels.

Forman's equation is not applicable to negative stress ratios. However, reducing the stress ratio below zero can accelerate growth. Eisenstadt and Rajan (ref 21) have shown that the crack growth rate under these conditions can be estimated from data obtained at R = 0 by means of an effective stress intensity K_{eff}. Denoting the maximum stress intensity during fatigue cycling at negative stress ratios as K_{max}, then the growth rate corresponds to that at R = 0 for a stress intensity level of K_{eff} where:

$$K_{eff} = K_{max}(1-R)^{1/2}$$

While this method has not been verified for pearlitic steels, it has been shown to be applicable to a variety of steels over a wide range of yield strengths (ref 21).

Beevers, et al. (ref 13) consider that only positive stress ratios influence the fatigue crack growth characteristics when the mode of fatigue crack growth involves substantial proportions of cleavage fracture. Our findings are consistent with this in that cleavage cracking was the predominant mode of crack growth in Region II (Section 3.8.3). The same investigators reported that a Region III is associated with cleavage cracking, and that the transition from Region II to Region III occurs at lower ΔK values with increasing R. They suggest that this is the result of developing high tensile stresses at the crack tip which promotes the linkage of isolated cleavage facets, and thus accelerates crack growth. However, as previously noted, a Region III is not observed in the crack growth curves reported herein.

A comparison of the crack growth curve scatter bands for the Class A wheel (fig. 22) and the Grades U and F axles (fig. 18) indicates similar but not identical behavior in Region II. Nevertheless, it is considered that the scatter band for the Class A wheels provides an adequate representation of the fatigue crack growth characteristics of axle materials.

Reducing the test temperature from RT to −40° F did not affect the fatigue crack resistance of the Class A wheel and Grade F axle materials (figs. 19 and 23). An increase in growth rate was expected based on the reduction in cleavage resistance with reduction in temperature.

Testing in 3½% aqueous sodium chloride solution reduced the fatigue crack growth rate relative to 100% RH air (fig. 25). While an increase in growth rate is more usually observed (ref 22), a reduction has also been reported to occur when 10Ni steel (180 ksi yield strength) is tested in a chloride-containing solution (ref 23). The reduced growth rates are attributed to crack tip blunting by corrosion and/or rust deposits on the fracture surface which limit the crack opening displacement range.

It has been well documented that tensile overloads can decrease the crack growth rates (ref 24). Both the material and the relative magnitudes of the loads experienced by the structural element determine the degree of retardation. Corbly and Packman (ref 24) reported that if the ratio of the peak stress to lower stress intensity factor is greater than 1.5, crack arrest occurs. In our tests under these conditions (fig. 26), no effect on crack growth rate was observed. These results indicate that pearlitic steels do not exhibit retardation effects, but this should be confirmed by more extensive testing. A possible explanation is that since the predominant mode of crack growth is cleavage, tensile overloads promote significant damage ahead of the crack tip and counteract the other effects (e.g., crack closure) which would tend to retard the crack.

5.0 SIGNIFICANCE OF FRACTURE TOUGHNESS RESULTS WITH RESPECT TO SERVICE

5.1 THERMAL CRACKS–WHEELS

Using the procedures fully documented in the first phase of this program (ref 4), the critical sizes of thermal cracks encountered under the most severe conditions of service are given in table 23 for the Class Sub A and B wheels. From this table, the minimum size of crack which must be detected by inspection can be obtained. Comparing these data with inspection limits documented previously (ref 4), it can be seen that the problem of crack detection in Class Sub A wheels is the least, in that the largest critical crack is developed. The critical crack size for Class B wheels for these service conditions remained unchanged from the estimates previously made.

TABLE 23.–CRITICAL SIZE OF THERMAL CRACKS AT AN APPLIED STRESS OF 55 ksi

Class	Critical crack length (in.)		K_{Ic} ksi $in^{1/2}$
	Corner crack	Surface crack	
Sub A	0.32	0.83	[a]45
A	0.25	0.65	40
B	0.14 (0.14)	0.36 (0.36)	30 (30)
C	0.10	0.26	25
U	0.10	0.26	25

( ) Estimated previously (ref. 4).

[a]Considered low due to invalidity.

Stresses equal to the yield strength can be developed at the tread surface during severe stop braking. Table 24 indicates the crack lengths which will become critical under these conditions.

TABLE 24.–CRITICAL LENGTH OF SURFACE CRACKS FOR FRACTURE AT STRESSES EQUAL TO YIELD STRENGTH

Class	Typical yield strength of rim (ksi)	Critical crack length (in.) (K_{Ic} = 0.9 TYS $C^{1/2}$)
Sub A	63	0.63
A	70	0.40
B	83 (87)	0.16 (0.15)
C	95	0.09
U	55	0.25

( ) Estimated previously (ref. 4).

From the foregoing, it is apparent that Class Sub A wheels give the greatest degree of confidence in finding thermal cracks before criticality.

5.2 PLATE CRACKS–WHEELS

As noted in Phase I of this report, brittle fracture of the wheel plate can result from the growth of fatigue cracks in the hub or plate fillets (ref 4). It was shown that the depth/length of surface cracks experienced in service was about 1/3. For this crack shape, the relationship between applied stress and critical crack length C is:

$$K_{Ic} = 0.9\,\sigma C^{1/2}$$

and is only applicable to cracks less than one-half the plate thickness. For through-thickness cracks, it was shown that:

$$K_{Ic} = 1.25\sigma C^{1/2}$$

In accordance with the previous analysis, it was decided that the more conservative approach of assuming dynamic conditions dominate in initiating brittle fracture, and hence K_{Id} has been substituted for K_{Ic}. The minimum K_{Id} value obtained for the Class Sub A wheels was 35 ksi $in^{1/2}$.

It was shown that stresses of yield strength magnitude can be experienced in wheel plates and the approximate value of yield strength was found to be 55 ksi (ref 4). The work of this investigation essentially confirms this approximate figure for yield strength.

Figure 63 shows that the critical crack size for surface cracks causing failure in the Class Sub A wheel is 0.50 in. Figure 64 gives a similar analysis for through-thickness cracks and should be used for cracks greater than 2 in. long since they will be on the verge of breaking through the thickness. For a given crack length the through-thickness crack represents the most dangerous situation.

Finally, if we consider that machining flaws and tears act as initiation sites for brittle failure (ref 1), the analysis given in Phase I of this work (ref 4, p 62) for Class A wheels would be valid for the Class Sub A wheel. This indicates that depth of a long, shallow critical flaw in the plate would be 0.084 in. at yield strength magnitudes (using a K_{Id} of 35 ksi $in^{1/2}$).

In the case of the Class B wheel, it was decided to retain the lower bound K_{Id} value of 25 ksi $in^{1/2}$ estimated in reference 4.

5.3 AXLES

The type of slow crack propagation experienced by axles, excluding hot journals, is essentially fatigue. These cracks occur in the wheel seat or between the wheels in the axle shaft at areas of stress concentration (ref 25).

The typical stresses experienced in an AAR 1940 standard axle under a freight car having 33-in. dia. wheels, a center of gravity 6 feet above the top of the rail, and a static load per axle of 40 kips, have been analyzed and are reported by Byrne (ref 26). Considering conditions of equal wheel loading for this Class D axle with a 5½- by 10-in. journal, the bending moment under the parameters defined is 200 in. kips in the journals and 200 in. kips in the axle body. This corresponds to approximately 6 ksi stress in the journal and 9.5 ksi stress in the axle shaft body. In extreme cases when side loading, imposed by wind gusts, super-elevation, etc., causes one wheel loading, the bending moment in the loaded journal can reach 580 in. kips and decreases linearly across the axle body, being 520 in. kips at the wheel seat rear fillet and about 350 in. kips in the center. These moments correspond to about 10 ksi in the journal and 17.5 ksi in the axle center.

Cannon and Allen (ref 27) have shown that the stress intensity K is related to the bending moment M, and the crack depth, a, as in figure 65. It is reasonable to assume that in a rotating axle with the conditions of track loading experienced, dynamic conditions prevail, and that the use of K_{Id} to calculate critical crack sizes is justifiable. The lowest K_{Id} that can be expected to be encountered in service has been shown to be approximately 35 ksi $in^{½}$ for all grades of axles investigated (sec. 3.4).

Using the curve in figure 65, and with values of K = 35 ksi $in^{½}$, M = 200 in. kips, and D (axle diameter at the center waisted position on the axle) = 5.9 in., the parameter $KD^{2.5}/M$ becomes 14.8. Entering the curve at 14.8, a/D is seen to be 0.50, which represents a crack 50% across the section. At the center position on the axle where the dia is 5.9 in., the crack depth "a" becomes approximately 3 in. It can be seen from the nature of this curve that increasing the toughness at this point by a factor of two would give a critical crack 65% through the section, an increase in crack depth of only about 0.8 in. from that shown above.

Considering the axle at the wheel seat, the other area of the axle prone to cracking, we find that D is approximately 7.6 in. The function $KD^{2.5}/M$ becomes 27.9 and extrapolating the curve shown in figure 65 gives an a/D of about 0.65 or a crack depth of approximately 5 in. These calculations represent average service conditions of loading and probably the lowest values of toughness which would be encountered.

Under extreme conditions such as one-wheel loading, where M becomes 520 in. kips, at the wheel seat rear fillet the value of $KD^{2.5}/M$ becomes 10.7. From figure 65, it can be seen that the a/D ratio is about 0.39, which for the 7.6-in. dia wheel seat rear fillet represents a crack approximately 3 in. deep. This value represents a lower bound based on static analysis and is in general agreement with reported evidence that fatigue cracks usually grow 50% and more through the section before failure (ref 25). Dynamic effects due to pitching and rolling of fully loaded cars can increase the axle loads by a factor of 3 (ref 28). In these conditions, the moment would be 600 in. kips, which on analysis would give a critical crack depth of 2.39 in., using the K_{Id} value of 35 ksi $in^{½}$ (a/D = 0.31). Thus, it seems likely that even for severe service conditions, cracks in excess of 2 in. will exist before criticality.

Figure 66 graphically defines the effect of temperature on critical crack size for axle loading of 520 in. kips. It should be remembered that these curves were generated for the standard Class D axle with the 5½- by 10-in. journal loaded under the parameters previously described. It can be seen that the effect of temperature is slight from −40° F to 32° F, the ratio of crack depth, a, to axle diameter, D, changing from approximately 0.4 to 0.56. Above 32° F no change in a/D is seen. For the purposes of these calculations, K_{Id} at −40° F was taken to be 35 ksi in and at 32° F and 75° F, it was taken to be 55 ksi in .

The critical crack depth as a function of applied stress for axles with a nominal diameter of 6 in. is shown in figure 67. This curve was generated by using the relationship between stress intensity and crack depth shown in figure 65. Axle bending moments were converted to maximum bending stress using the relationship

$$\sigma(\text{stress}) = \frac{\text{M(moment)}}{\left(\frac{\pi}{4}\right)\left(\frac{D^2}{2}\right)}$$

where D is the axle diameter (ref 26). The value of K_{Id} for this curve was taken to be 35 ksi $\text{in}^{1/2}$.

6.0 SIGNIFICANCE OF FATIGUE RESULTS WITH RESPECT TO SERVICE

6.1 WHEELS

Service experience shows that the initiation sites for fatigue cracking of wheel plates are frequently associated with defects. These include rough machining marks, embedded mill scale, and decarburization. References 4 and 29 indicate that the depth of these defects is frequently on the order of 0.030 in. and can be as high as 0.050 in.

The minimum size of a crack-like defect which will grow under specified cyclic loading conditions can be calculated from the threshold stress intensity parameter ΔK_t. As discussed in section 4.3, the value of ΔK_t for wheel materials appears to be about 7 ksi $in^{1/2}$ for a stress ratio R of zero, and can be estimated for other values of R. For surface defects, the relationship between the minimum depth of defect a_{min} and ΔK_t is given by (ref 4):

$$\Delta K_t = 1.1\,\Delta\sigma\left(\frac{\pi a_{min}}{Q}\right)^{1/2}$$

Where

$\Delta\sigma$ = cyclic stress range

Q = a parameter determined by the defect shape (ref 4)

Typical defects in wheels have a length much greater than their depth, and for this defect shape, Q has a value of 1.0. Figure 68 shows the relationship between $\Delta\sigma$ and a_{min} for four values of R.

The use of figure 68 can be illustrated by using the wheel stress data reported by Bruner, et al. (ref 30). These investigators measured the stresses experienced in a 33-in.-dia freight car wheel under a variety of loading conditions. Estimates of the minimum size of defect which can initiate fatigue crack growth at the front hub fillet are given in table 25 for some of the loading conditions reported by Bruner, et al. (ref 28). For a wheel subjected to a maximum vertical design load of 30 000 lb, and assuming a sustained residual tension stress of 10 ksi, the minimum defect depth is 0.096 in. This is larger than the defects usually experienced in wheels, and possibly explains why the incidence of plate failures is small relative to the number of wheels in service. If the design load is increased by a factor of two to allow for dynamic effects, for example due to car rocking, the minimum size is reduced to 0.061 in. Furthermore, if the residual stress is increased to 20 ksi under these conditions, the depth is reduced to 0.023 in.

Thermal effects, due to drag braking, can result in high sustained stresses at the wheel fillets during brake application (ref 4). These stresses act in combination with the residual stresses. Table 25 indicates that if the magnitude of the sustained stress is 40 ksi, it reduces the minimum defect size to less than 0.01 in. for a fully loaded freight car.

TABLE 25.—ESTIMATE OF MINIMUM DEFECT SIZE TO INITIATE FATIGUE CRACK GROWTH UNDER VARIOUS SERVICE CONDITIONS

Service conditions	Stress range[a] (ksi)	Sustained stress[b] (ksi)	R	$\Delta\sigma$ (ksi)	Minimum crack depth a_{min} (in.)
Fully loaded car (30 000-lb/wheel)	-9.6 to + 2.0	10	0.03	11.6	0.096
Fully loaded car, Dynamic loading on wheels (60 000-lb/ wheel)	-19.1 to + 4.5	10	-0.63	23.6	[c]0.061
Fully loaded car, dynamic loading on wheels (60 000-lb/ wheel)	-19.1 to + 4.5	20	0.04	23.6	0.023
Fully loaded car, drag braked	-9.6 to + 2.0	40	0.72	11.6	0.008
Fully loaded car, dynamic loading on wheels, drag braked	-19.1 to + 4.5	40	0.47	23 6	0.006

[a]Reference 30.

[b]Residual and/or thermal stress.

[c]Tension portion of stress cycle used to calculate crack size.

Yontar (ref 29) reported that fatigue cracking of wheel plates in rapid transit service was initiated by defects which were up to 0.050 in. deep. Strain gage measurements showed that stress ranges of 20 ksi and higher were frequently experienced at the failure locations. Figure 68 is in good agreement with this service behavior in that defects exceeding 0.030-in. depth will initiate cracking at the measured stresses. However under some service conditions, conventional fatigue analyses have shown that pre-existing defects are not a prerequisite for fatigue cracking (ref 30).

Once a fatigue crack is initiated, the subsequent growth is controlled by the stress intensity range ΔK and the stress ratio R. Provided that the stresses are known, a curve of crack length versus cycles can be constructed from the ΔK versus da/dN data given earlier. Service experience has shown that a fatigue crack growing into a wheel plate rapidly assumes a semi-elliptical shape with a depth/length typically equal to 1/3 (ref 4). For a cyclic stress range $\Delta\sigma$, the stress intensity range experienced at the tip of the plate crack depth a is given by:

$$K = 1.1\ \Delta\sigma\left(\frac{\pi a}{Q}\right)^{1/2}$$

Where

Q = 1.73 for a crack depth/length of 1/3 (ref 4).

The growth rate in the wheel plate (of all classes) is given by the relationship developed in section 4.3:

$$\frac{da}{dN} = \frac{5.638 \times 10^{-9} \Delta K^{2.99}}{(1 - R)K_{Ic} - \Delta K}$$

and is applicable for the environments normally experienced by wheels. A typical K_{Ic} value of 35 ksi $in^{1/2}$ can be used for calculation purposes. Thus, by integration of the above equations, the number of cycles to grow a crack between specified limits can be determined, and a curve of crack length versus cycles developed.

Such a curve (fig. 69) has been constructed for rather severe service conditions using the stress data developed by Bruner, et al. (ref 30) for the front hub fillet of a 33-in. dia freight car wheel. A maximum design load of 26 400 lb (ref 31) was used, and dynamic loading conditions were assumed to exist. The fluctuating stresses developed under these conditions are 17 ksi compression to 4 ksi tension. In addition, a sustained tension stress of 30 ksi was considered to act at the wheel fillet as a result of residual and/or thermal stresses. An initial flaw depth of 0.05 in., based on earlier discussion, was used. The crack length/cycles curve developed for these conditions is shown in figure 69. The curve indicates that the 0.05 in. initial flaw grows to a critical depth of 0.48 in. (1.44 in. in length) after approximately 360 000 cycles.

In the absence of dynamic loading conditions, the fluctuating stress range decreases to −8.5 ksi to +2 ksi. Furthermore, in the absence of thermal loads, Bruner, et al. (ref 30) state that the sustained stresses are of the order of +10 ksi due to residual stresses. Using these stress values in conjunction with the threshold ΔK_t data given in section 4.3, it can be shown that a crack less than 0.46 in. long will not propagate. In other words, the above loading conditions will not cause the crack to grow until at least 80% of the cyclic life has expired (fig. 69). Details of the stress spectra experienced by wheels are not available, but in view of the above it appears that many of the wheel revolutions will not influence the crack growth. More refined analyses could be conducted when stress spectra data become available.

The crack growth and critical crack length data discussed above provide a basis for establishing inspection criteria. It was shown in reference 4 that stresses of yield strength magnitude can be developed at the wheel fillets under severe drag braking conditions. Under these circumstances, the minimum critical crack length for brittle fracture is 0.16 in. for Class U and C wheels (ref 4). These are less than the minimum length of crack which can be detected by NDT with a high degree of confidence. As these conditions can be experienced at any time in the service life of the wheel, it may be concluded that for the worst case no useful inspection criteria can be specified for these materials.

Consideration of Class A and Sub A wheels, however, indicates that the critical crack length for plate cracks at yield strength stresses is 0.5 in. Figure 70 shows that propagation of the crack to a detectable size (0.2 in. length) occurs after approximately 10^5 cycles. An additional 2×10^5 cycles are required to propagate the crack to critical length (0.5 in.). If it is assumed that the loads used to construct figure 69 occur only

7.0 CONCLUSIONS

The results of this Phase II study have confirmed that fracture toughness, K_{Ic}, of railroad wheels and axles is controlled primarily by their carbon content.

It has been shown that fracture toughness was essentially constant over the range of temperature experienced in service. Dynamic fracture toughness, K_{Id}, for the Class Sub A wheel did not show any improvement over that for the Class A wheel since the relative percentages of free ferrite appear to be the dominant factor controlling this property. This was also shown when comparing the K_{Id} values obtained for the axles.

Estimates were made for critical thermal crack sizes in the presence of residual tensile stresses of 55 ksi in the flange (which could be developed under conditions of severe drag braking). The critical crack length for a Class Sub A wheel was 0.63 in. and for a Class B wheel was 0.16 in. Analysis of critical crack lengths in the plate for Class Sub A and A wheels under conditions of yield strength magnitude stresses showed critical crack lengths of 0.50 in. for both classes. Furthermore, analysis for machining tears or other surface discontinuities exceeding 0.084 in. in depth could result in wheel failure.

Critical crack sizes for both Grade U and F axles were calculated as a function of axle diameter. These were calculated for three conditions using stresses typically seen in Class D axles. The first condition representing average service gave the critical crack depth as 50% diameter. For conditions of one wheel loading, this was reduced to 31%.

Fatigue crack growth rate curves for all wheel materials and axles were similar and were relatively unaffected by the environmental variations experienced in service. The effect of the stress ratio R on fatigue crack growth rate was found to conform to that predicted by the Forman equation. It was demonstrated that no reliable inspection criterion is currently available for the detection of plate fatigue cracks before potential criticality in Class U, B, and C wheels.

It appears that cracks in Class A and Sub A wheels should be detectable prior to initiating brittle fracture. Similarly for axles, it was shown that for both Grade U and F axles, the critical size crack was above the minimum inspection limits. It is concluded that a reliable inspection procedure for axles would be possible given a suitable stress spectrum.

7.0 CONCLUSIONS

The results of this Phase II study have confirmed that fracture toughness, K_{Ic}, of railroad wheels and axles is controlled primarily by their carbon content.

It has been shown that fracture toughness was reasonably constant over the range of temperature experienced in service. Typical fracture toughness, K_{Ic}, for the Class Sub A wheel did not show any improvement over that for the Class A wheel since the relative percentages of fine ferrite appear to be the dominant factor controlling this property. This was also shown when comparing the K_{Ic} values obtained for the axles

Estimates were made for critical internal crack sizes in the presence of residual tensile stresses of 35 ksi in the flange region could be developed under conditions of severe drag braking. The critical crack length for a Class Sub A wheel was 0.69 in. and for a Class B wheel was 0.16 in. Analysis of critical crack lengths in the plate for Class Sub A and A wheels under conditions of yield strength magnitude stresses showed critical crack lengths of 0.50 in. for both classes. Furthermore, analysis for machining or other surface discontinuities exceeding 0.084 in. in depth could result in wheel failure.

Critical crack sizes for both Grade U and F axles were calculated as a function of axle diameter. These were calculated for three conditions using stresses typically seen in Class D axles. The first condition representing average service gave the critical crack depth as 30% diameter. For conditions of one wheel loading, this was reduced to 31%.

Fatigue crack growth rate curves for all wheel materials and axles were similar and were relatively unaffected by the environmental variations experienced in service. The effect of the stress ratio R on fatigue crack growth rate was found to conform to that predicted by the Forman equation. It was demonstrated that no reliable inspection criterion is currently available for the detection of plate fatigue cracks before potential criticality in Class U, B, and C wheels.

It appears that cracks in Class A and Sub A wheels should be detectable prior to initiating brittle fracture. Similarly for axles, it was shown that for both Grade U and F axles, the critical size crack was above the minimum inspection limits. It is concluded that a reliable inspection procedure for axles would be possible given a suitable stress spectrum.

REFERENCES

1. *Railroad Accident Report: Southern Railway Company Train 154 Derailment with Fire and Explosion, January 25, 1969,* National Technical Information Service Report PB 190208, 1969. Published by NTSB.

2. Accident Bulletin Number 138 1969, 139 (1970), and 140 (1971), *Summary and Analysis of Accidents on Railroads in the United States,* Federal Railroad Administration, Department of Tranportation (published annually).

3. Circular No. D. V. 815 AAR Operation and Maintenance Department, Mechanical Division, 1974.

4. C. S. Carter and R. G. Caton, "Fracture Resistance of Railroad Wheels," Boeing Company, Report No. FRA-ORD/75-12, September 1974, (available from National Technical Information Service as PB 243 638/AS).

5. Telephone conversation between Rene Gauthier of the National Railroad Passenger Corporation and J. L. Guthrie of the Boeing Company, June 12, 1975.

6. P. Fox and G. Hewitt, "Wheel and Tyre Development of British Railways," *Proc. Fourth International Wheelset Congress,* Paris, 2, 1972, p. 67.

7. S. Mostovoy, P. B. Crosley, and E. J. Ripling, "Use of Crack Line Loaded Specimens for Measuring Plane Strain Fracture Toughness," *J. Materials,* Vol. 2, no. 3, 1967, p. 661.

8. M. O. Speidel and M. V. Hyatt, "Stress Corrosion Cracking of High Strength Aluminum Alloys," in *Advances in Corrosion Science and Technology,* M. G. Fontana and R. W. Staehle, eds., Plenum Press, 1972.

9. T. Gladman and J. H. Woodhead, "The Accuracy of Point Counting in Metallographic Investigation," *J. Iron and Steel Inst.,* 194, 1960, p. 189.

10. J. M. Wandrisco and F. J. Dewey, "Service Defects in Treads of Railroad Wheels During Service," ASME paper 60-RR-1, 1960.

11. H. R. Wetenkamp, O. M. Sidebottom, and H. R. Schrader, "The Effect of Brake Shoe Action on Thermal Cracking and Failure of Wrought Steel Railway Car Axles, "University of Illinois, Experimental Engineering Station Bulletin 387, 1960.

12. T. Gladman, T. D. McIvor, and F. B. Pickering, "Some Aspects of the Structure-Property Relationships in High Carbon Ferrite-Pearlite Steels," J.I.S.I. 210, 1972, p. 916.

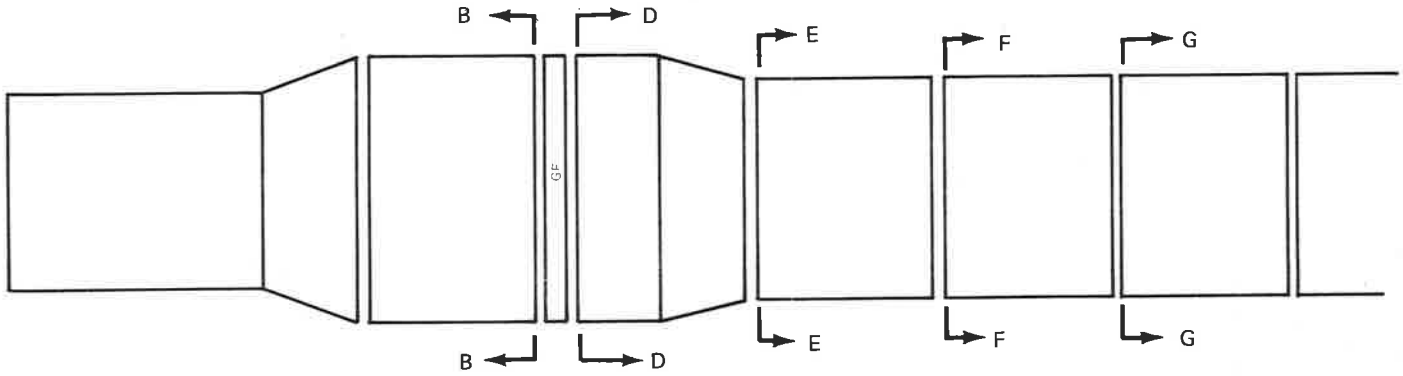

Note: Specimen types

K = Fracture toughness
T = Tensile specimen
F = Fatigue specimen
KD = Dynamic toughness
GF = Grain flow

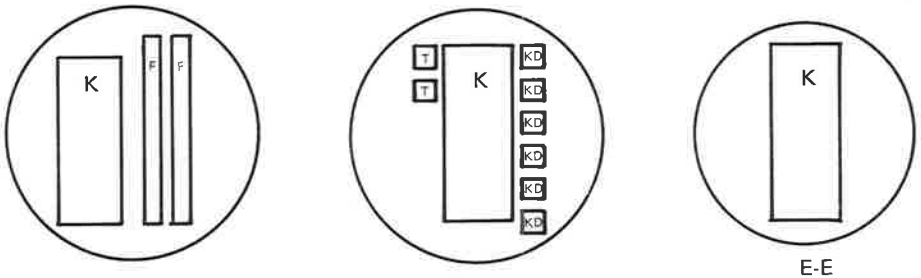

FIGURE 1.–AXLE SPECIMEN LOCATIONS

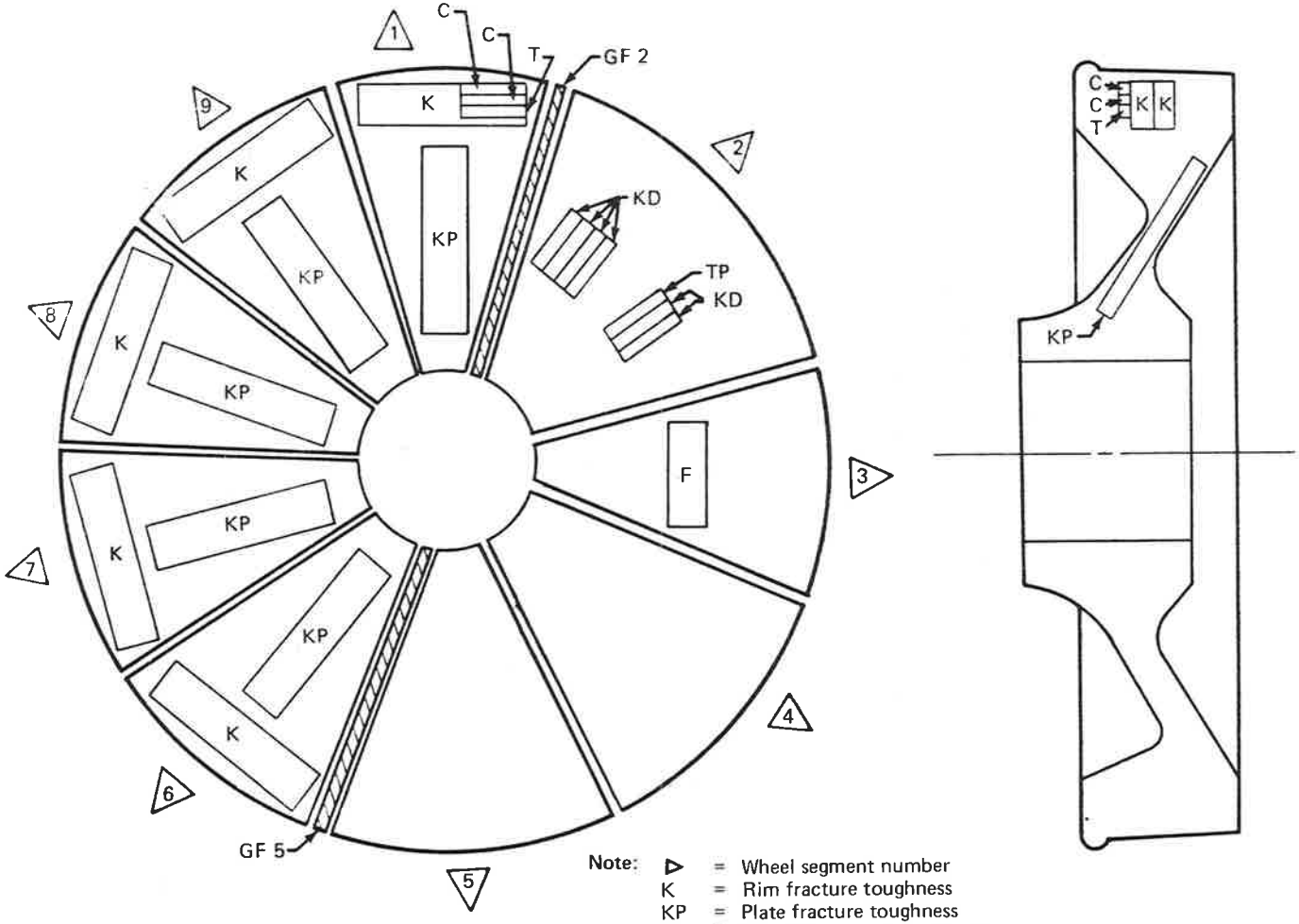

FIGURE 2.—LOCATION OF SPECIMENS WITHIN WHEEL

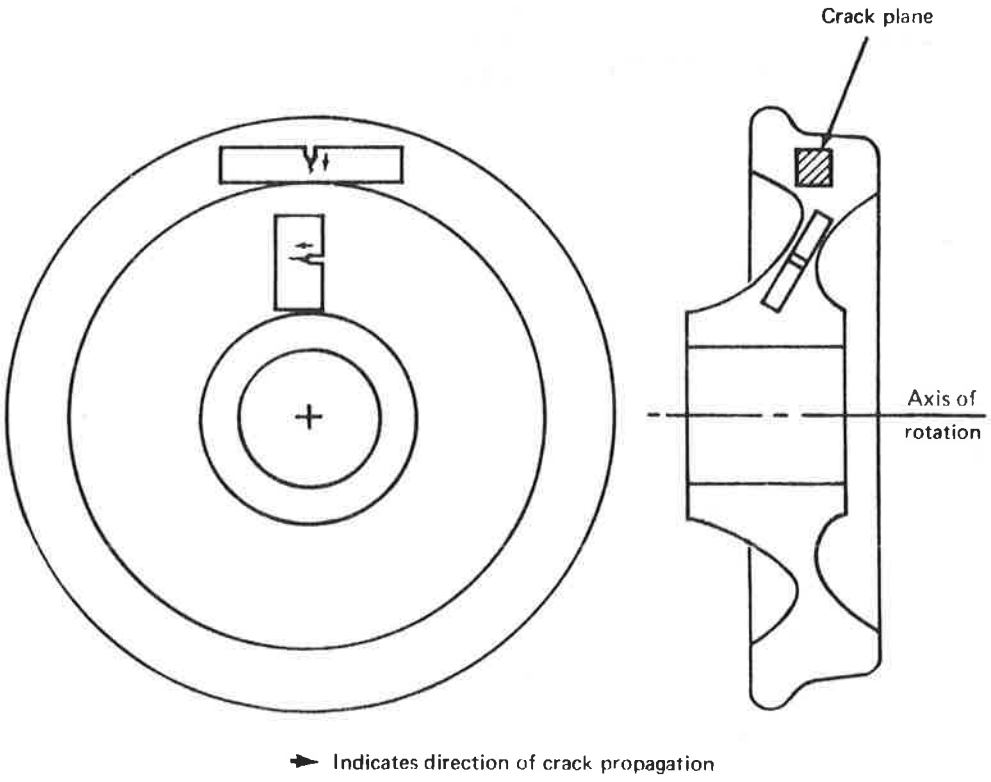

FIGURE 3.—ORIENTATION OF SPECIMENS WITH RESPECT TO WHEEL

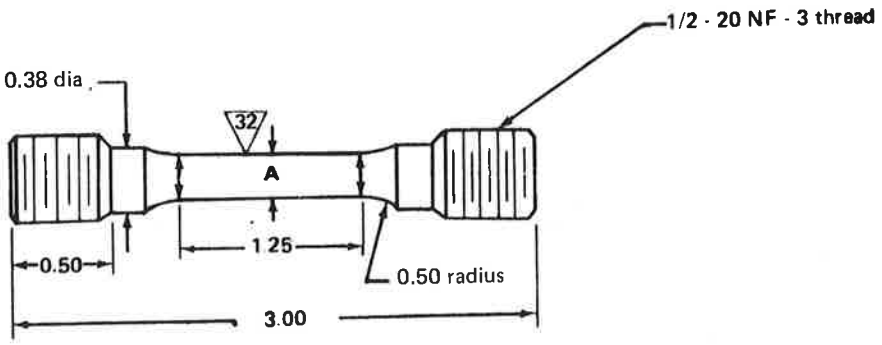

A = 0.250 max to 0.247 min

All dimensions in inches

FIGURE 4.—TENSILE SPECIMEN CONFIGURATION

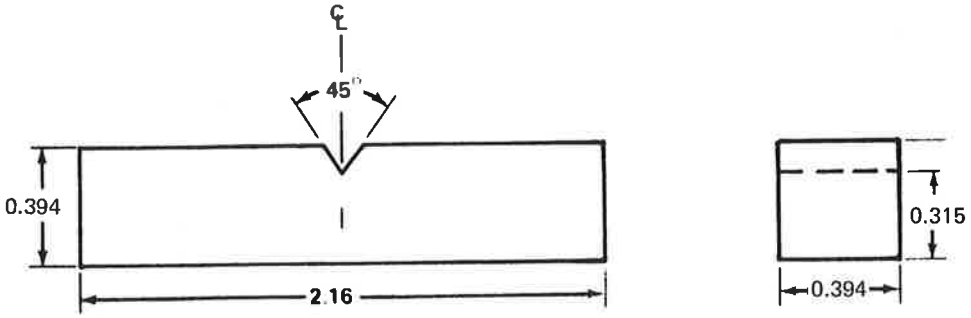

All dimensions in inches

Dynamic fracture toughness specimens have a fatigue crack grown at the notch root

FIGURE 5.—CHARPY AND DYNAMIC FRACTURE TOUGHNESS SPECIMEN CONFIGURATION

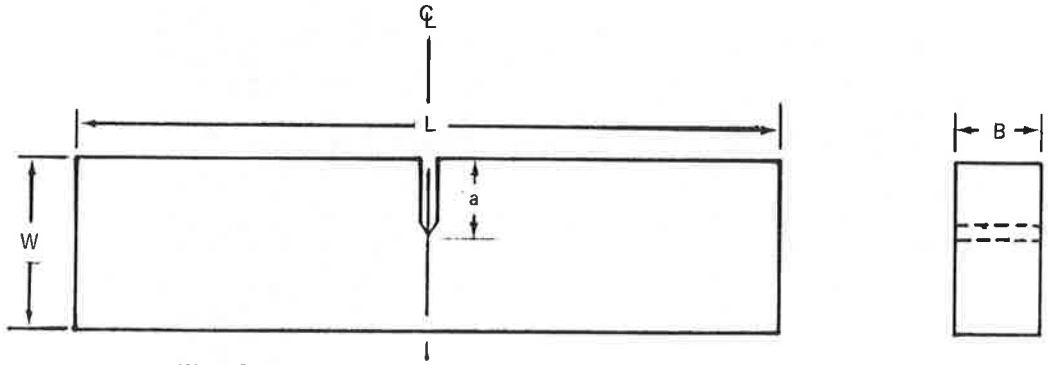

W = Specimen width (recorded with results, see table 12)
B = Specimen thickness (recorded with results, see table 12)
a = Crack length including notch (see table 12)
L = 4.1W

FIGURE 6.—NOTCH-BEND FRACTURE TOUGHNESS SPECIMEN USED FOR TESTING WHEELS

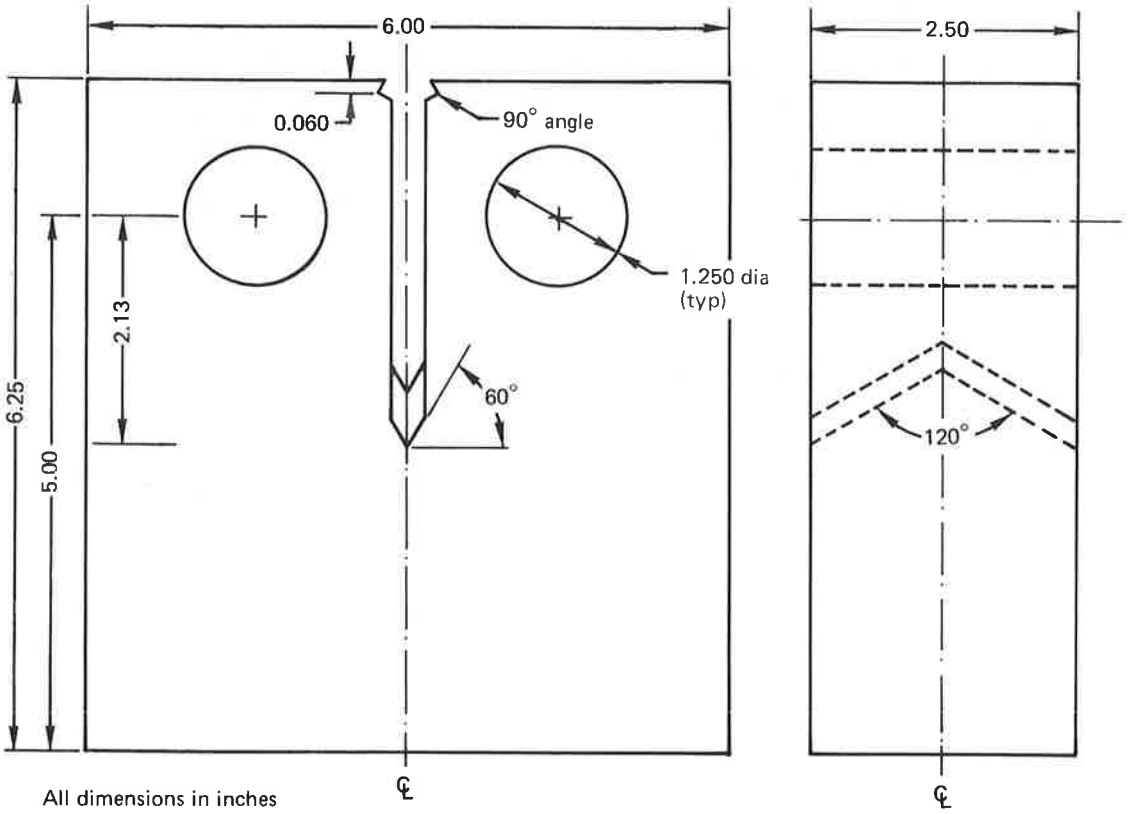

FIGURE 7.—COMPACT TENSION FRACTURE TOUGHNESS SPECIMEN

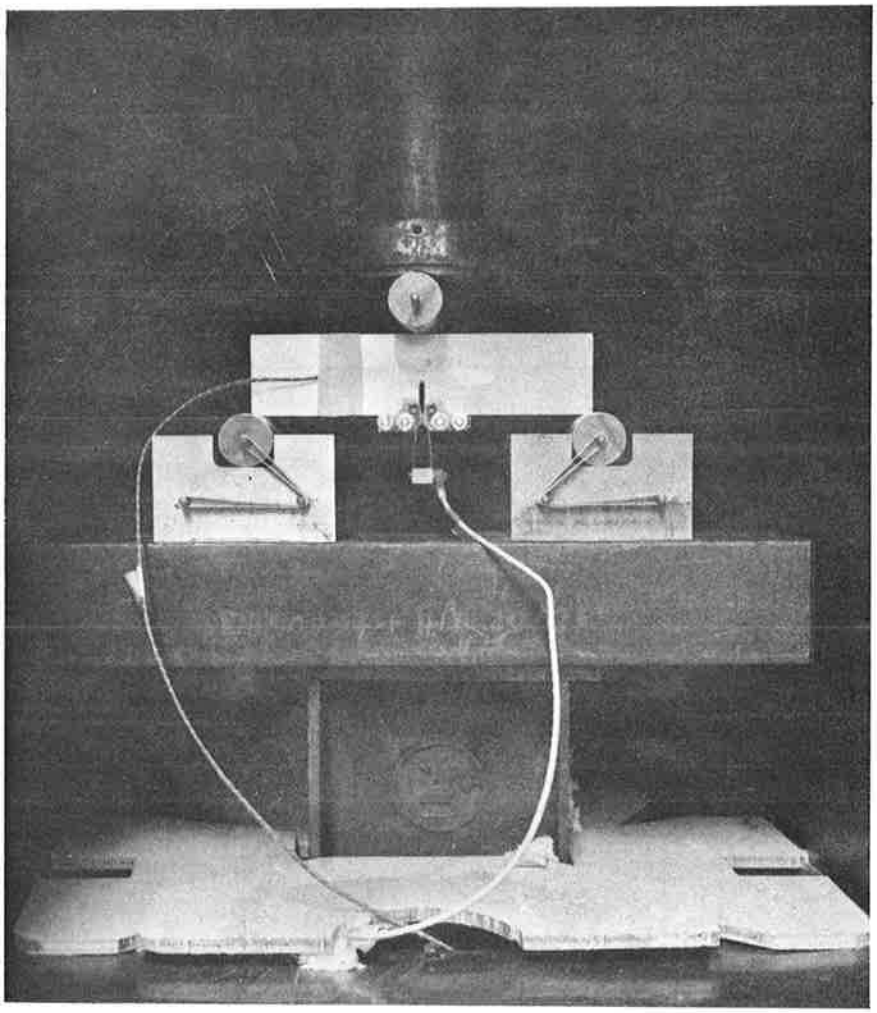

FIGURE 8.—NOTCH-BEND FRACTURE TOUGHNESS SPECIMEN TEST SETUP

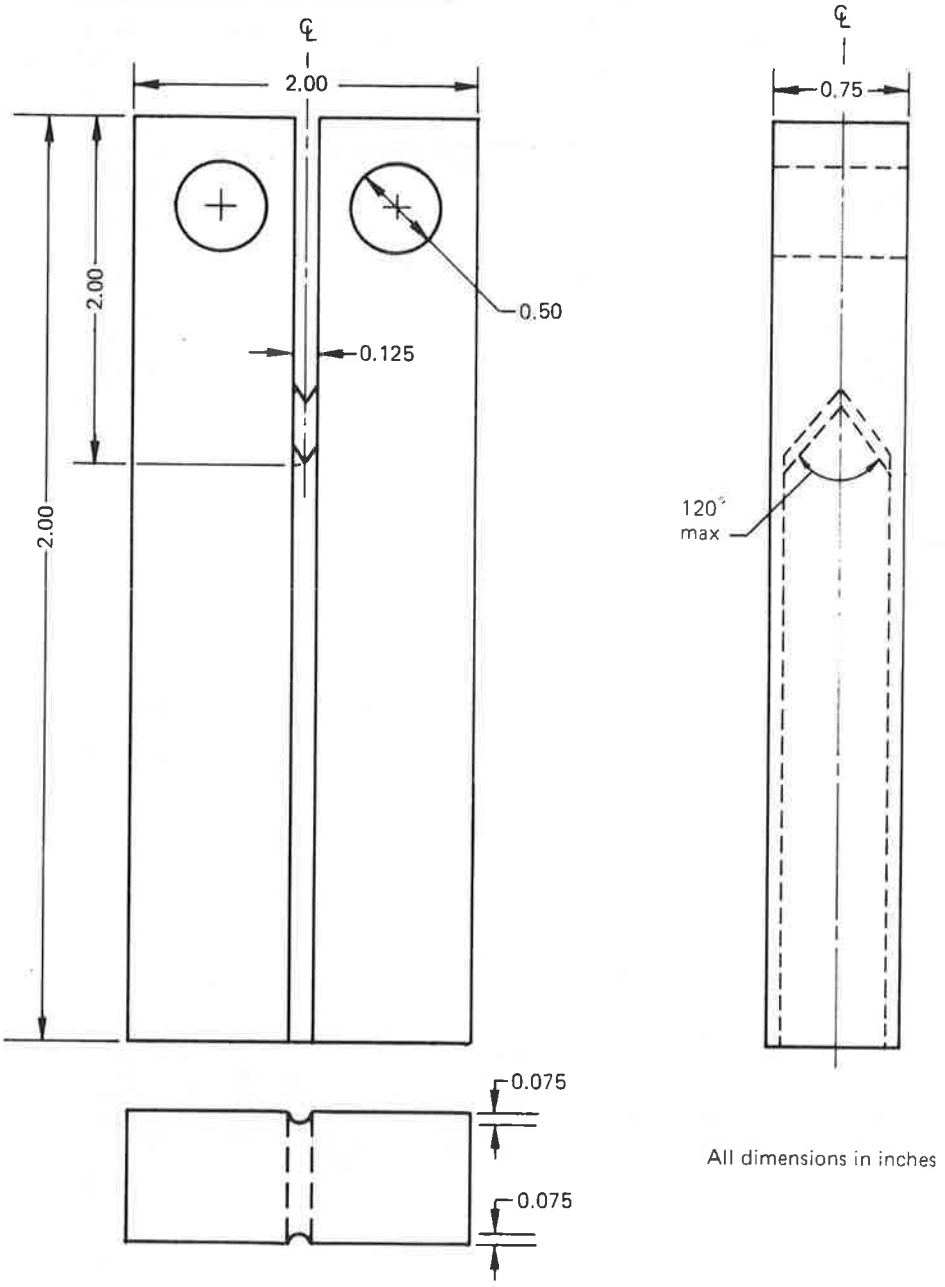

FIGURE 9.–FATIGUE SPECIMEN CONFIGURATION

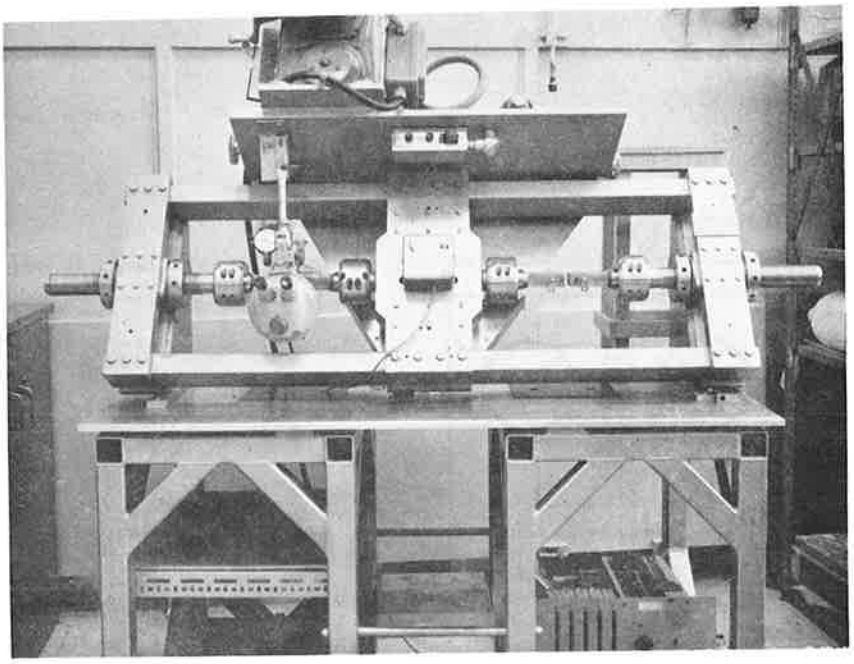

a) OVERALL VIEW OF FATIGUE MACHINE

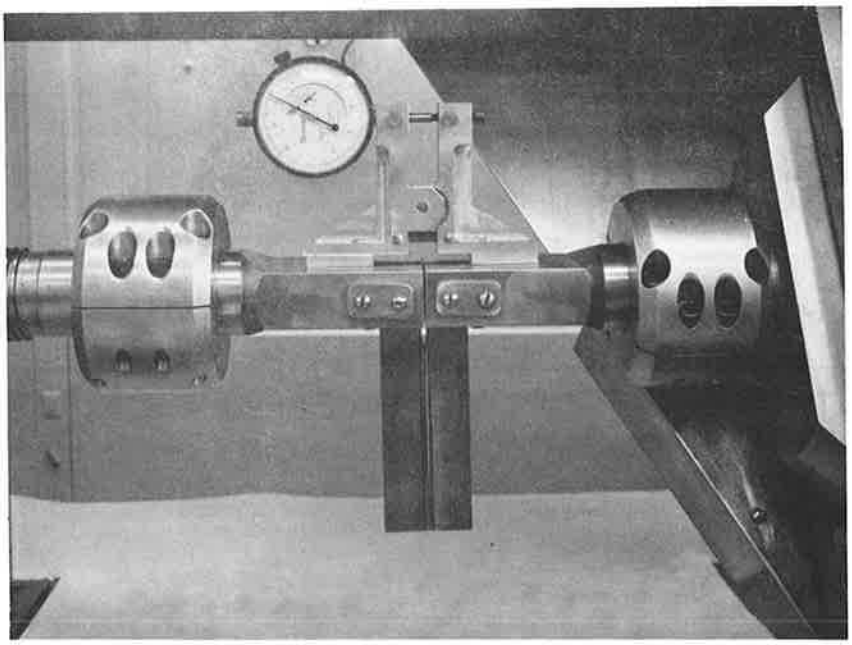

b) CLOSEUP VIEW OF SPECIMEN PLACEMENT

FIGURE 10.–FATIGUE MACHINE SHOWING SPECIMEN AND GRIP ARRANGEMENT

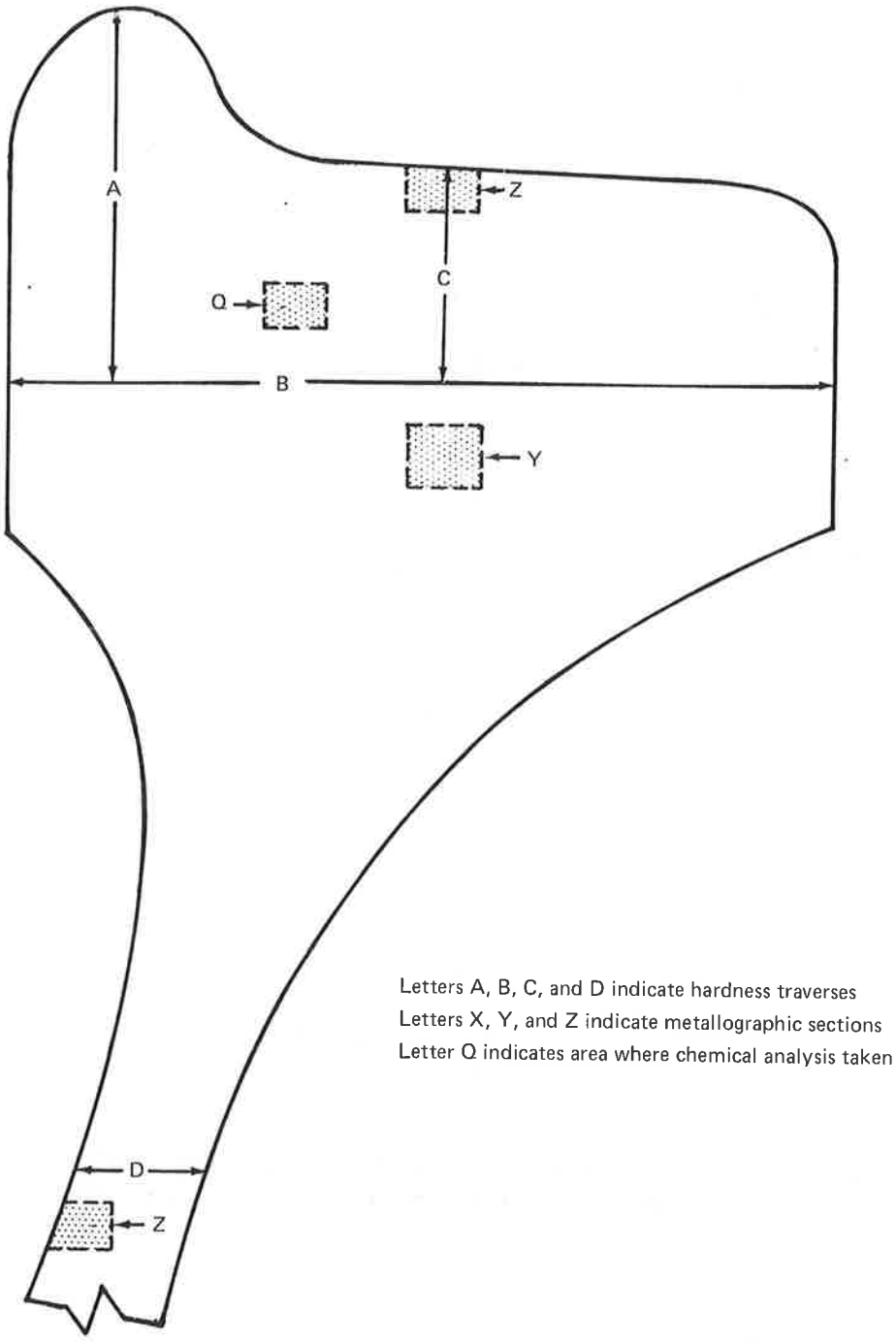

FIGURE 11.–WHEEL SECTION LOCATION OF HARDNESS TRAVERSES, MICROSECTIONS, AND CHEMICAL ANALYSIS SPECIMENS

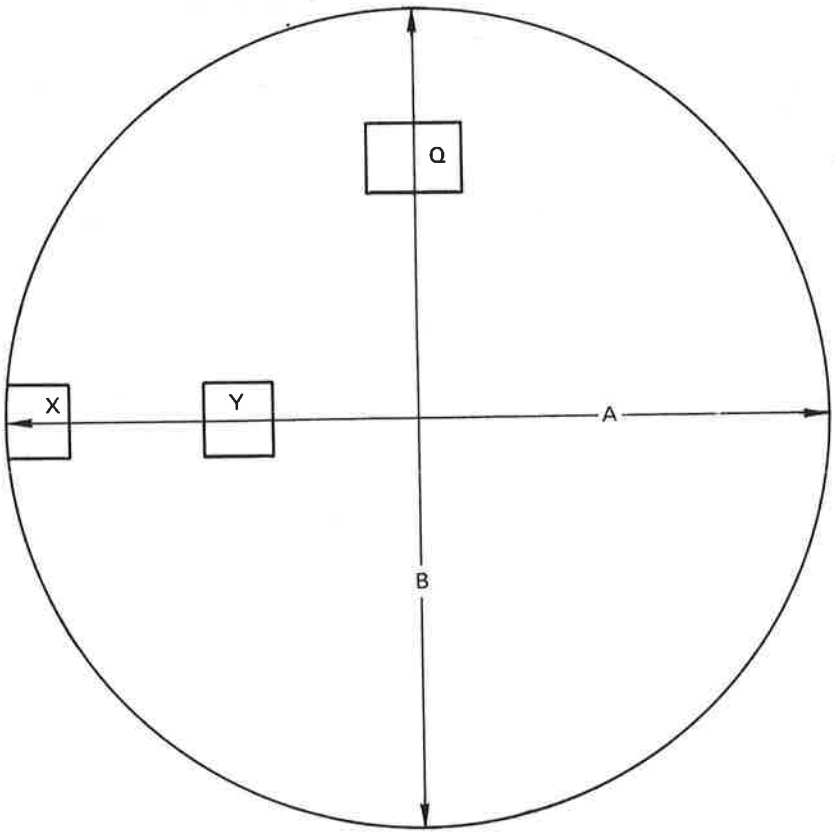

Letters A and B indicate hardness traverses
Letters X and Y indicate metallographic sections
Letter Q indicates location of chemical analysis sample

FIGURE 12.–AXLE SECTION LOCATION OF HARDNESS TRAVERSES, MICROSECTIONS, AND CHEMICAL ANALYSIS SPECIMEN

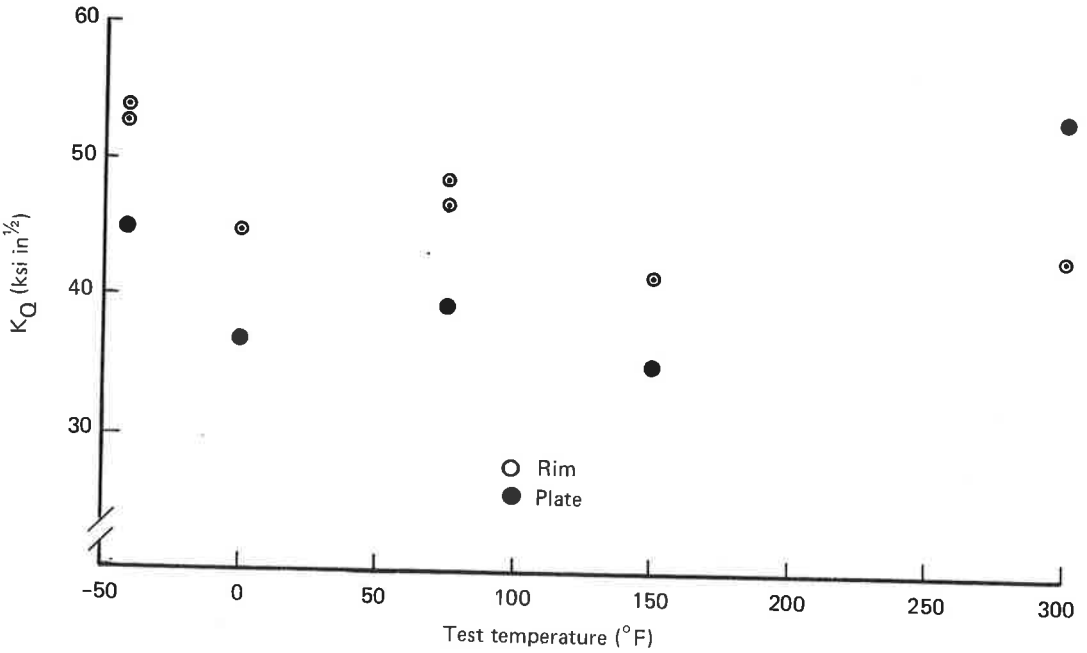

FIGURE 13.–EFFECT OF TEMPERATURE ON FRACTURE TOUGHNESS OF CLASS SUB A WHEEL

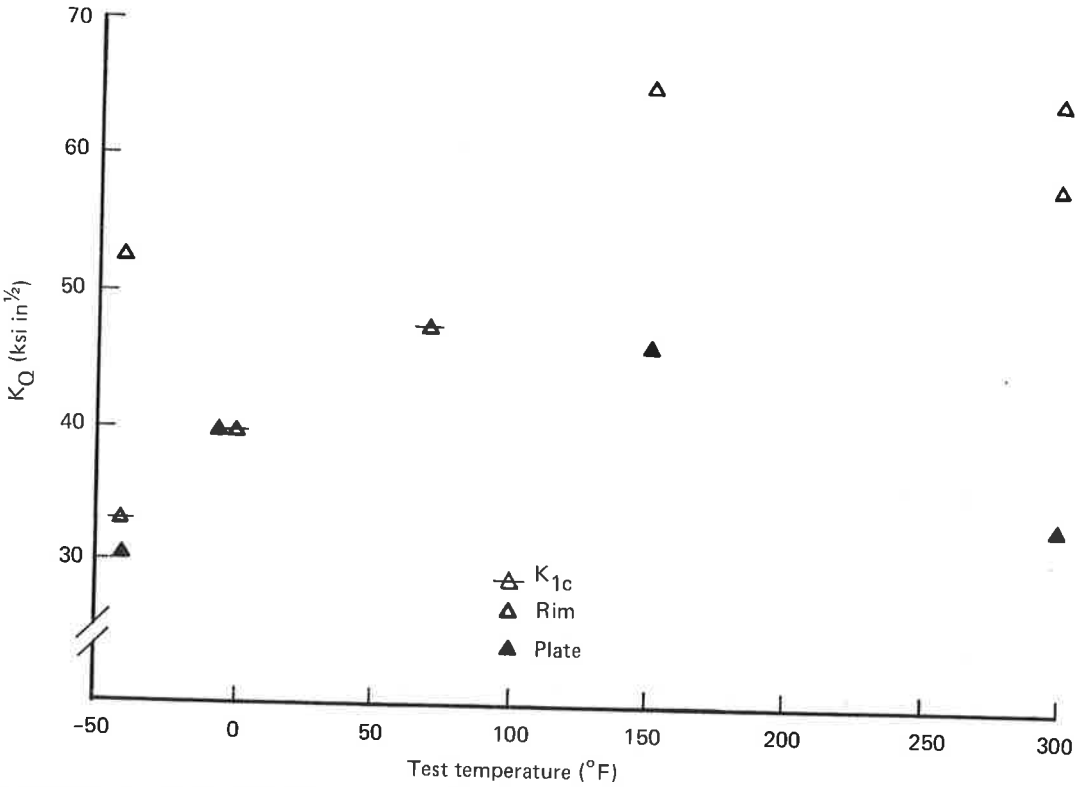

FIGURE 14.–EFFECT OF TEMPERATURE ON FRACTURE TOUGHNESS OF CLASS B WHEEL

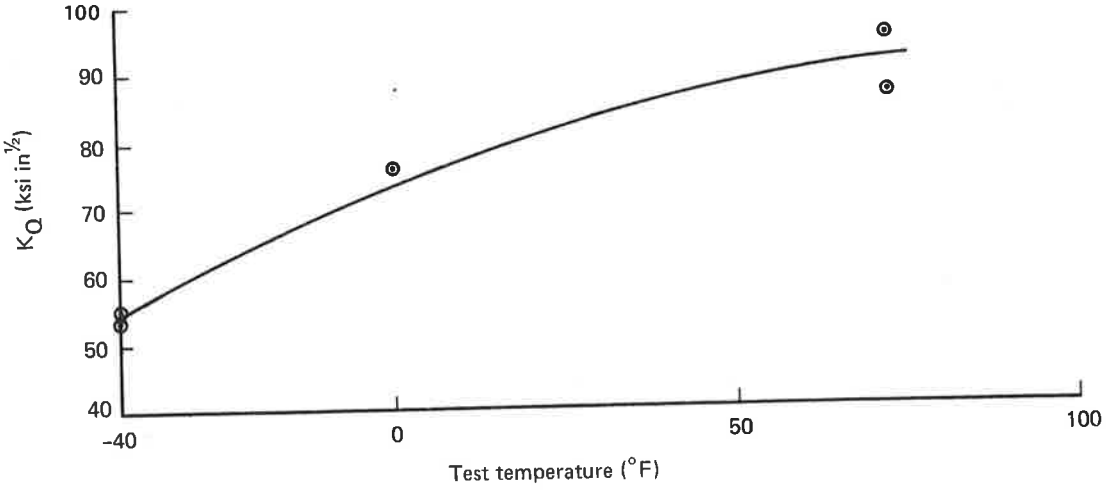

FIGURE 15.—EFFECT OF TEMPERATURE ON TOUGHNESS OF GRADE U AXLE

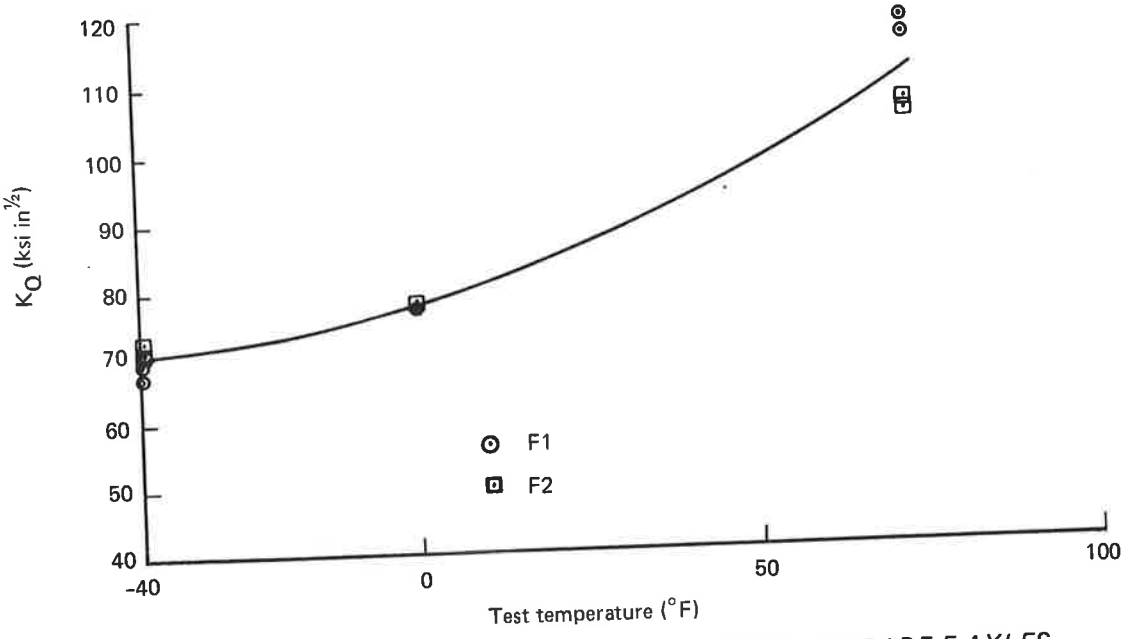

FIGURE 16.—EFFECT OF TEMPERATURE ON TOUGHNESS OF GRADE F AXLES

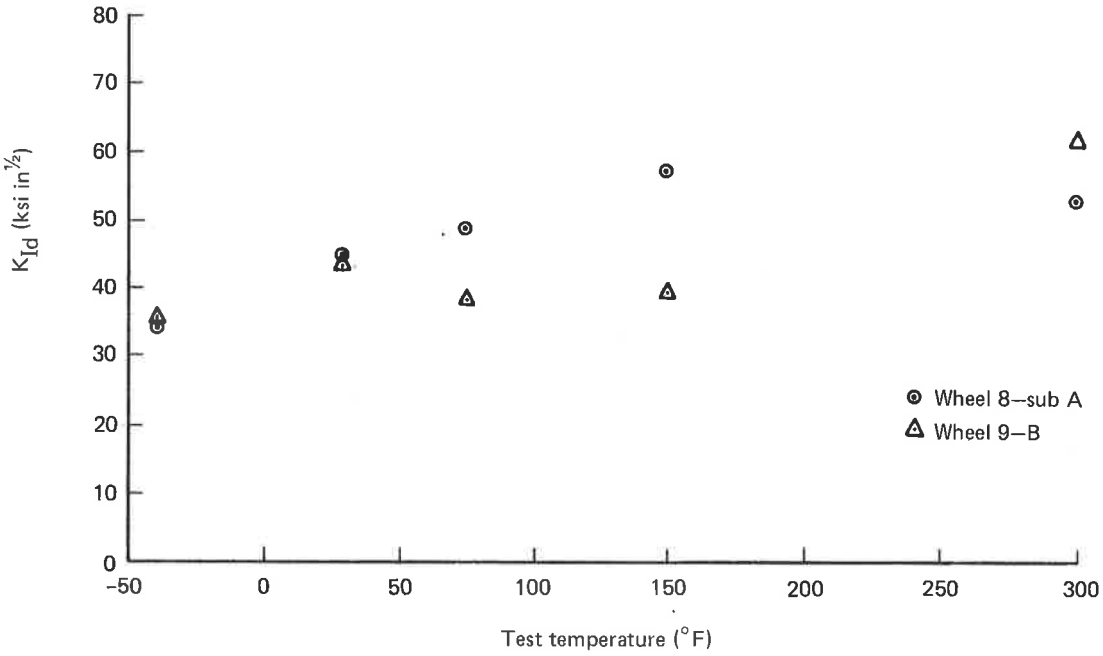

a) WHEELS

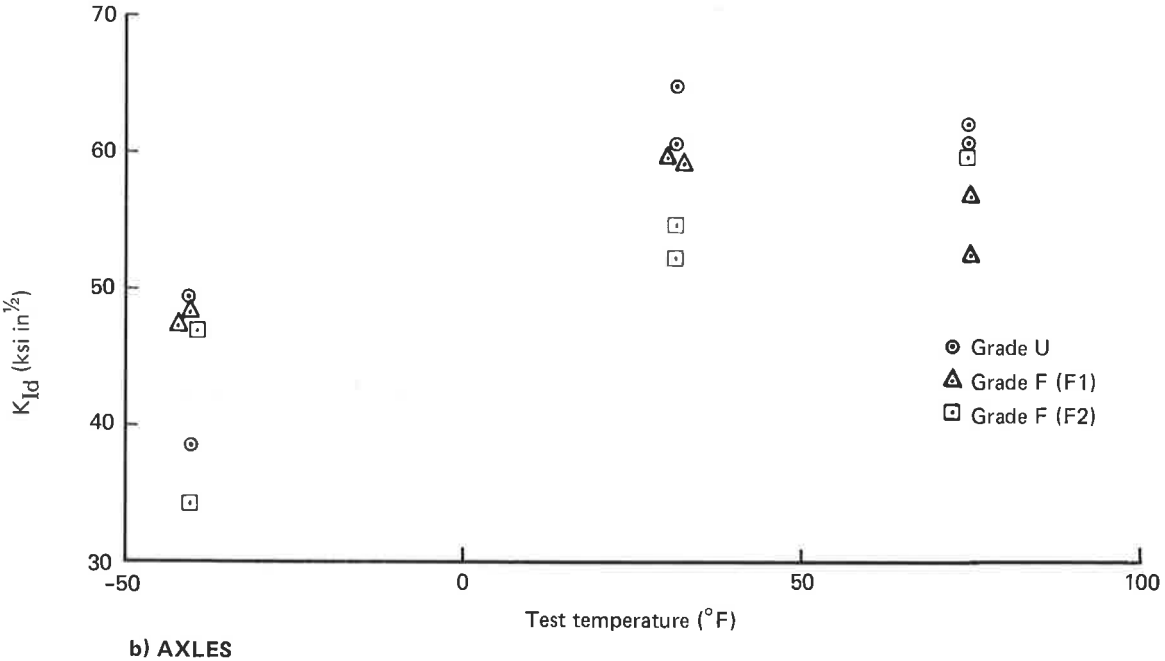

b) AXLES

FIGURE 17.–EFFECT OF TEST TEMPERATURE ON DYNAMIC FRACTURE TOUGHNESS

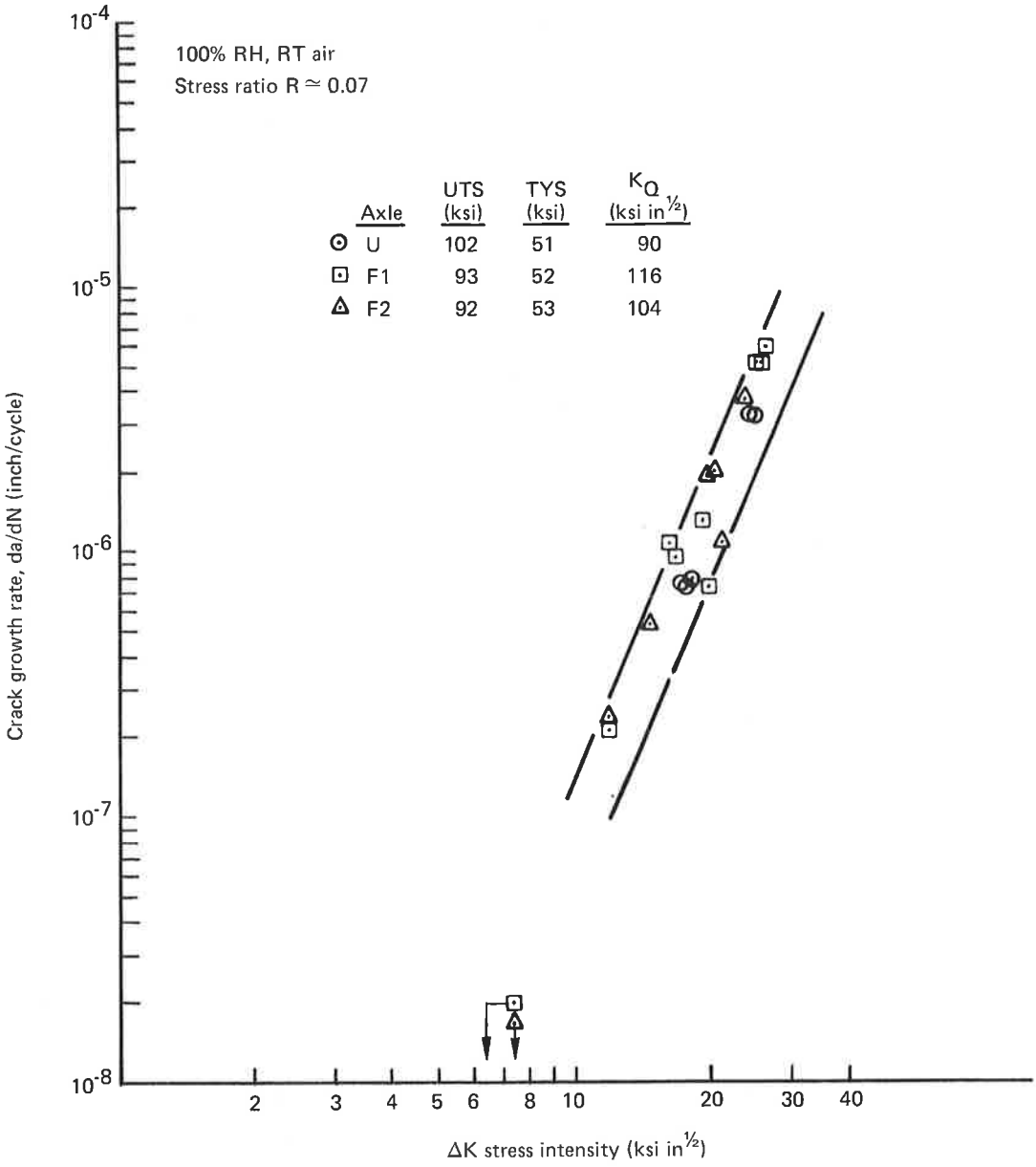

FIGURE 18.–FATIGUE CRACK GROWTH RATES OF AXLE MATERIALS

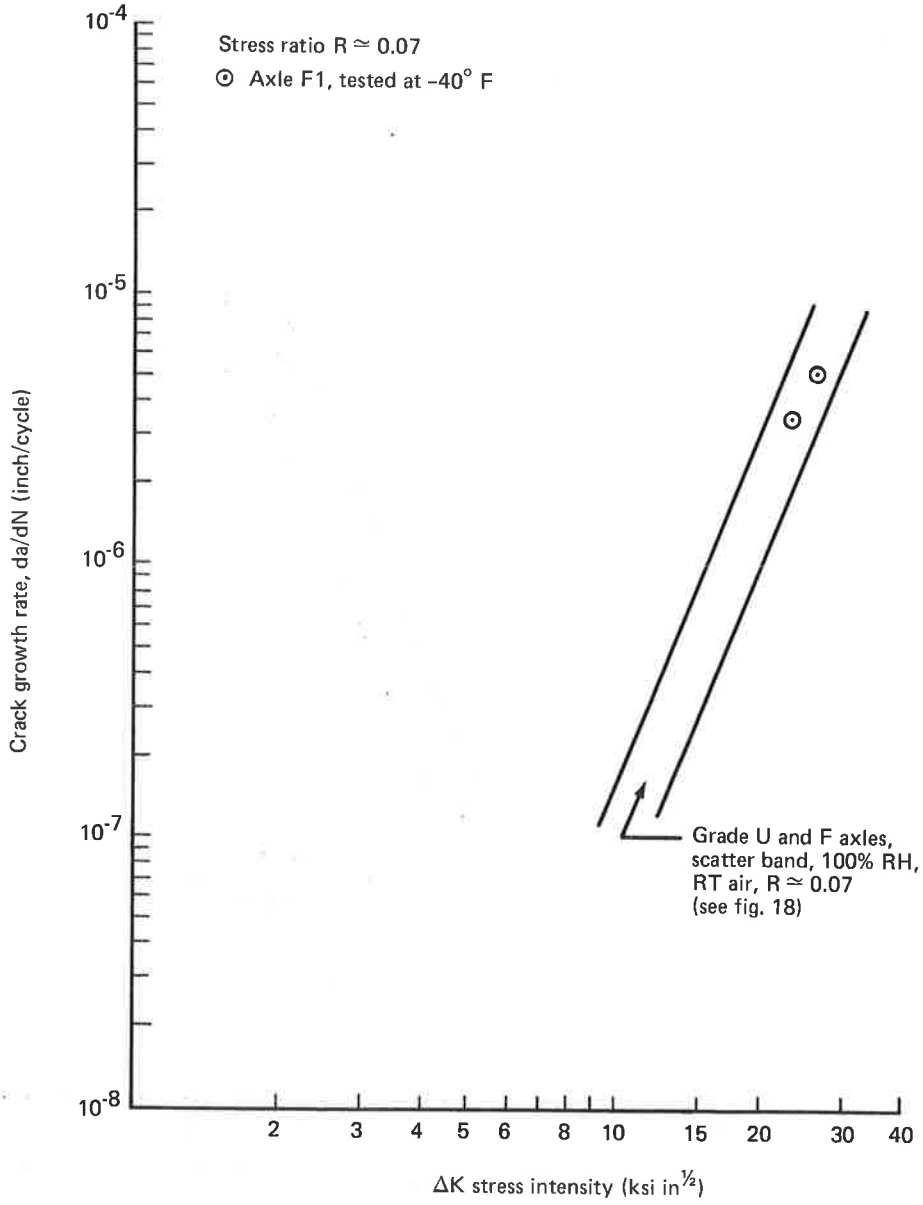

FIGURE 19.–GRADE U AND F AXLES, EFFECT OF -40° F TEMPERATURE ON CRACK GROWTH RATES

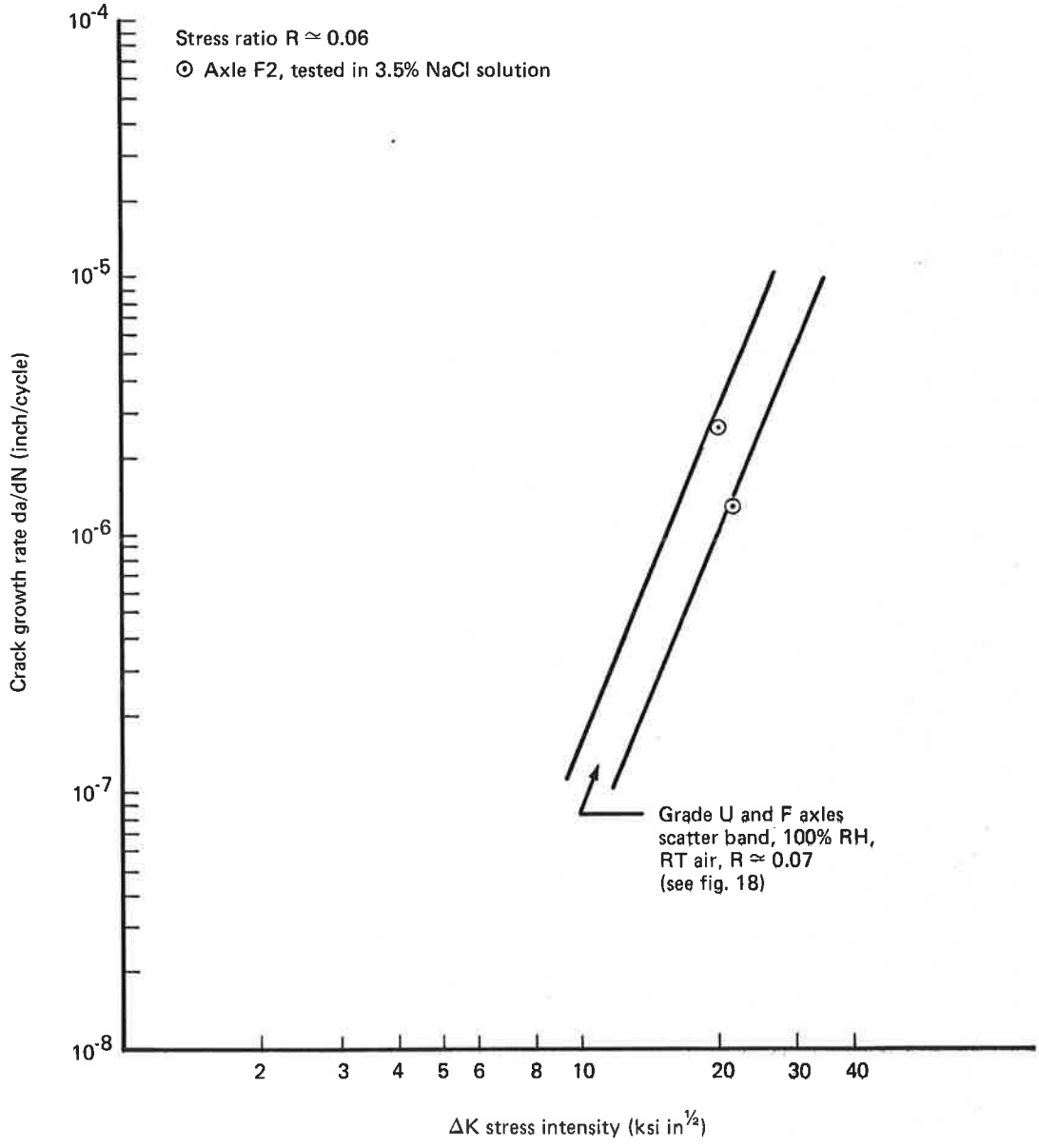

FIGURE 20.—GRADE F AXLE, EFFECT OF 3.5% NaCl AQUEOUS SOLUTION ON CRACK GROWTH RATES

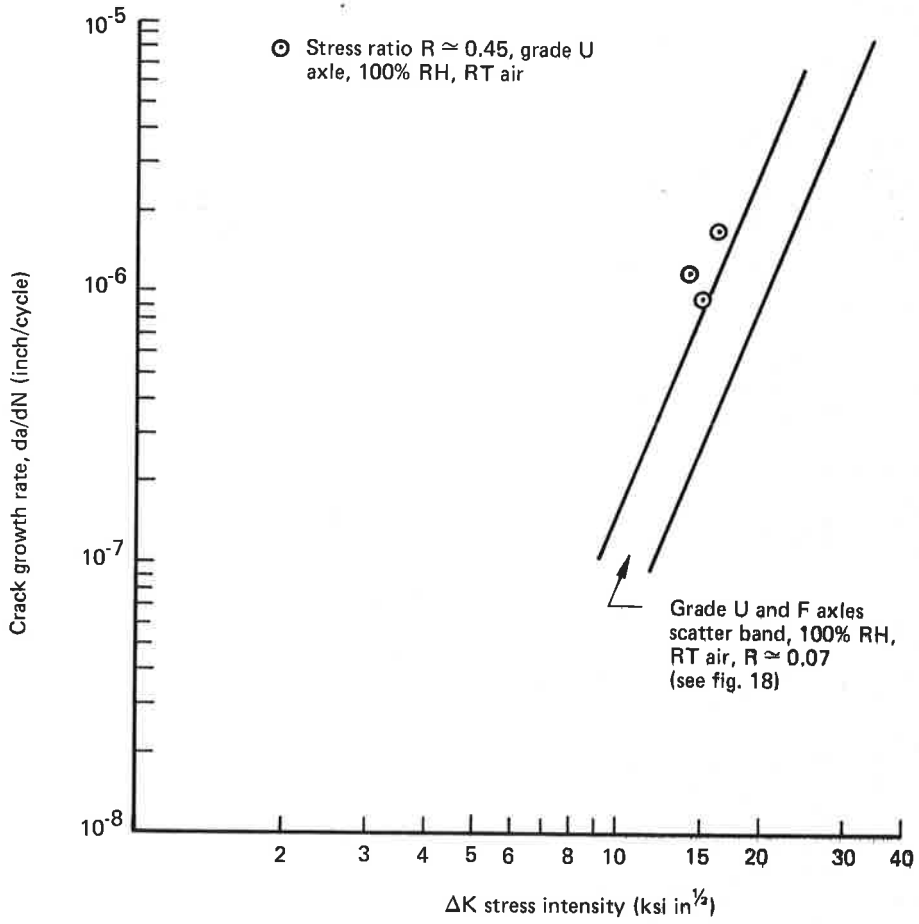

FIGURE 21.—GRADE U AXLE, EFFECT OF STRESS RATIO ON CRACK GROWTH RATES

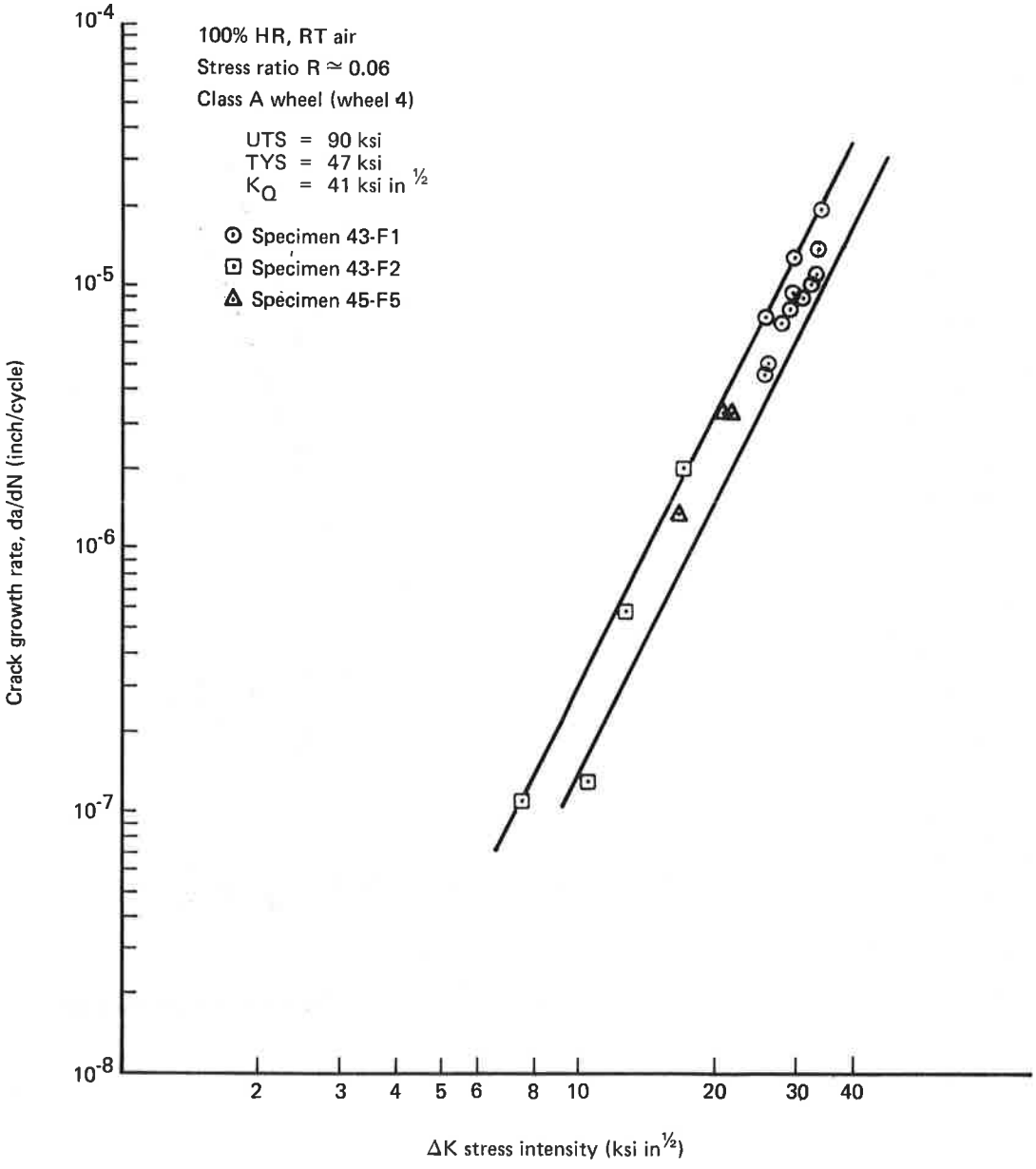

FIGURE 22.—CLASS A WHEEL FATIGUE CRACK GROWTH DATA

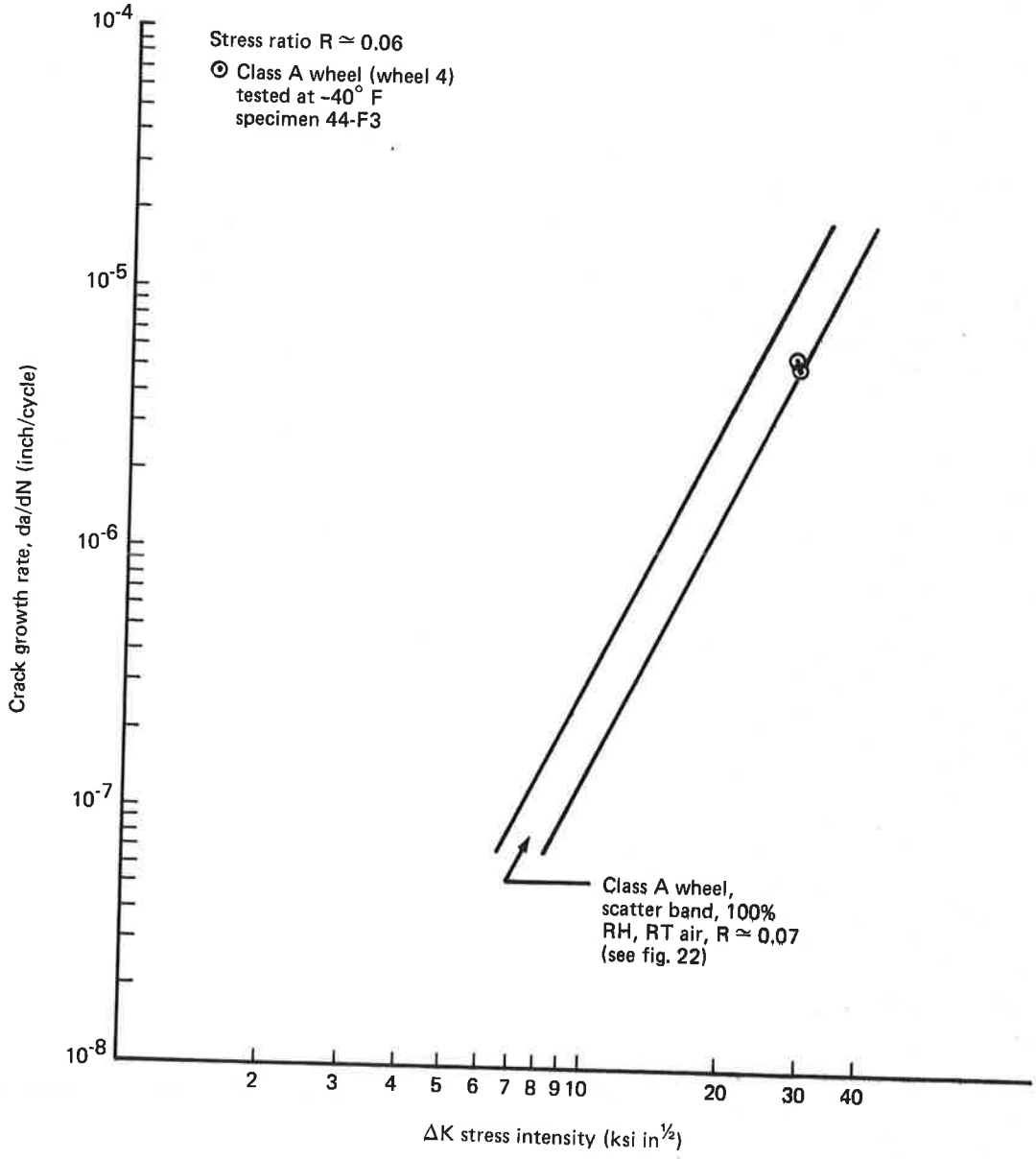

FIGURE 23.—CLASS A WHEEL, EFFECT OF -40° F TEMPERATURE ON FATIGUE CRACK GROWTH RATE

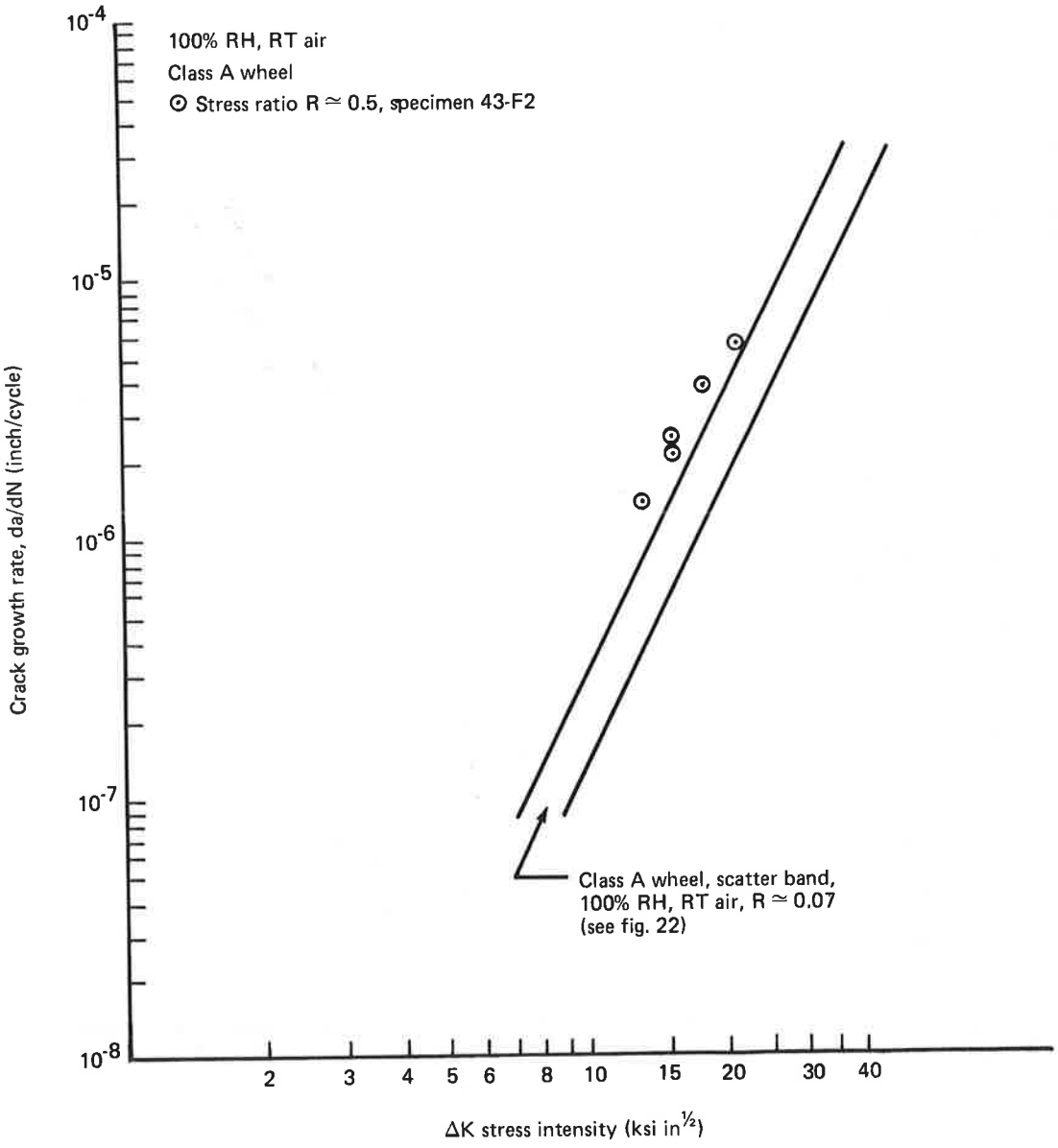

FIGURE 24.—CLASS A WHEEL, EFFECT OF R ≃ 0.5 ON CRACK GROWTH RATE

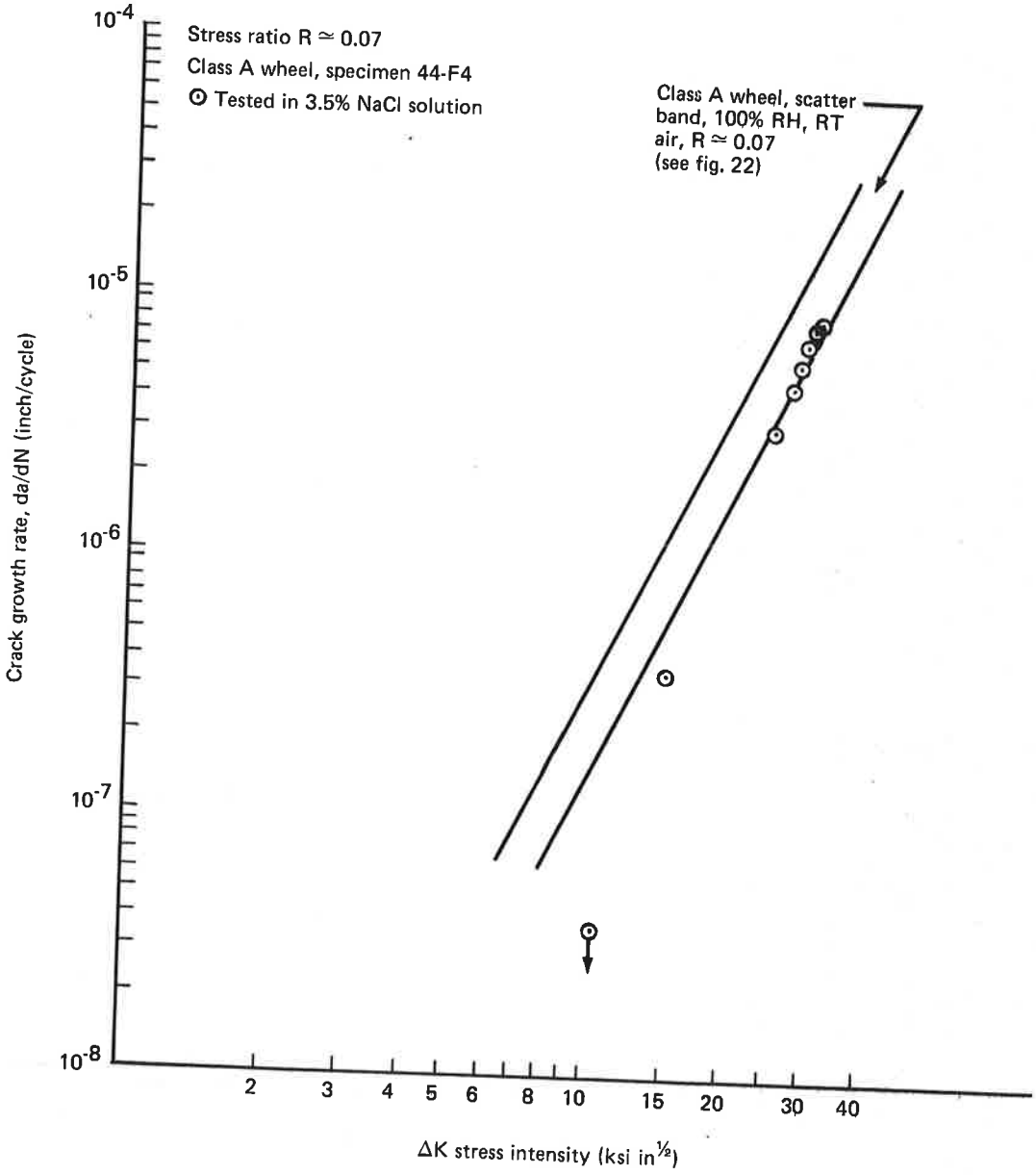

FIGURE 25.—CLASS A WHEEL, EFFECT OF 3.5% NaCl AQUEOUS SOLUTION ON CRACK GROWTH RATE

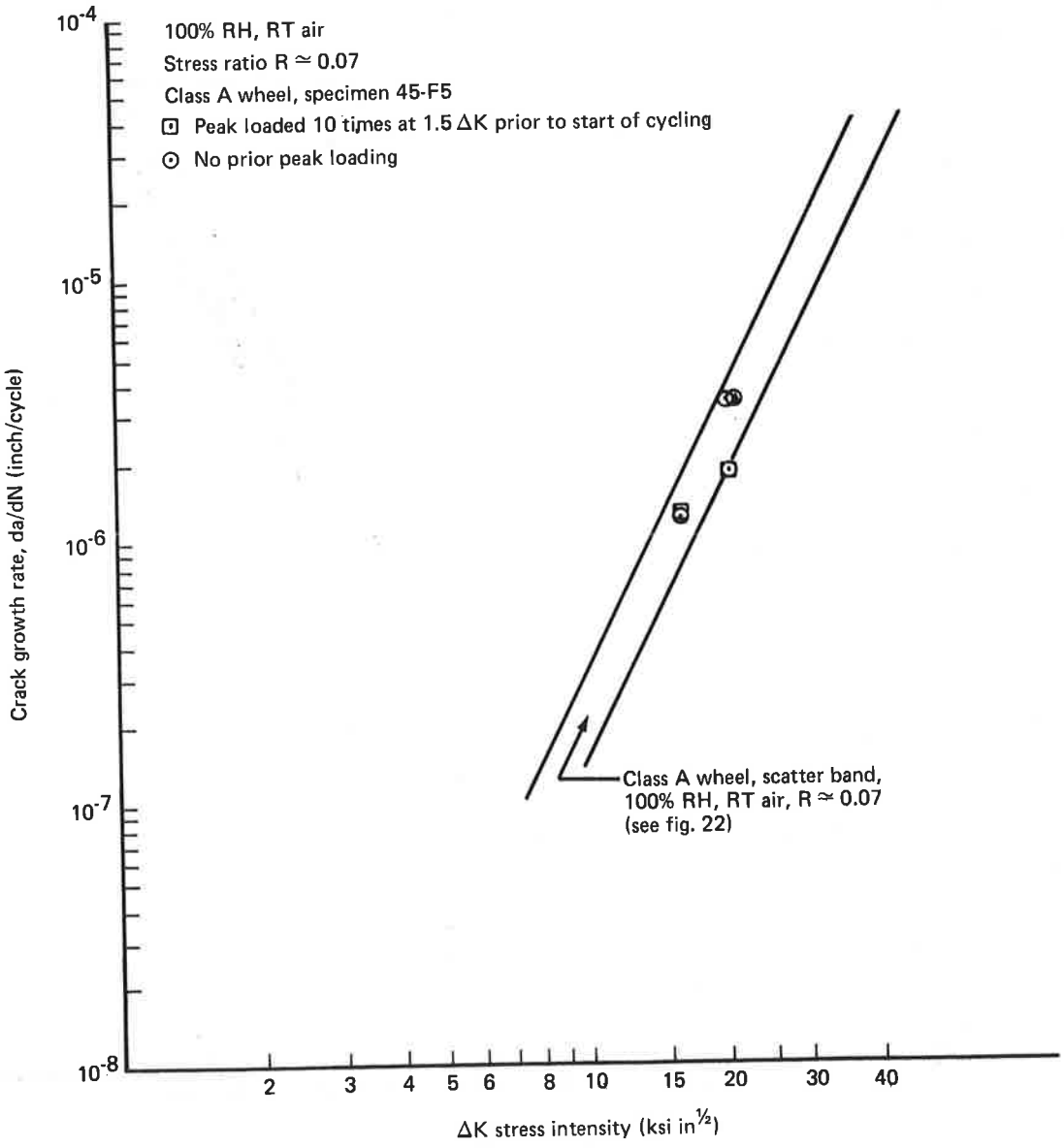

FIGURE 26.—CLASS A WHEEL, EFFECT OF PEAK LOADING PRIOR TO START OF CYCLING

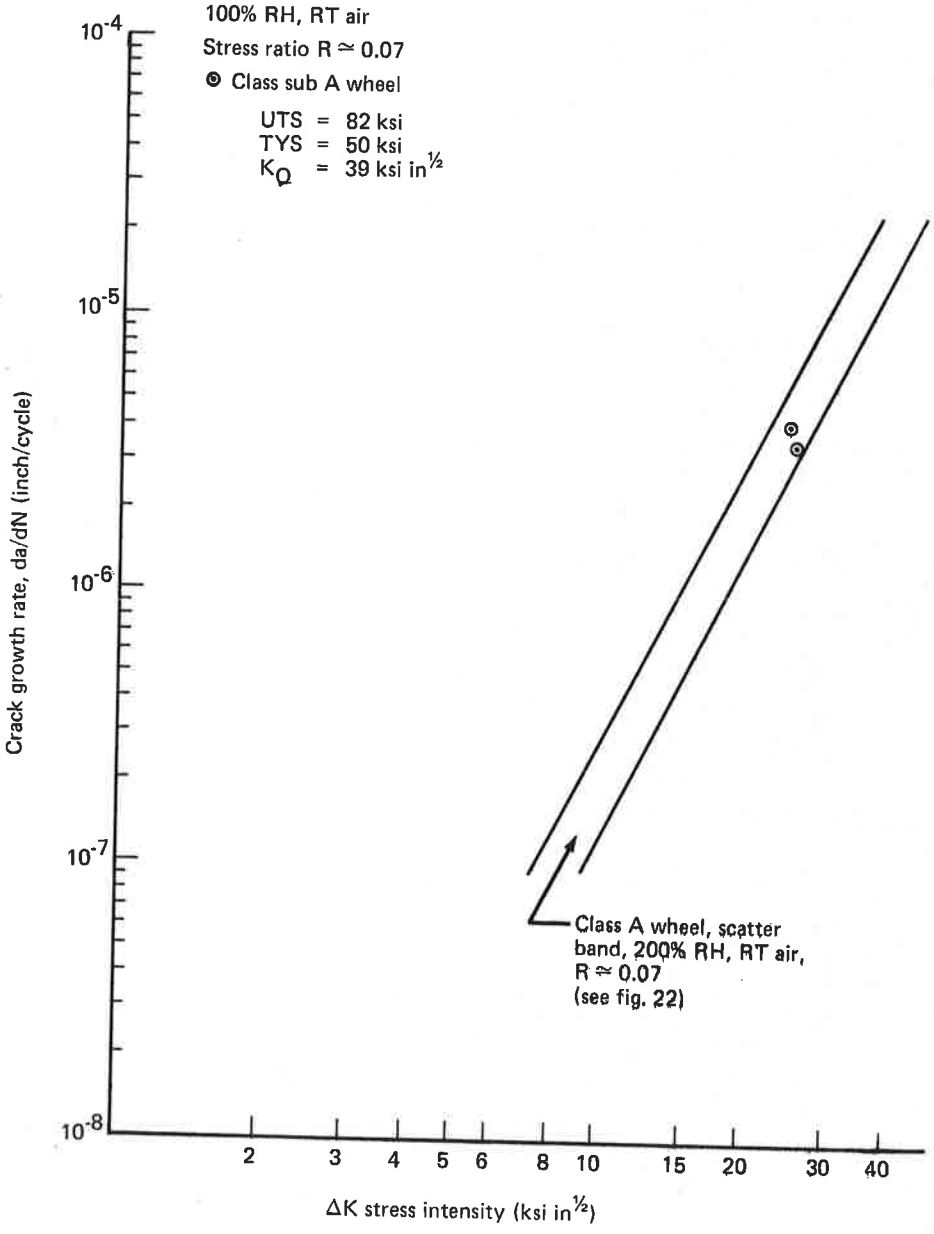

FIGURE 27.–COMPARISON OF CLASS A WHEEL AND CLASS SUB A WHEEL CRACK GROWTH RATES

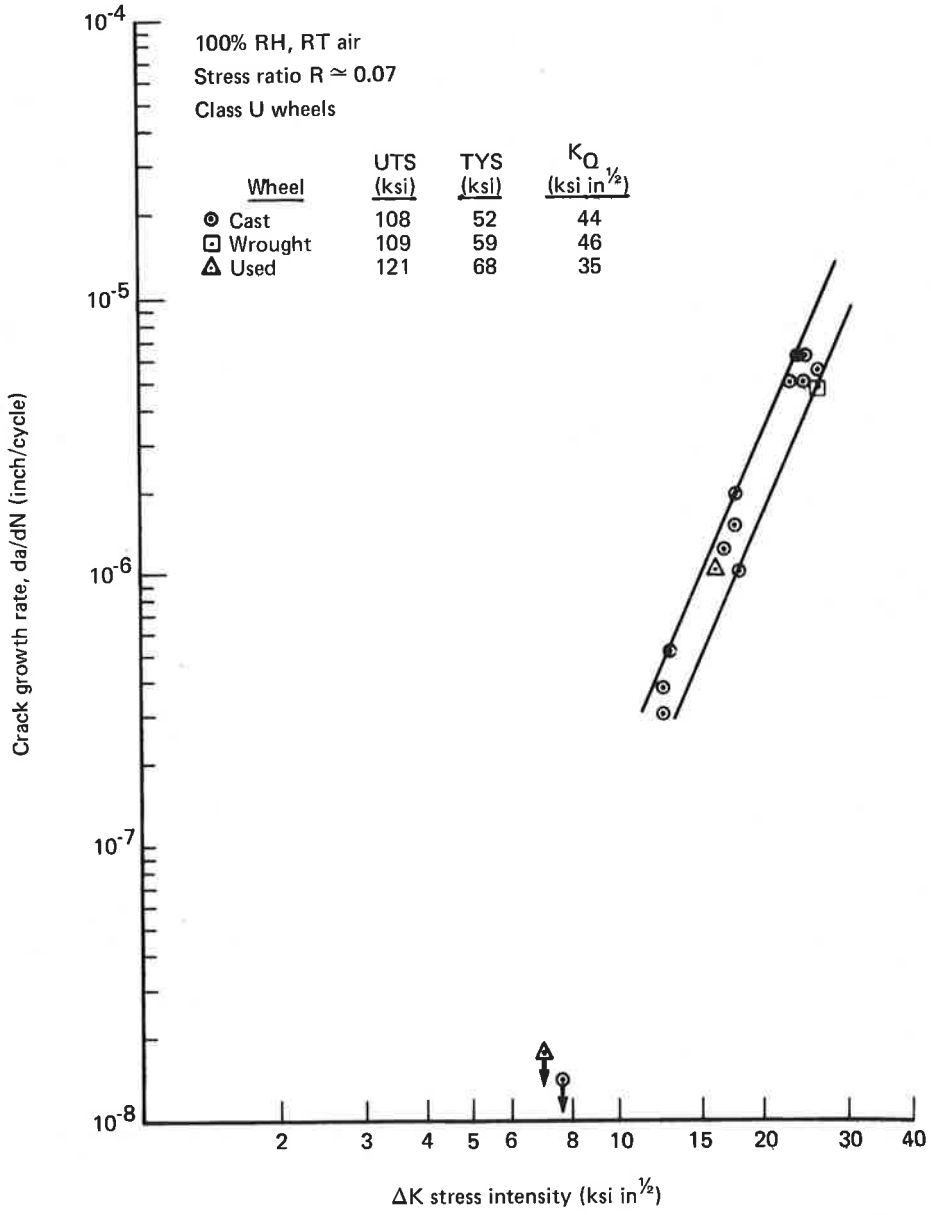

FIGURE 28.—FATIGUE CRACK GROWTH RATES OF CLASS U WHEELS

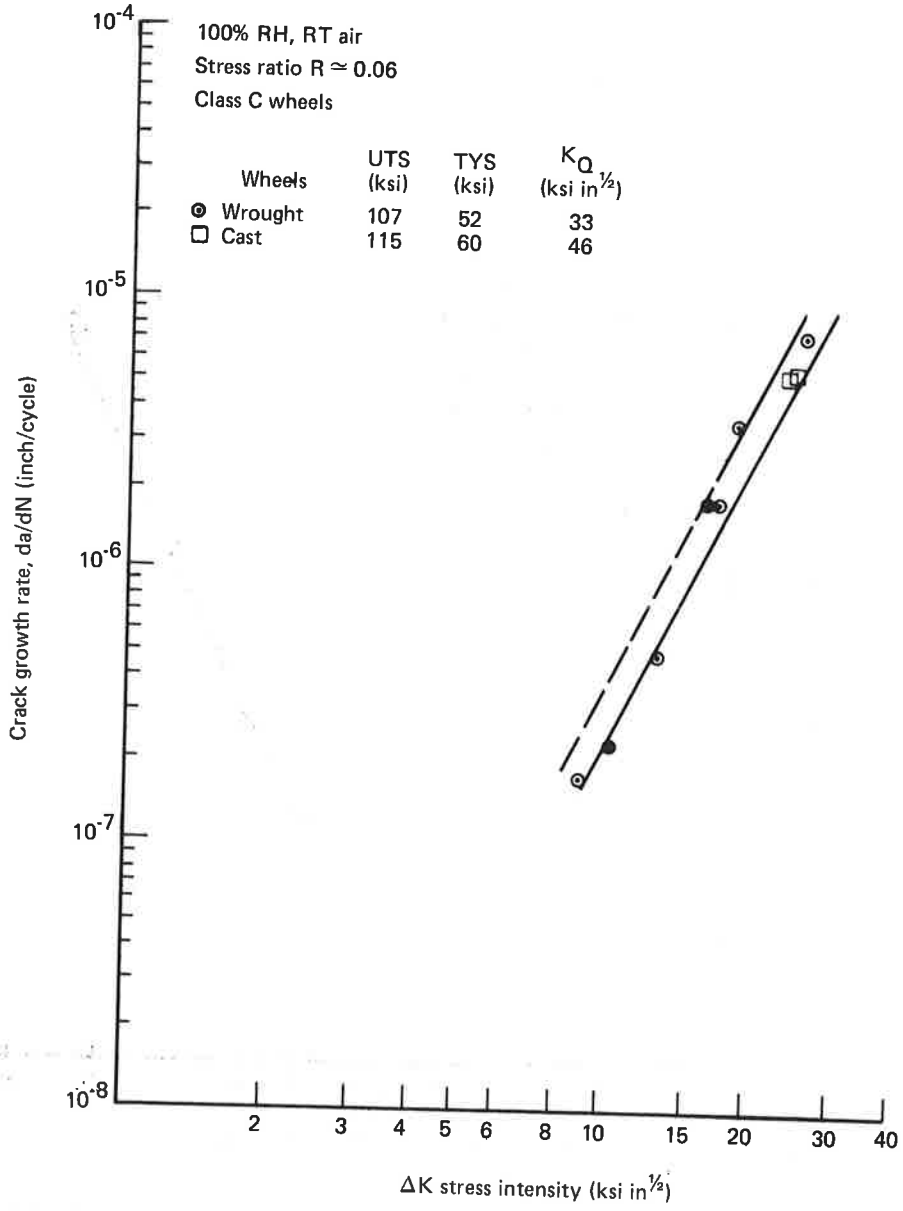

FIGURE 29.–FATIGUE CRACK GROWTH RATES OF CLASS C WHEELS

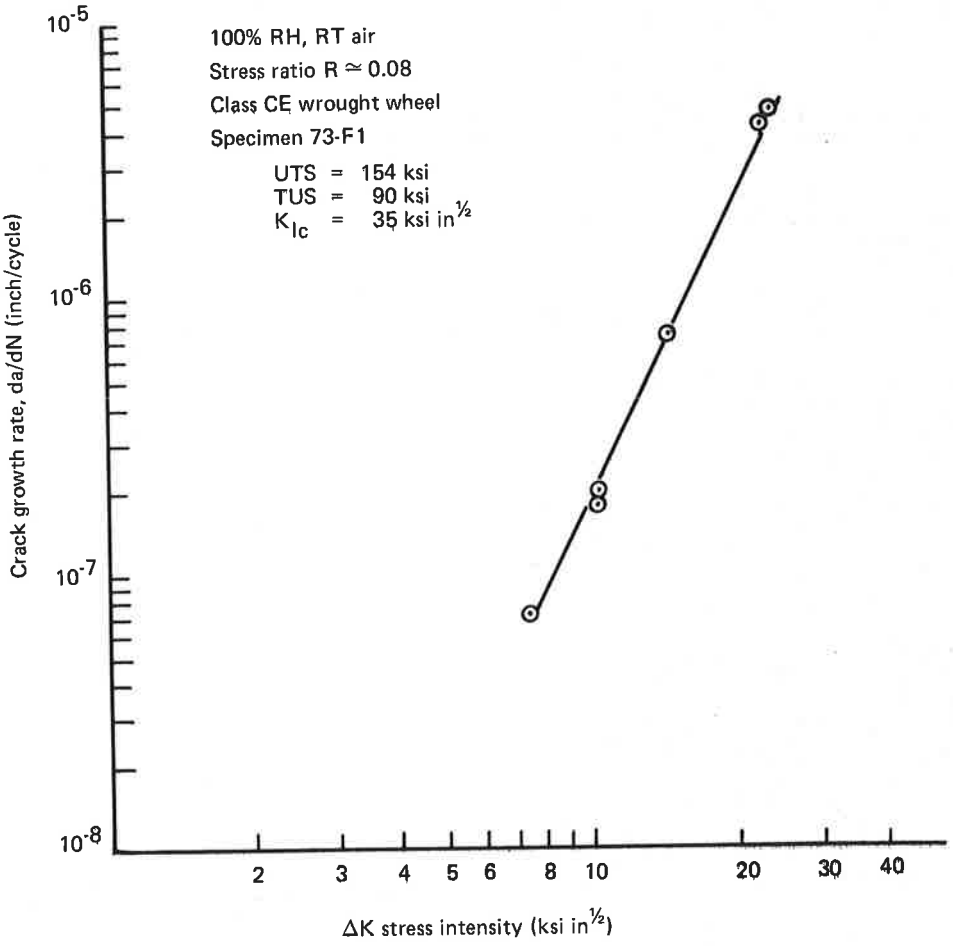

FIGURE 30.—CLASS CE WROUGHT WHEEL FATIGUE CRACK GROWTH DATA

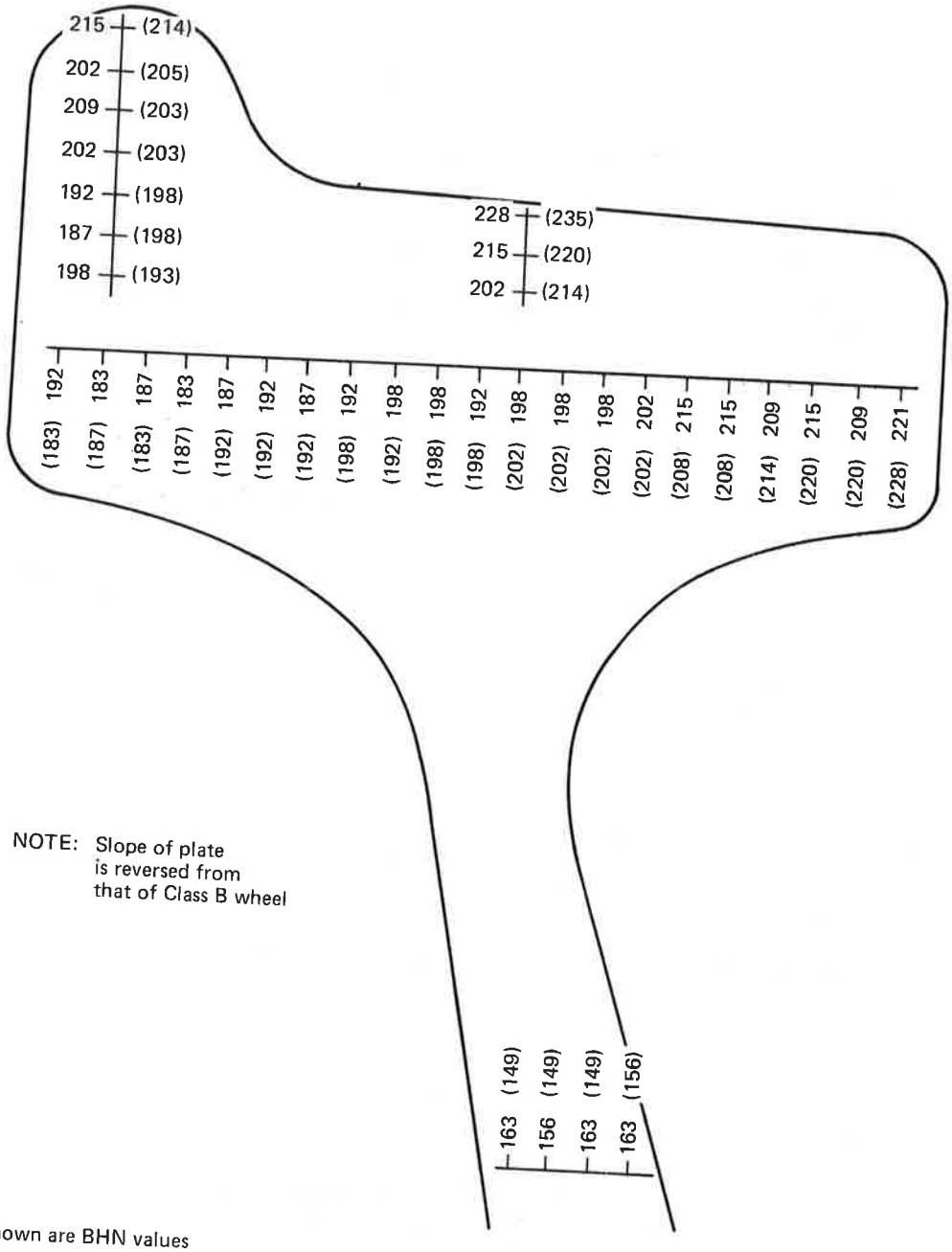

Numbers shown are BHN values

Numbers in parenthesis are for the GF5 location (fig. 2)

FIGURE 31.–HARDNESS TRAVERSE FOR CLASS SUB A WHEEL

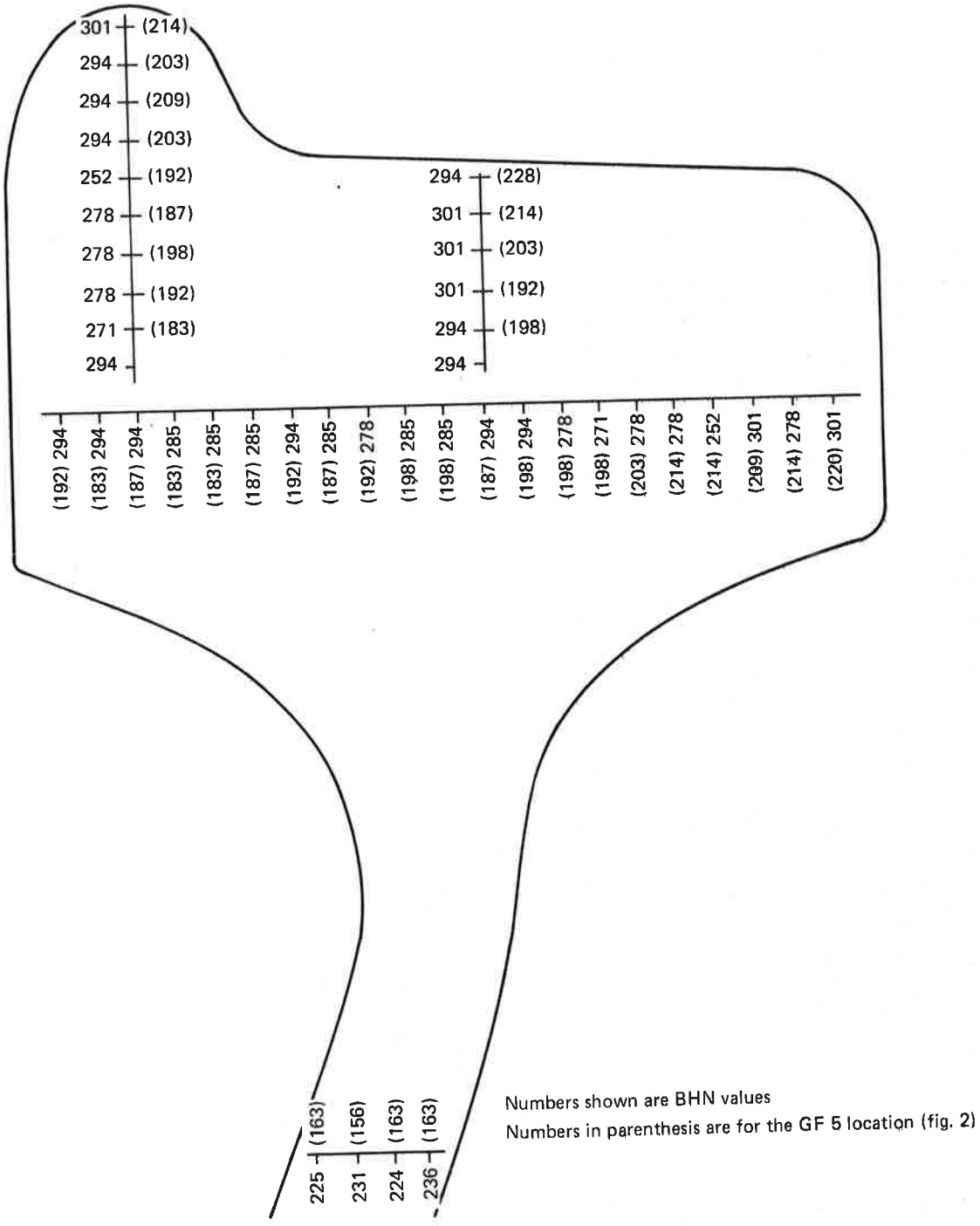

FIGURE 32.–HARDNESS TRAVERSE FOR CLASS B WHEEL

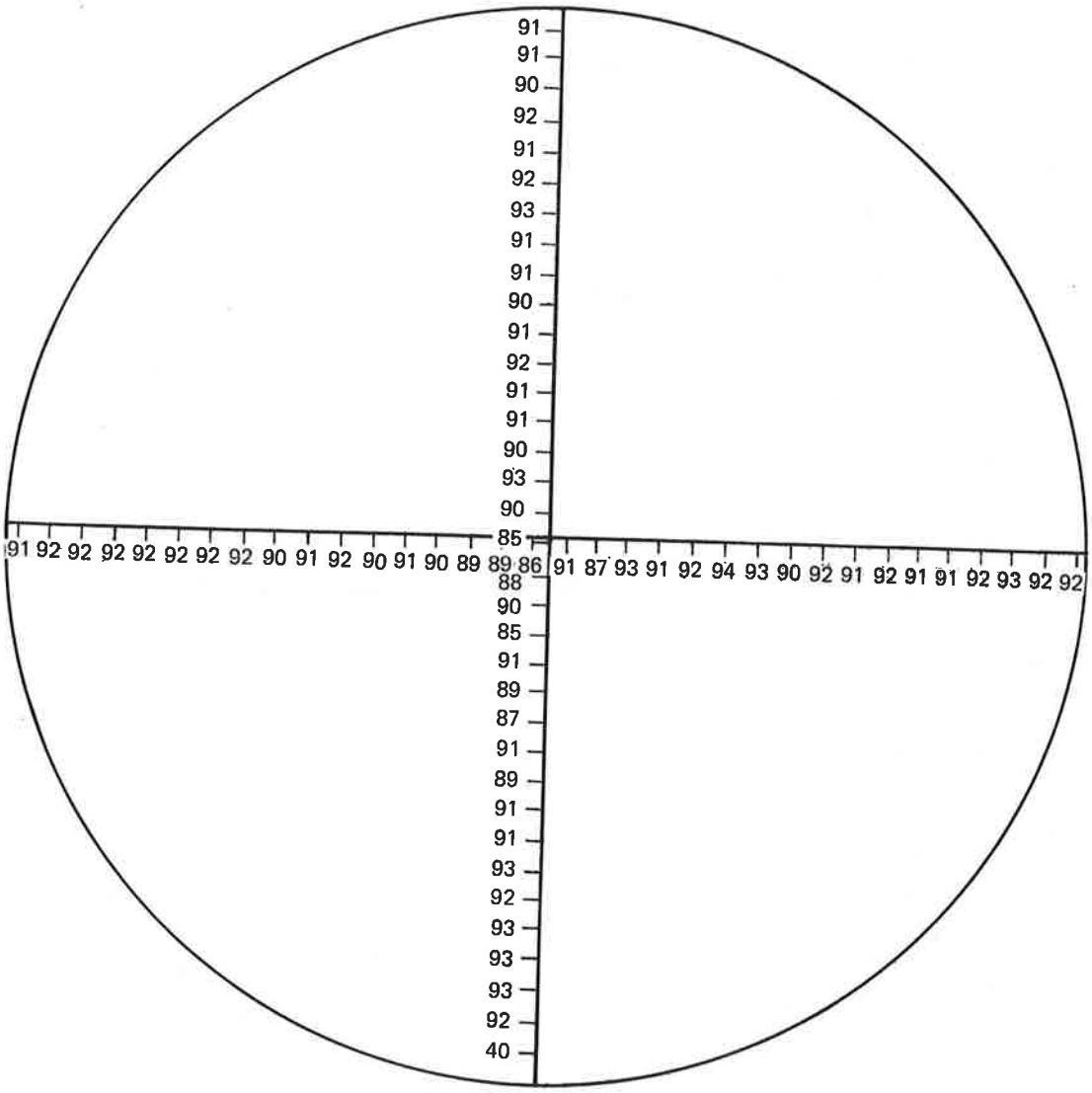

Note: Hardness measurements spaced approximately 0.25-in. across 8.8 in. diameter section.

FIGURE 33.—GRADE U (NONHEAT TREATED) AXLE ROCKWELL B HARDNESS TRANSVERSE

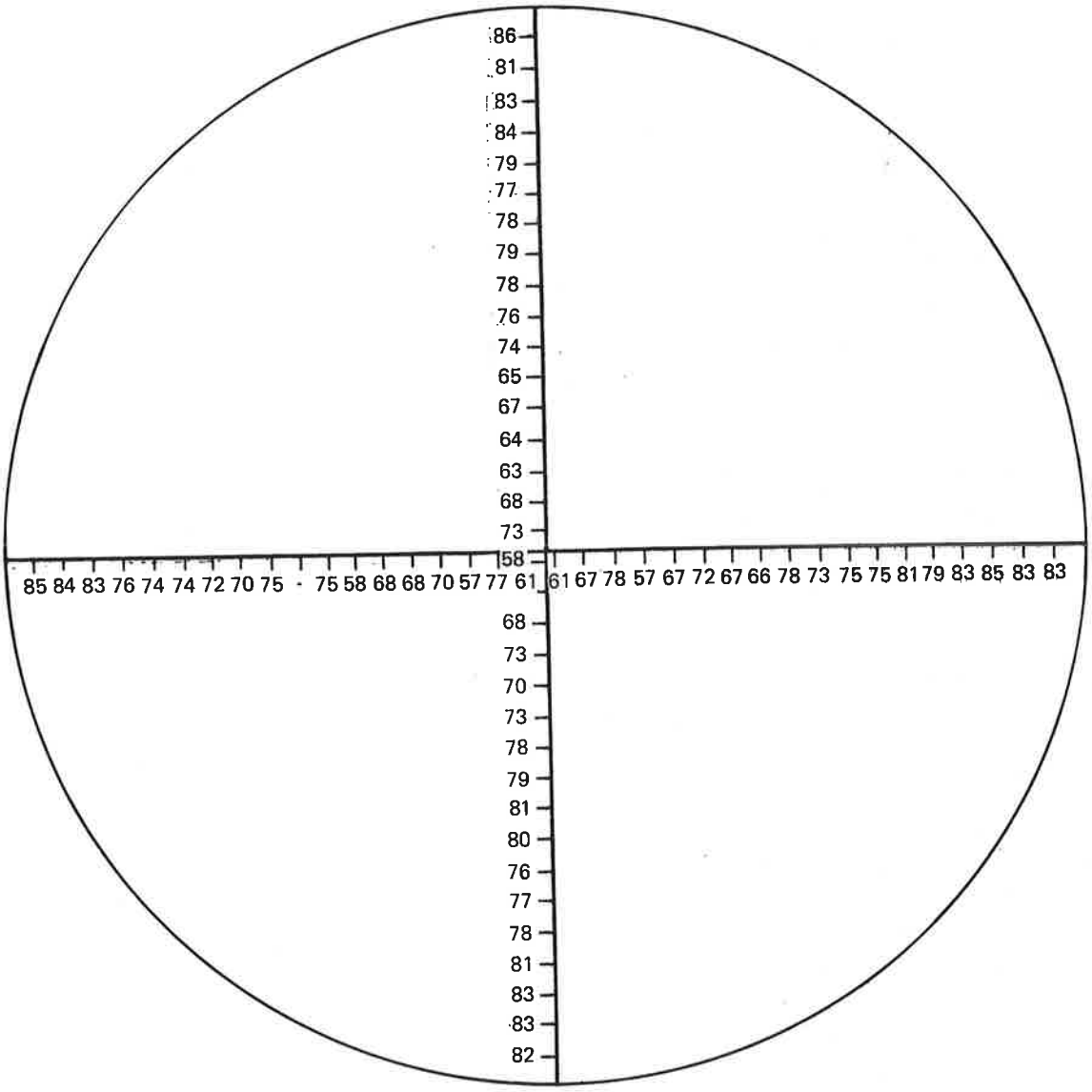

Note: Hardness measurements spaced approximately 0.25-in. across 9.0-in. diameter section.

FIGURE 34.—GRADE F (DOUBLE NORMALIZED AND TEMPERED) F1 AXLE ROCKWELL B HARDNESS TRANSVERSE

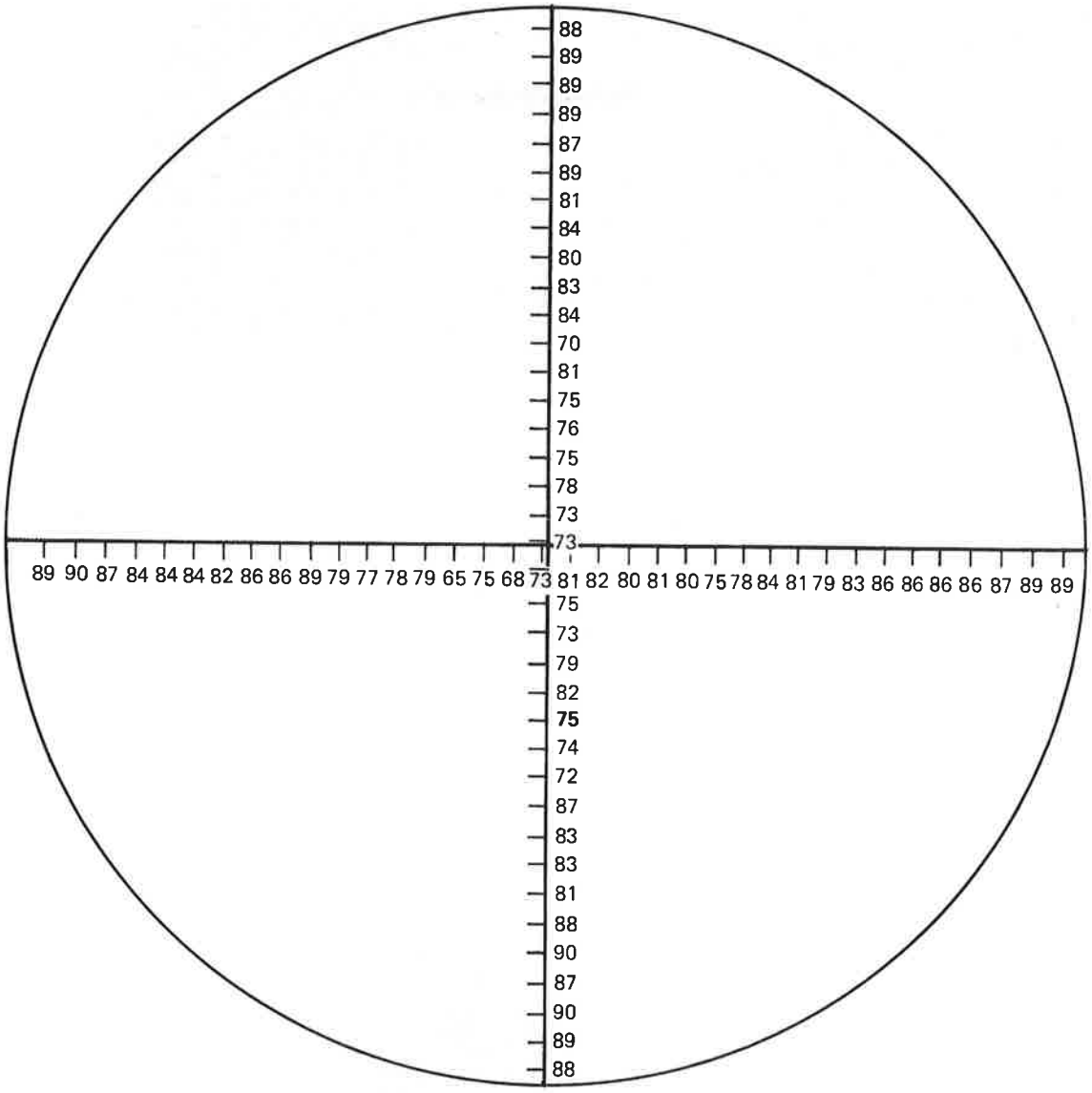

Note: Hardness measurements spaced approximately 0.25-in across 9.2-in. diameter section.

FIGURE 35.—GRADE F (DOUBLE NORMALIZED AND TEMPERED) F2 AXLE ROCKWELL B HARDNESS TRANSVERSE

Approximately actual size

FIGURE 36.—MACROSECTION OF CLASS SUB A WHEEL (WHEEL 8), GRAIN FLOW SECTION GF2 (METROLINER TYPE WHEEL

FIGURE 37.—MACROSECTION OF CLASS B WHEEL (WHEEL 9), GRAIN FLOW SECTION GF5

Approximately 0.7X

FIGURE 38.–MACROSECTION OF GRADE F AXLE (F1)

Approximately 0.7X

FIGURE 39.—MACROSECTION OF GRADE F AXLE (F2)

Approximately 0.7X

FIGURE 40.—MACROSECTION OF GRADE U AXLES (U)

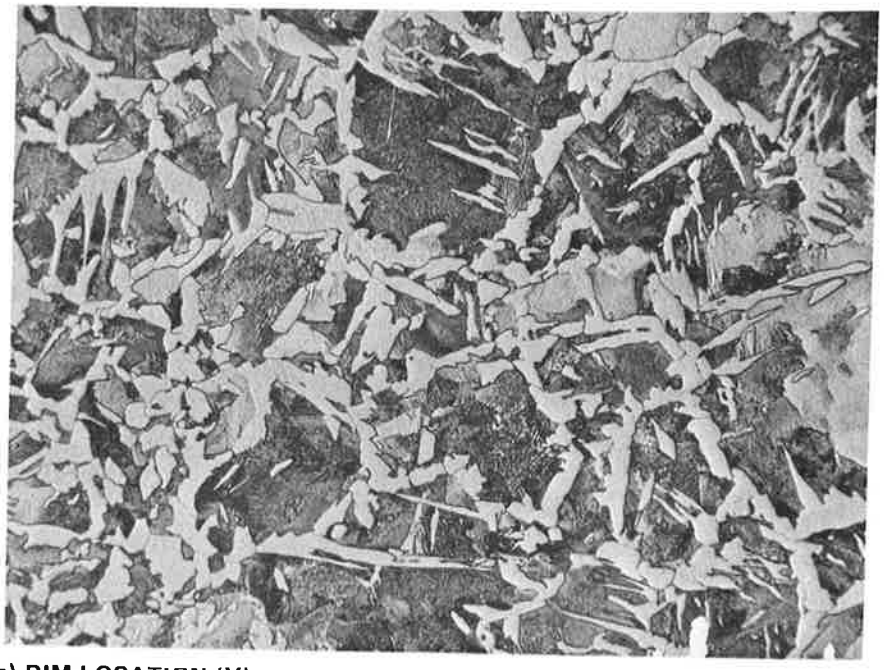

a) RIM LOCATION (Y) 360X—etch 2% Nital

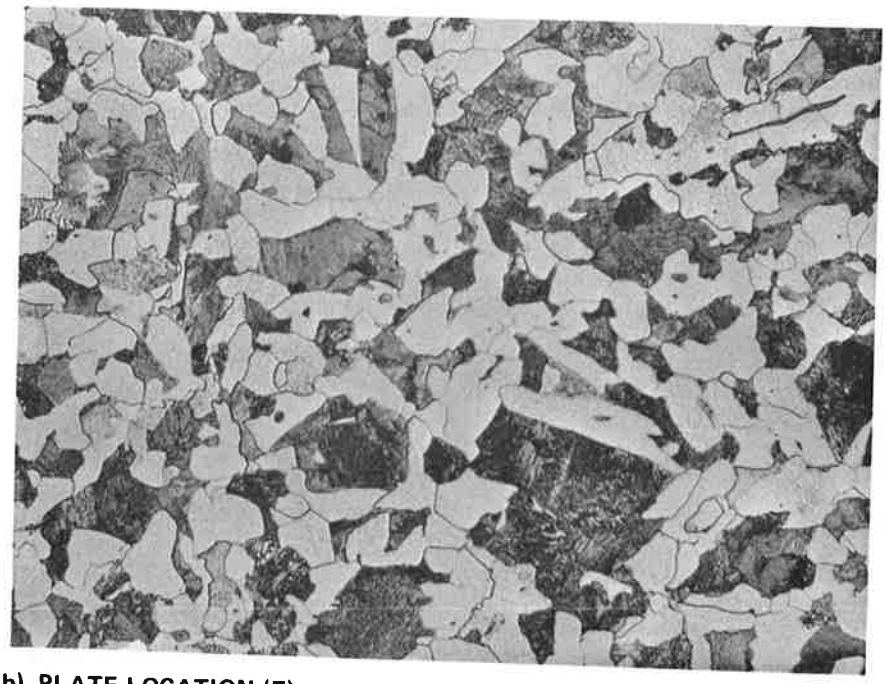

b) PLATE LOCATION (Z) 360X—etch 2% Nital

FIGURE 41.—PHOTOMICROGRAPH OF CLASS SUB A (WHEEL (WHEEL 8)

a) RIM LOCATION (Y) 360X—etch 2% Nital

b) PLATE LOCATION (Z) 360X—etch 2% Nital

FIGURE 42.—PHOTOMICROGRAPHS OF CLASS B WHEEL (WHEEL 9)

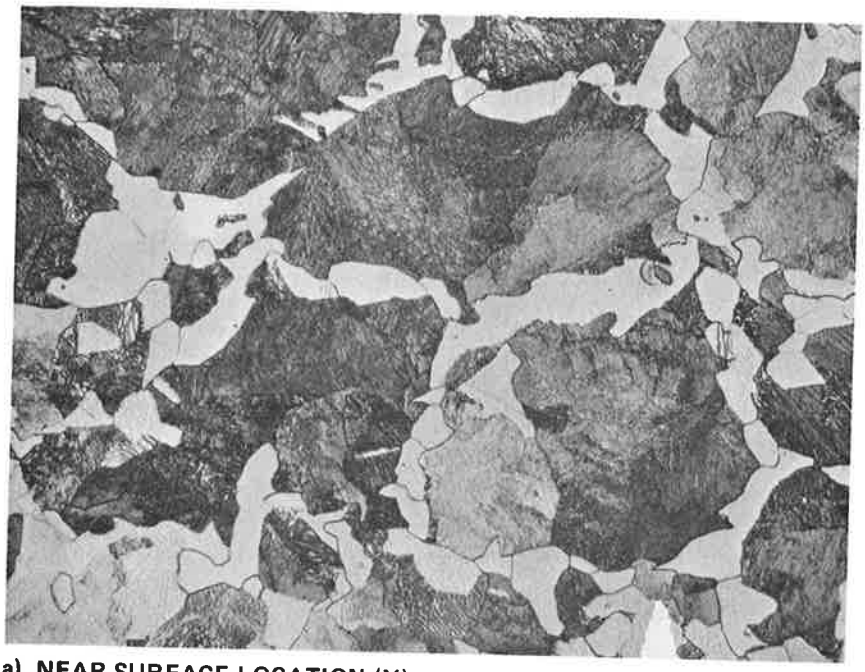

a) NEAR-SURFACE LOCATION (X) 360X—etch 2% Nital

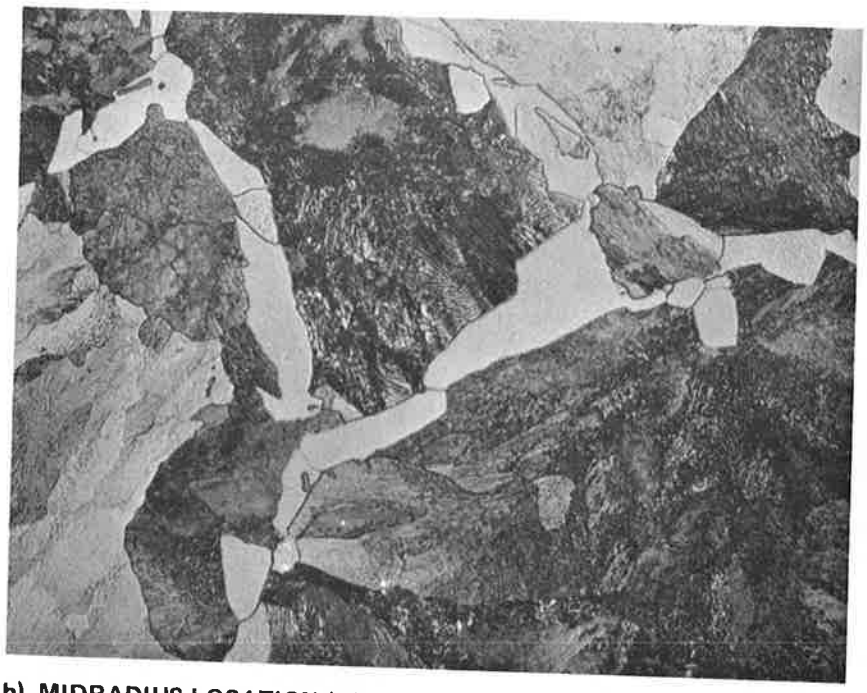

b) MIDRADIUS LOCATION (Y) 360X—etch 2% Nital

FIGURE 43.—PHOTOMICROGRAPHS OF GRADE U AXLE (U)

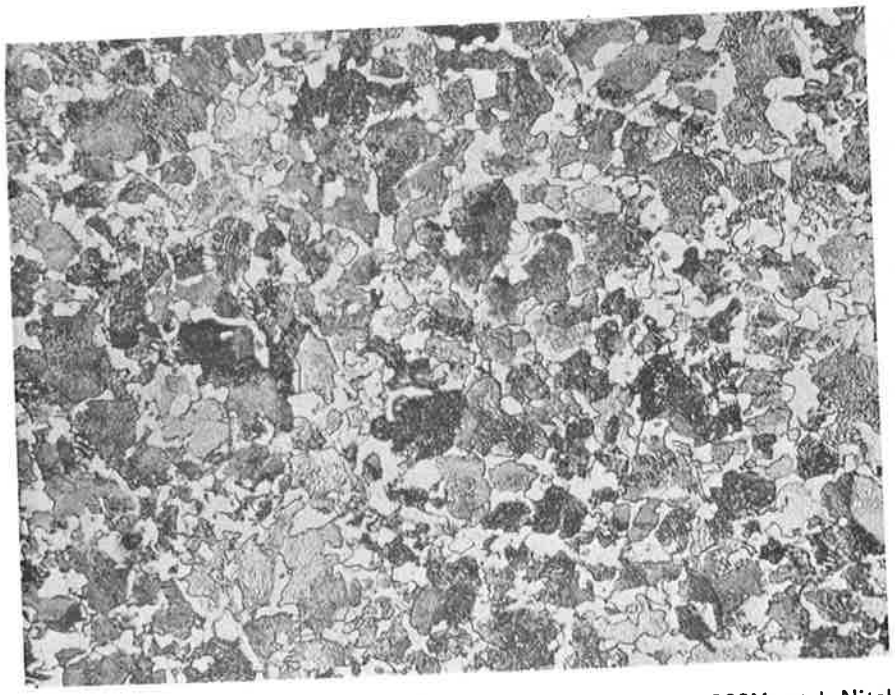

a) NEAR-SURFACE LOCATION (X) 360X—etch Nital

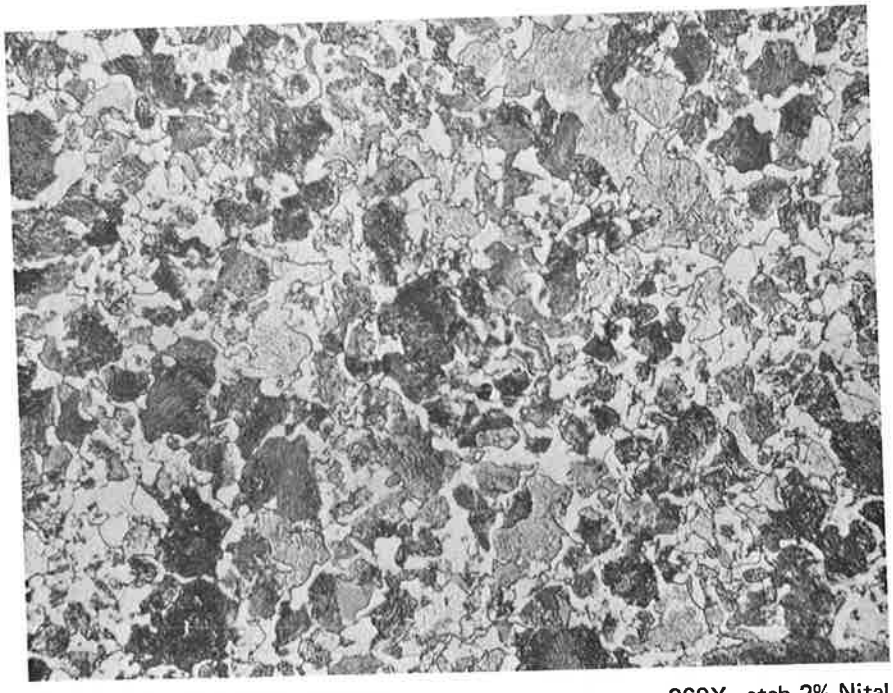

b) MIDRADIUS LOCATION (Y) 360X—etch 2% Nital

FIGURE 44.—PHOTOMICROGRAPHS OF GRADE F AXLE (F1)

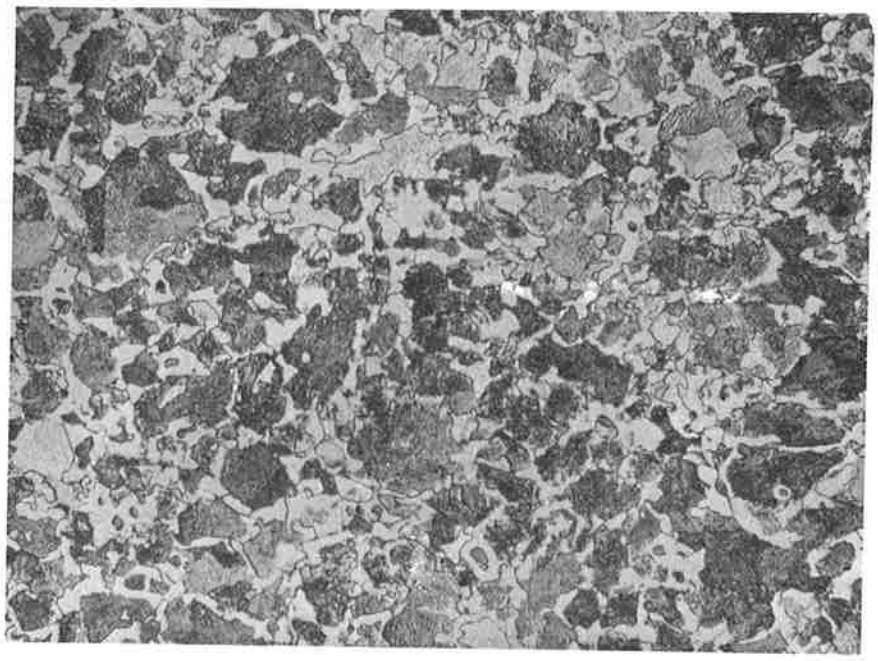

a) NEAR-SURFACE LOCATION (X) 360X—etch 2% Nital

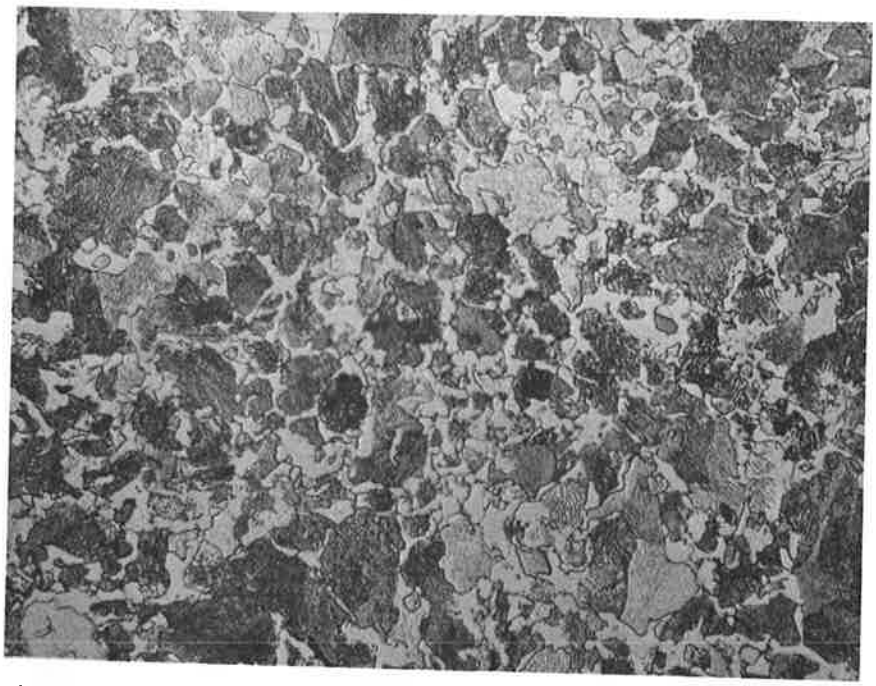

b) MIDRADIUS LOCATION (Y) 360X—etch 2% Nital

FIGURE 45.—PHOTOMICROGRAPHS OF GRADE F AXLE (F2)

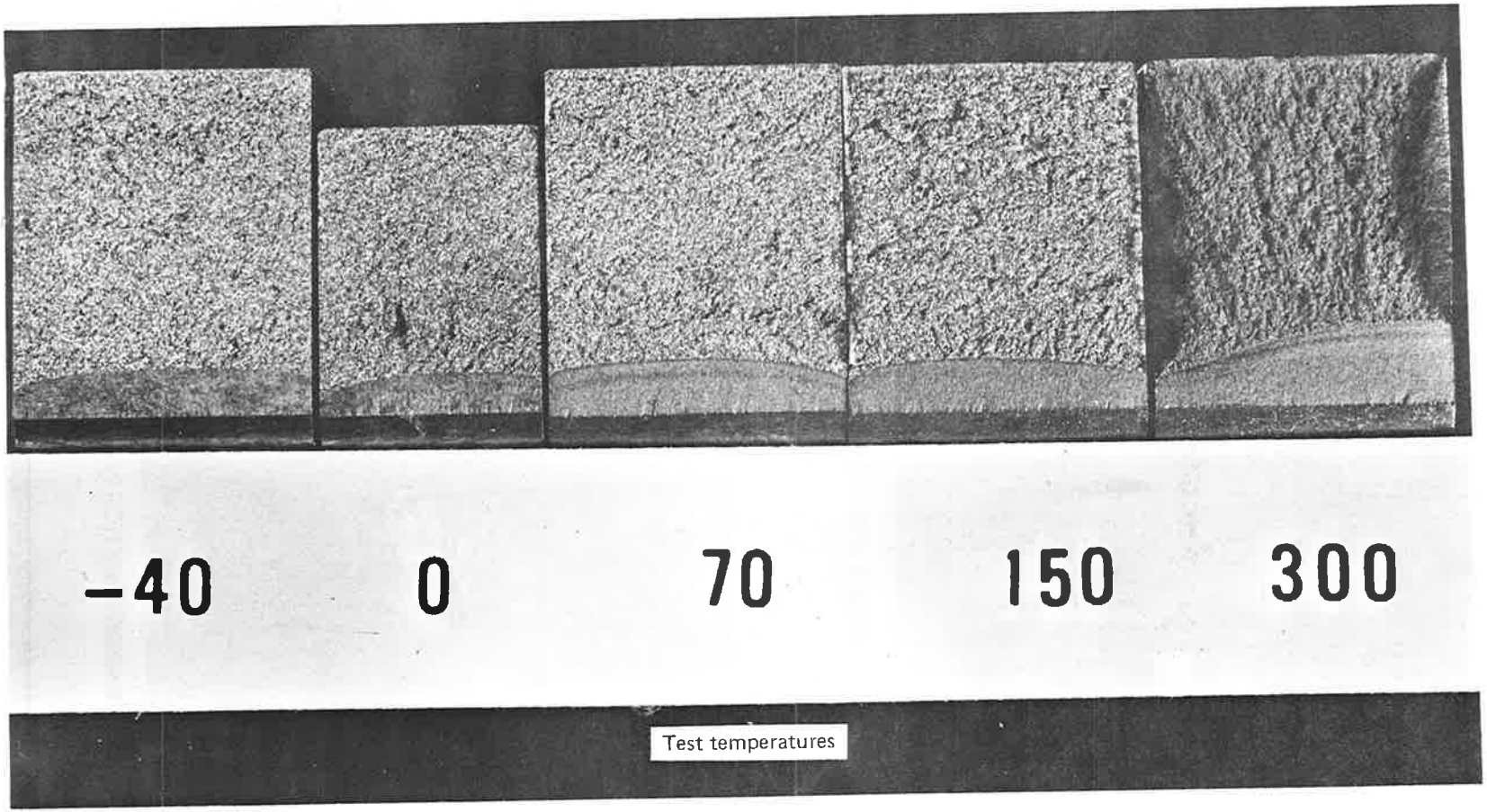

FIGURE 46.—K_{Ic} FRACTURES FROM THE WROUGHT CLASS B WHEEL RIM

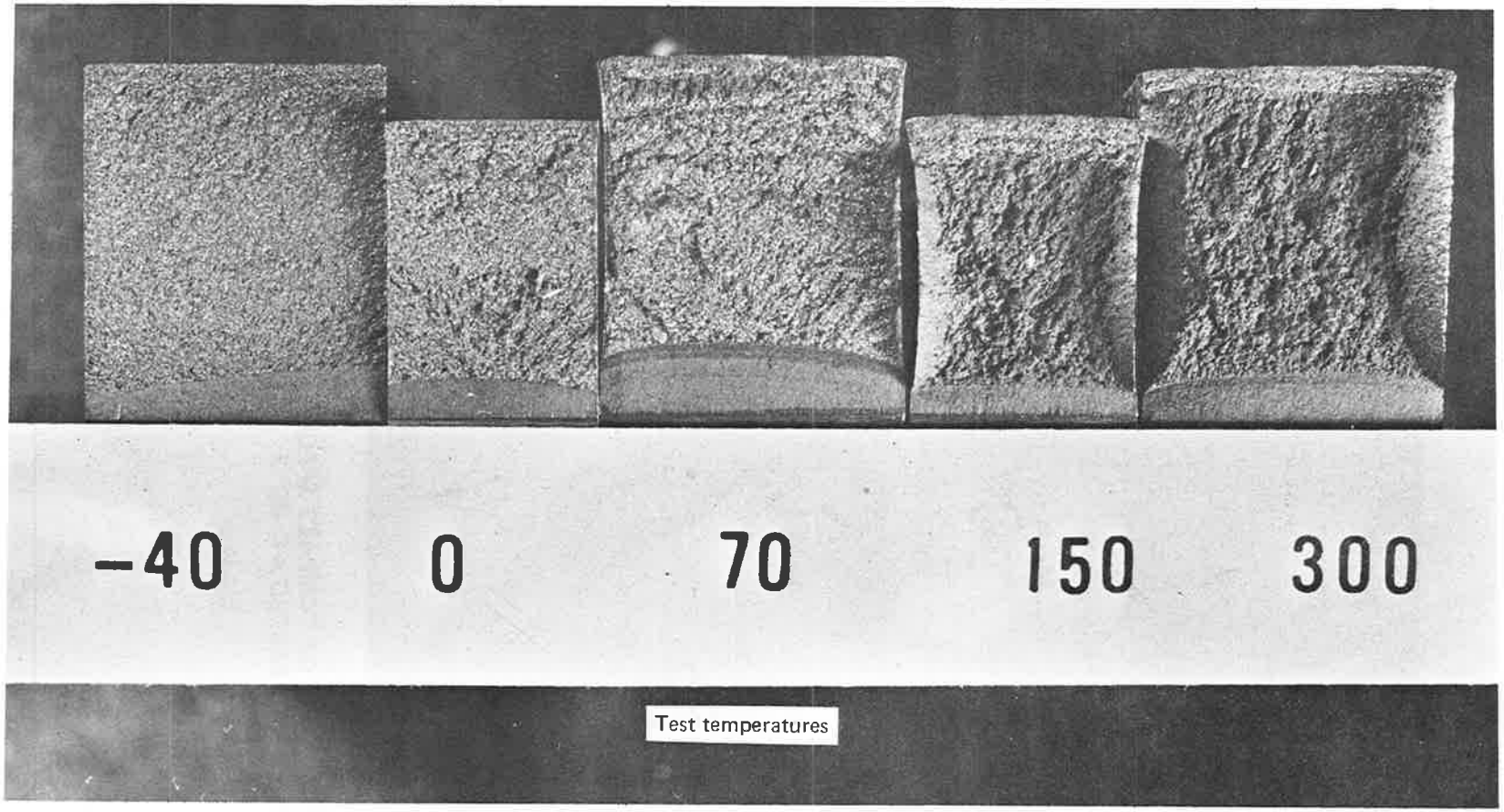

FIGURE 47.–K_{Ic} FRACTURES FROM THE WROUGHT CLASS SUB A WHEEL RIM

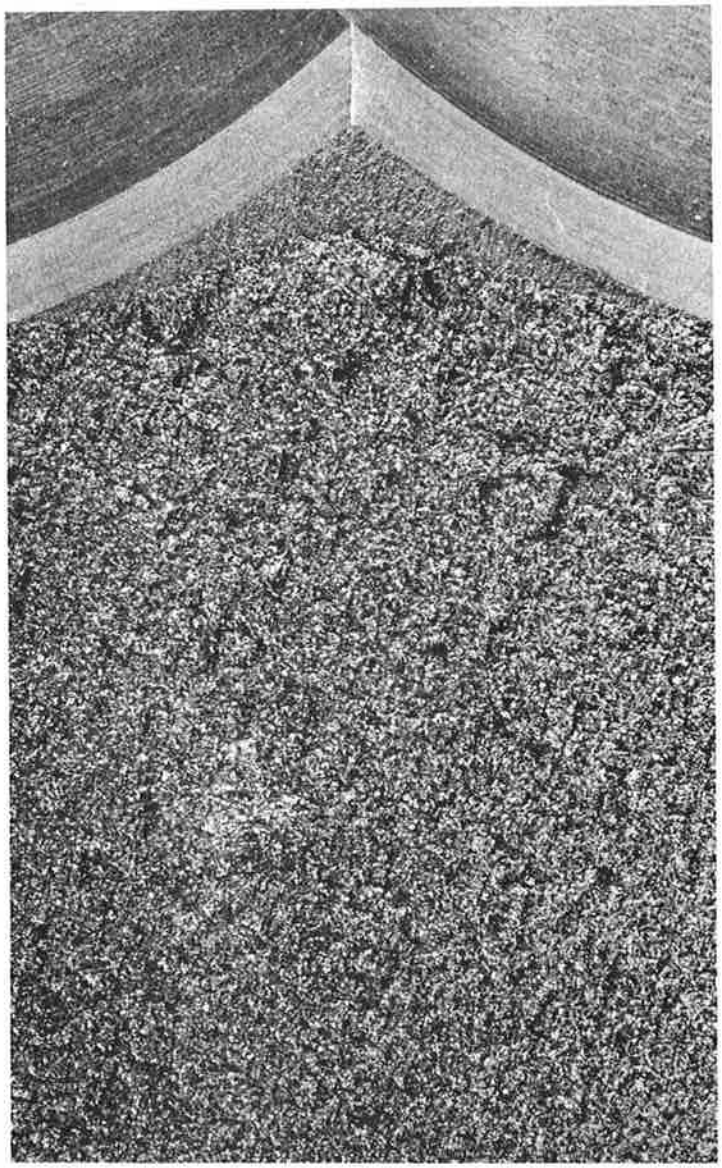

FIGURE 48.—FRACTURE OF COMPACT SPECIMEN UUE-KC4 TAKEN FROM GRADE U AXLE AND TESTED AT -40° F

FIGURE 49.—FRACTURE OF COMPACT SPECIMEN UUB-KC2 TAKEN FROM GRADE U AXLE AND TESTED AT 70° F

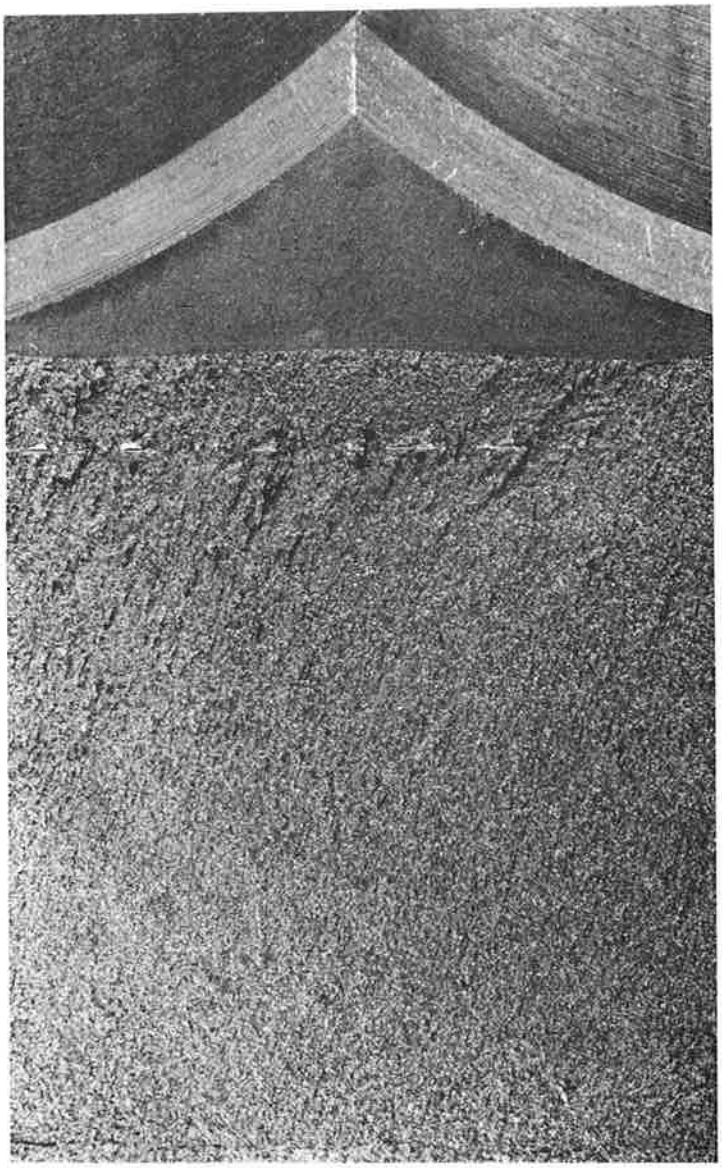

FIGURE 50.—FRACTURE OF COMPACT SPECIMEN FFE-KC4 TAKEN FROM GRADE F AXLE AND TESTED AT -40° F

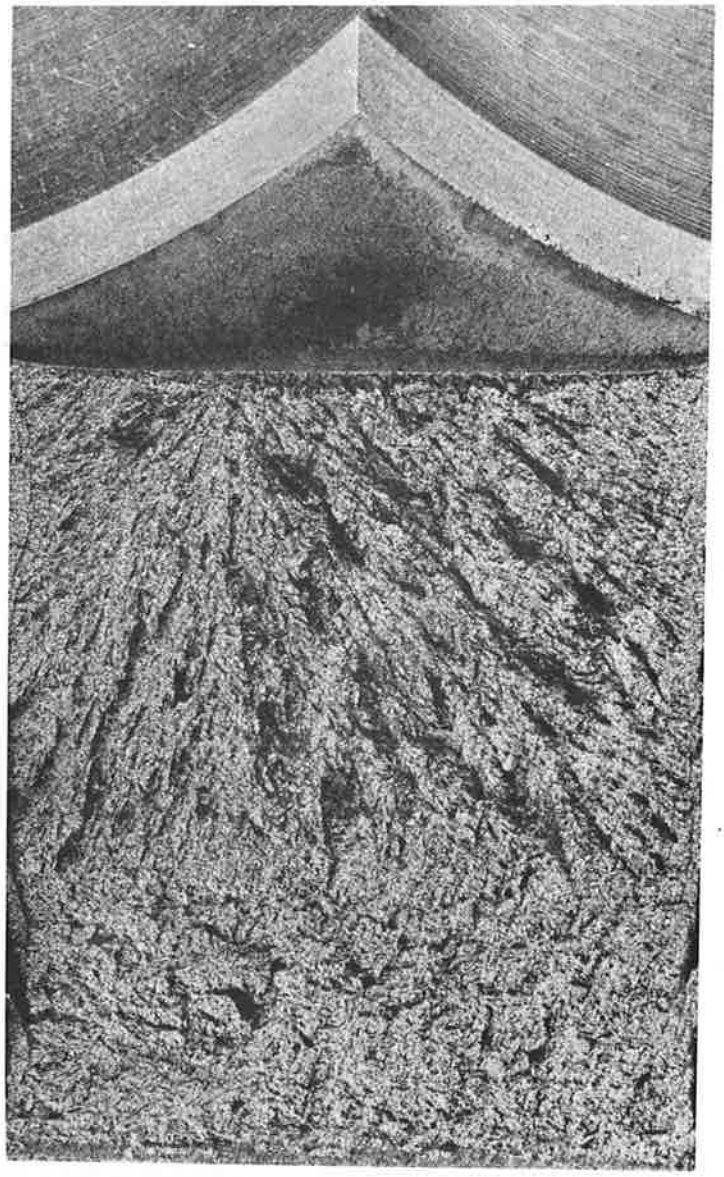

FIGURE 51.—FRACTURE OF COMPACT SPECIMEN HHB-KC2 TAKEN FROM GRADE F AXLE AND TESTED AT 70° F

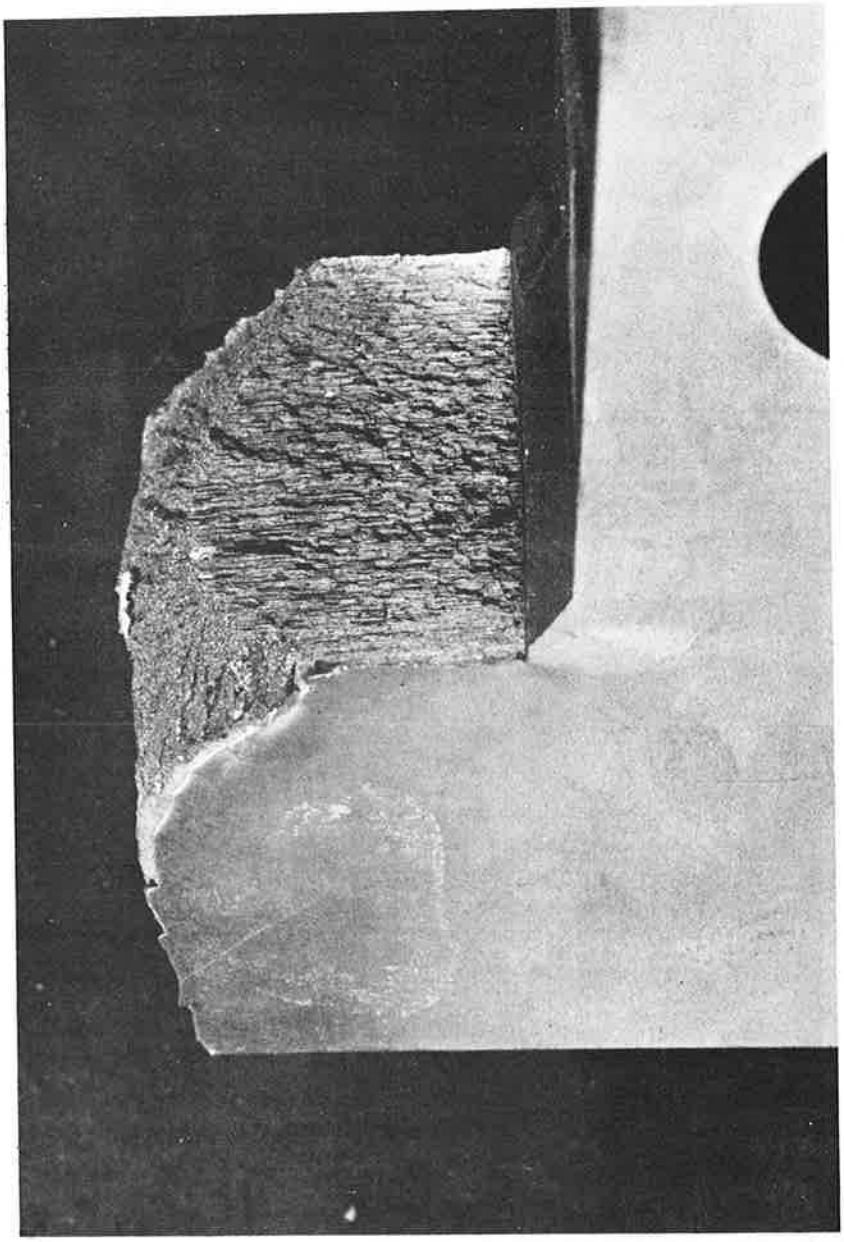

FIGURE 52.—FRACTURE APPEARANCE OF COMPACT SPECIMEN FFG-KC1 TESTED AT 70° F

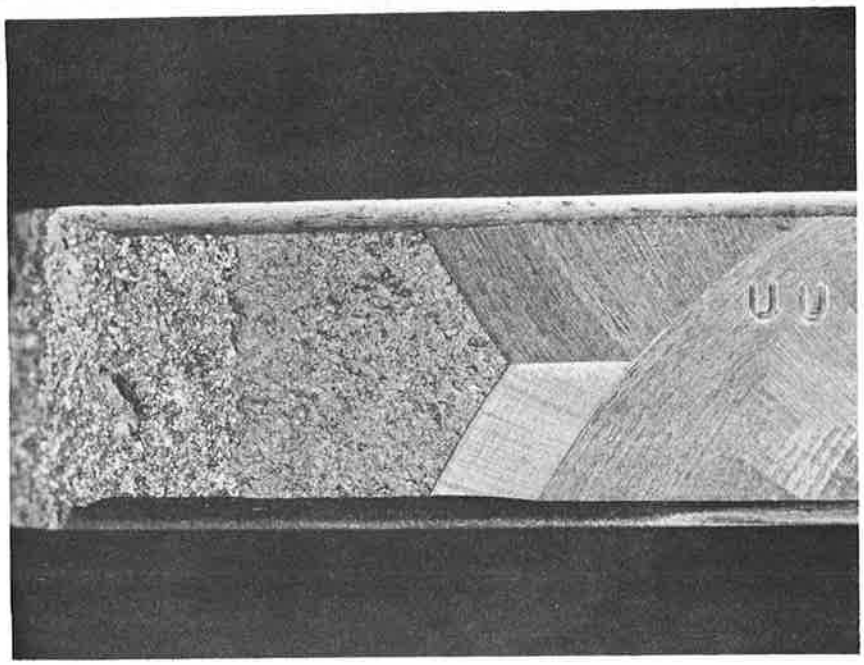

FIGURE 53.—FRACTURE APPEARANCE OF SPECIMEN UUB-F1 TAKEN FROM GRADE U AXLE, TESTED IN 100% RH, R ≃ 0.06

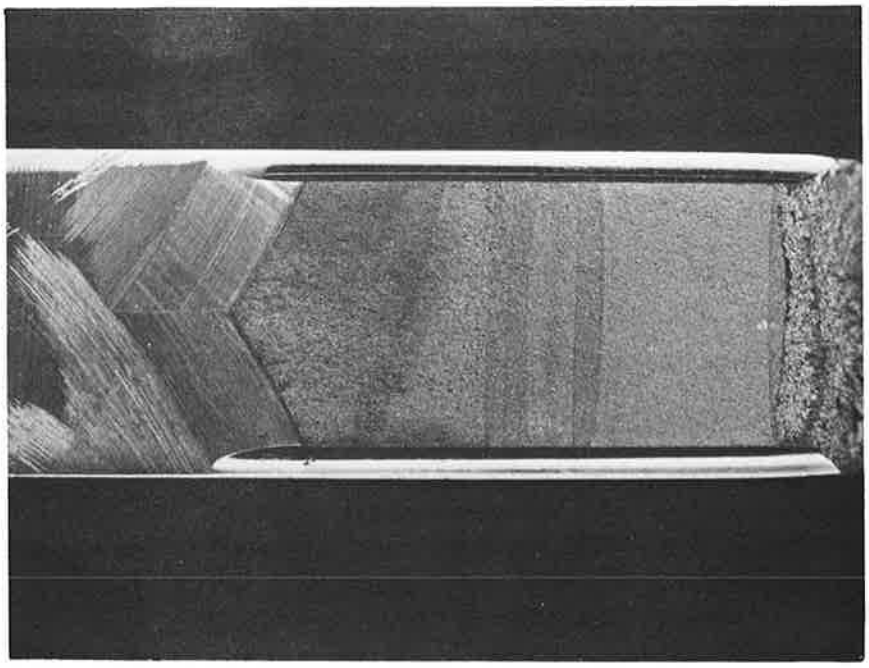

FIGURE 54.—FRACTURE APPEARANCE OF SPECIMEN 43-F2 TAKEN FROM CLASS A WHEEL, TESTED IN 100% RH, R ≃ 0.06

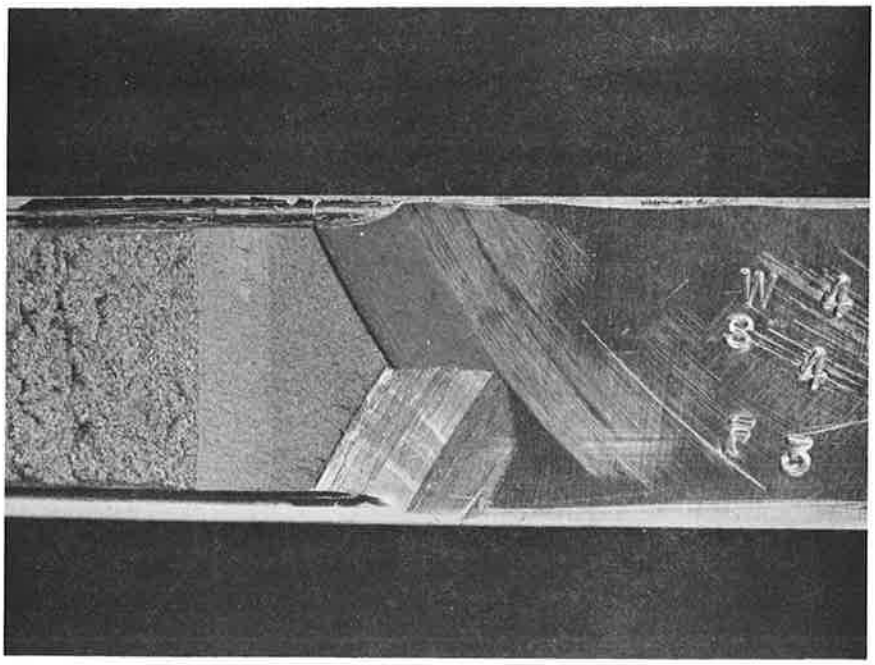

FIGURE 55.—FRACTURE APPEARANCE OF SPECIMEN 44-F3 TAKEN FROM CLASS A WHEEL

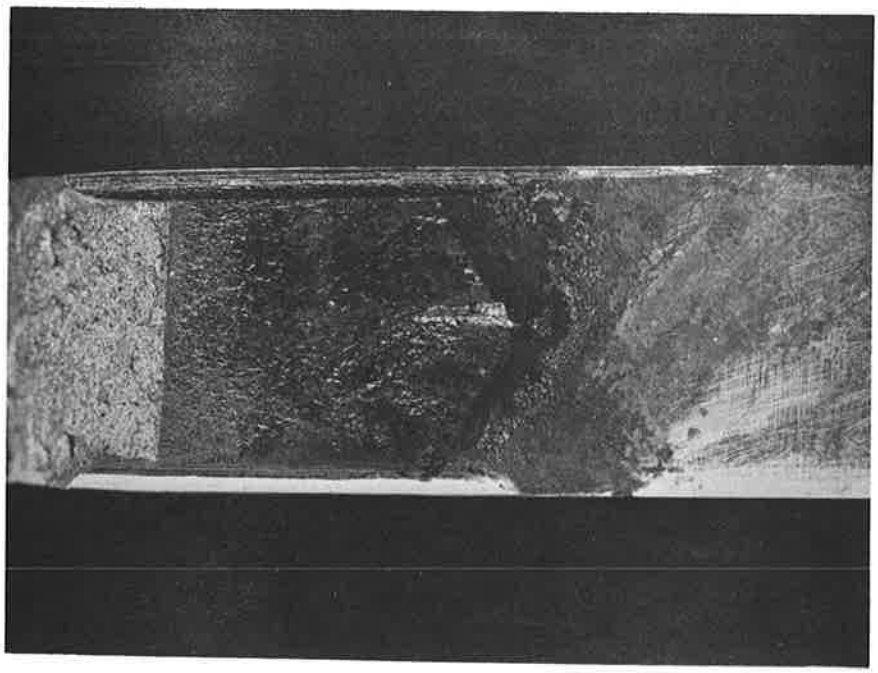

FIGURE 56.—FRACTURE APPEARANCE OF SPECIMEN 44-F4 TAKEN FROM (CLASS A WHEEL TESTED IN 3.5% NaCl AQUEOUS SOLUTION

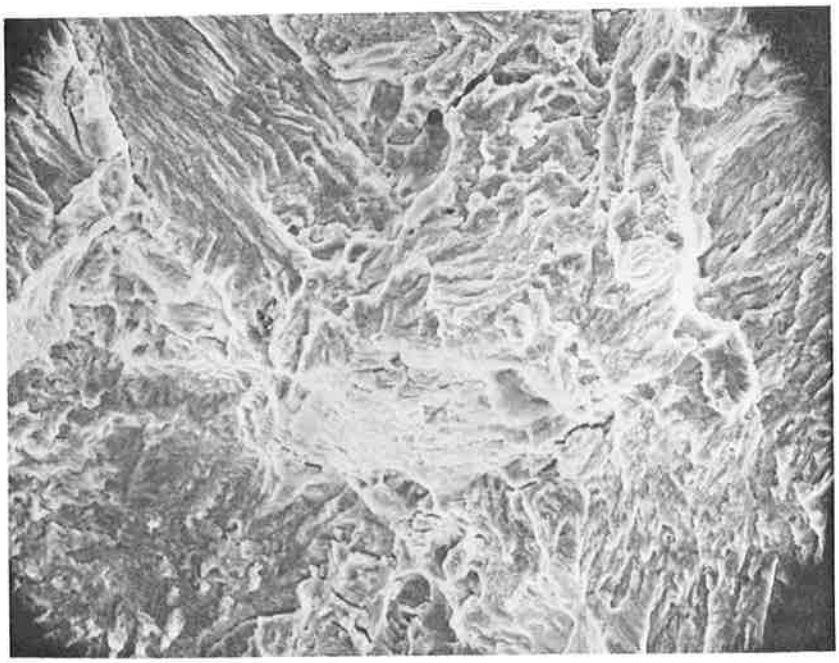

500X

FIGURE 57.–SCANNING ELECTRON MICROGRAPH OF SPECIMEN UUB-F1; $\Delta K \simeq 18$ KSI $IN^{1/2}$ AND $da/dN \simeq 7.6$ μIN./CYCLE

450X

FIGURE 58.–SCANNING ELECTRON MICROGRAPH OF SPECIMEN 44-F4 TAKEN FROM CLASS A WHEEL, TESTED IN 3.5% NaCl AQUEOUS SOLUTION

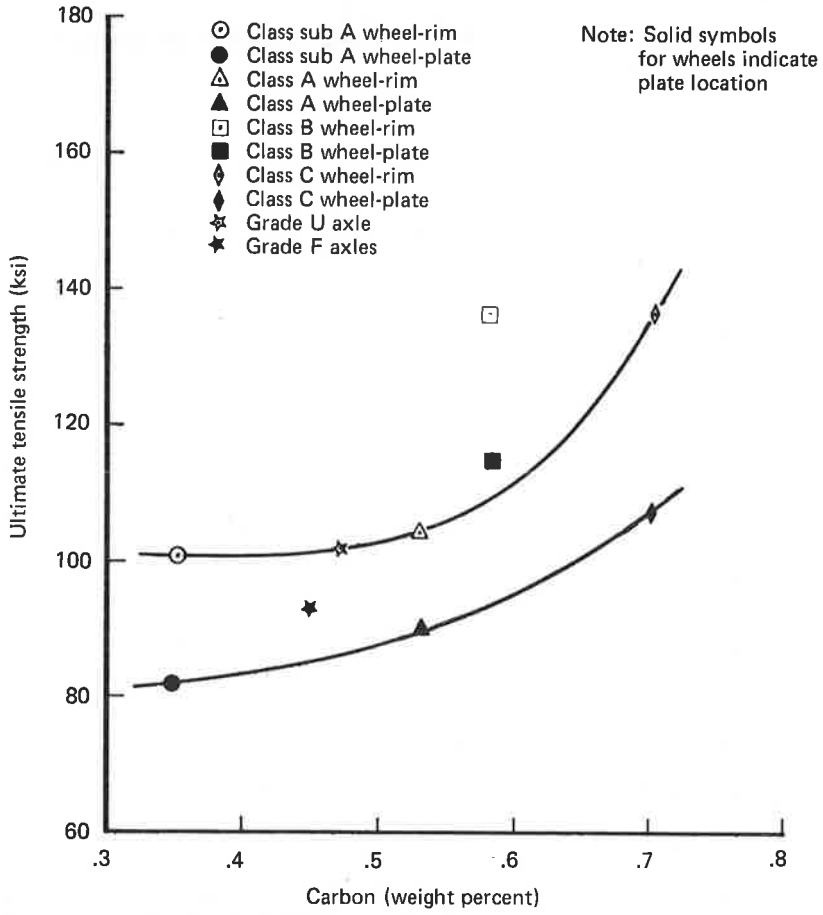

FIGURE 59.—RELATIONSHIP BETWEEN ULTIMATE TENSILE STRENGTH AND CARBON CONTENT FOR AXLES AND RIM TOUGHENED WHEELS

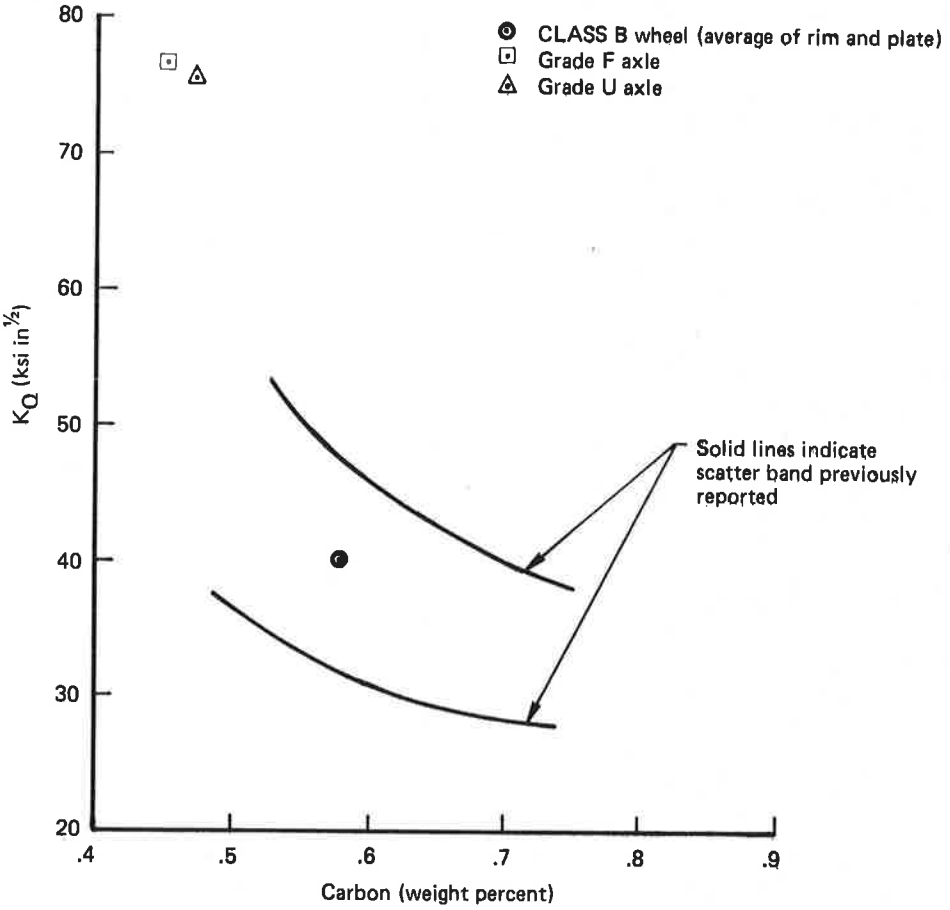

FIGURE 60.—EFFECT OF CARBON CONTENT ON FRACTURE TOUGHNESS (0° F TO 5° F)

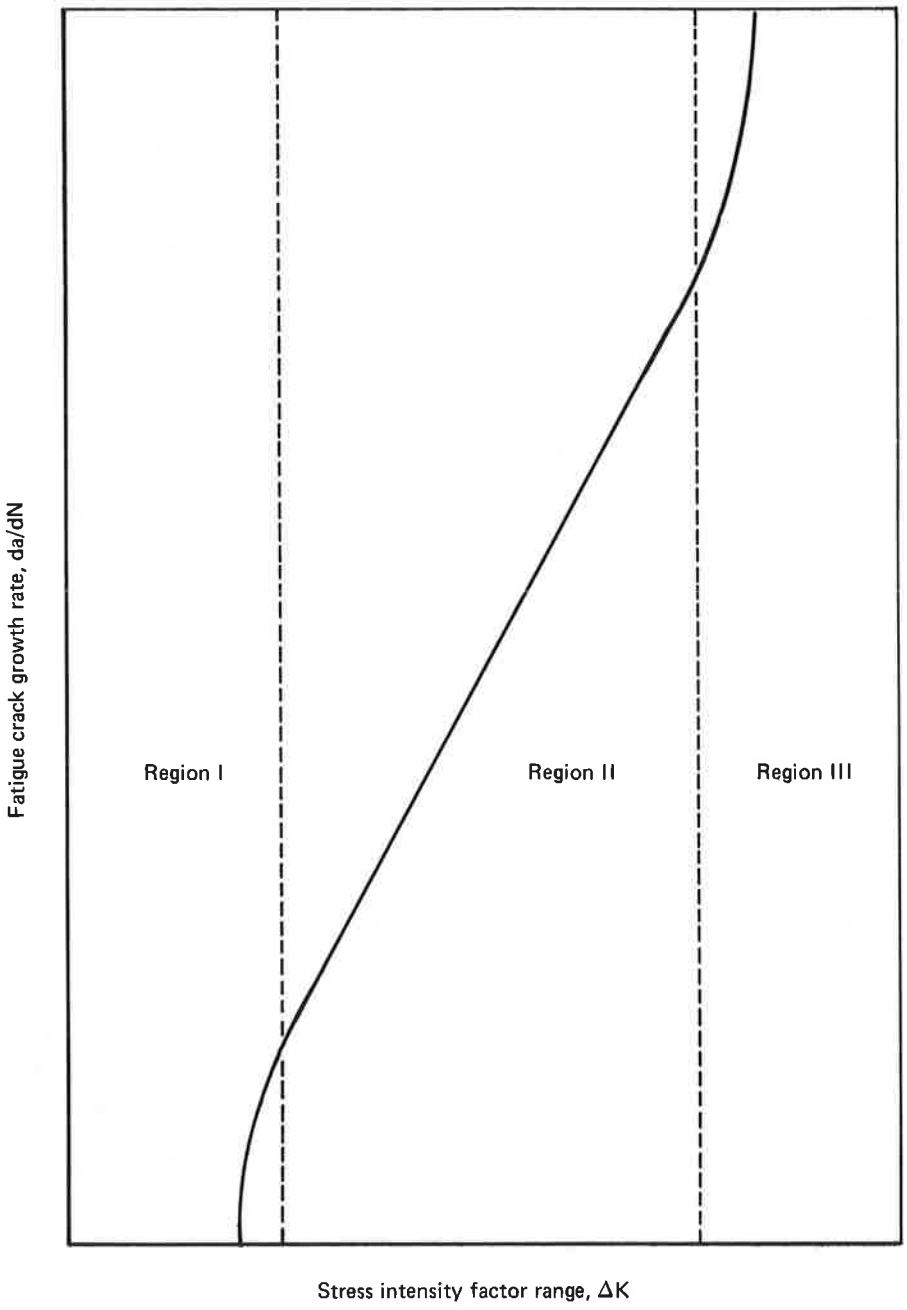

FIGURE 61.—FATIGUE CRACK PROPAGATION CURVE

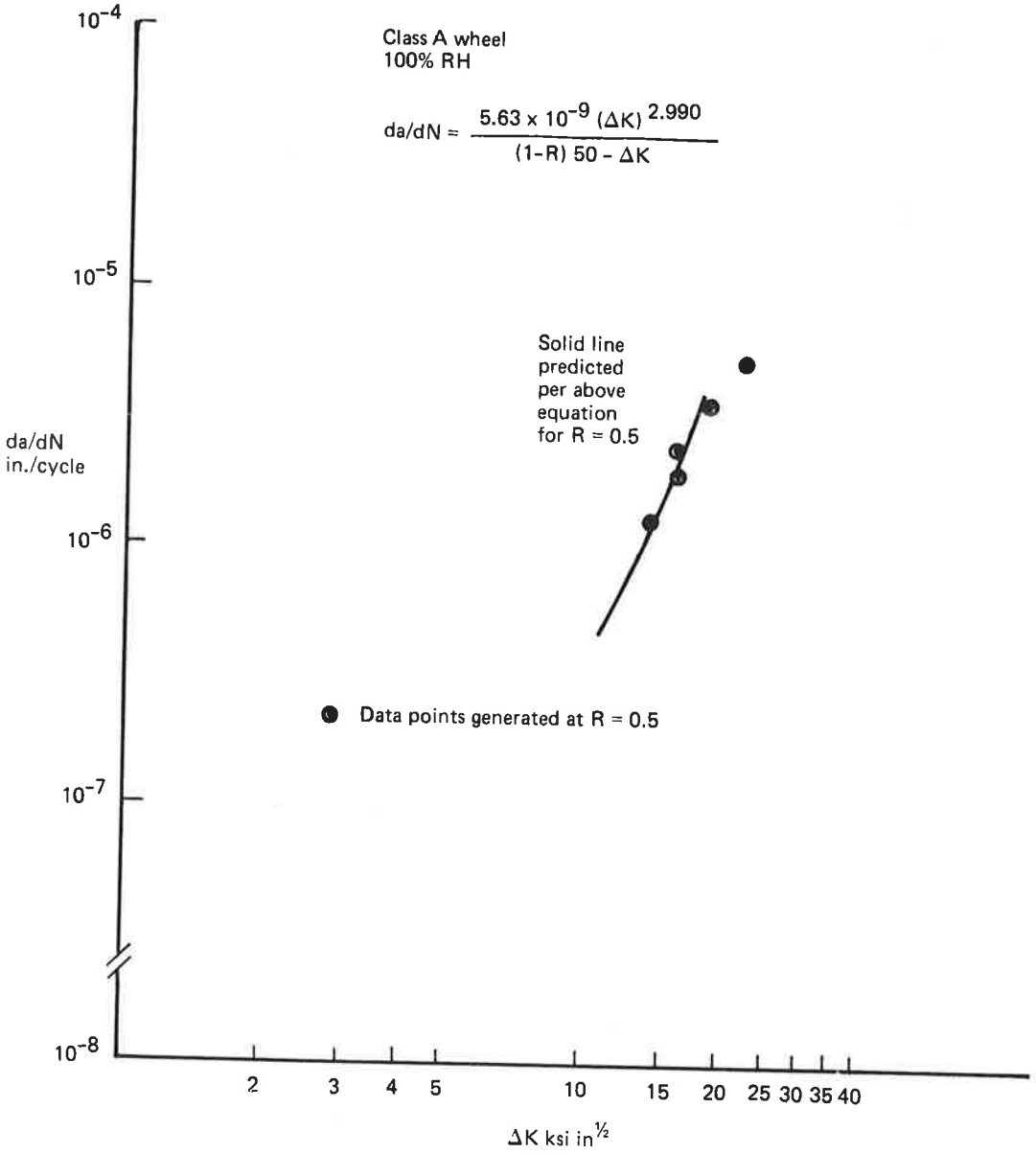

FIGURE 62.—CONFORMANCE OF TEST DATA GENERATED AT AN R = 0.5 WITH THAT PREDICTED BY FORMAN'S EQUATION (REF 19)

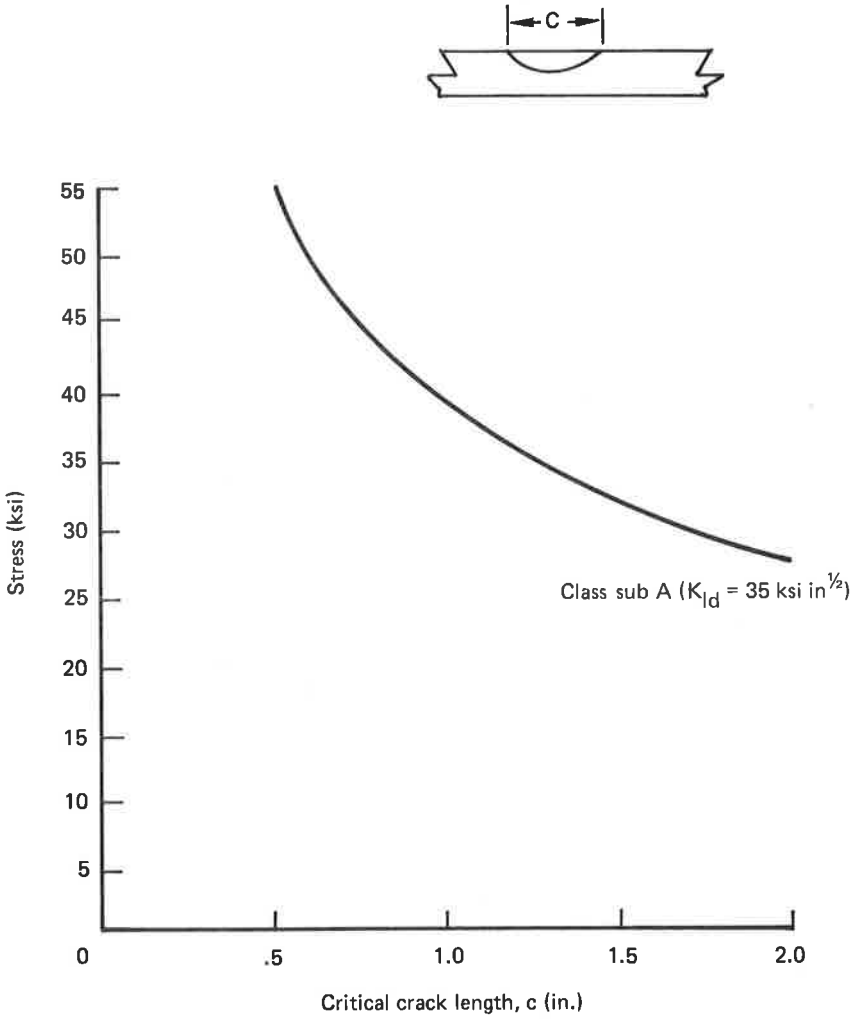

FIGURE 63.—APPLIED STRESS/CRITICAL CRACK LENGTH RELATIONSHIPS FOR SURFACE CRACKS IN WHEEL PLATES

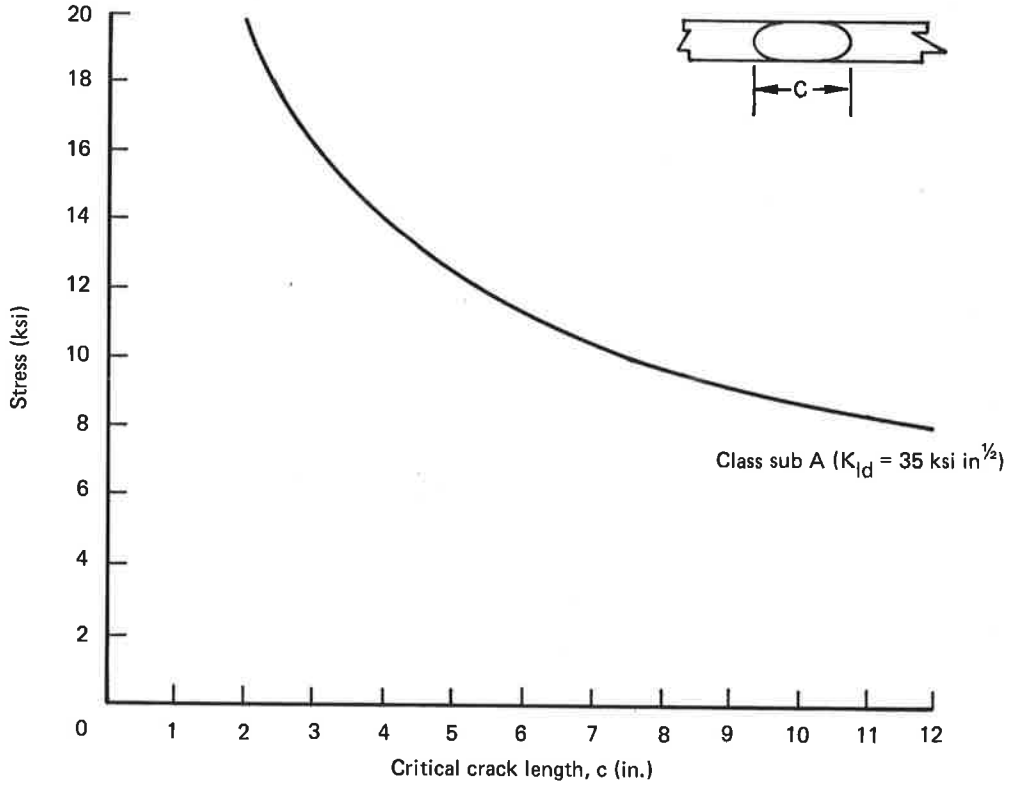

FIGURE 64.—APPLIED STRESS/CRITICAL CRACK LENGTH RELATIONSHIPS FOR THROUGH-THICKNESS CRACKS IN WHEEL PLATES

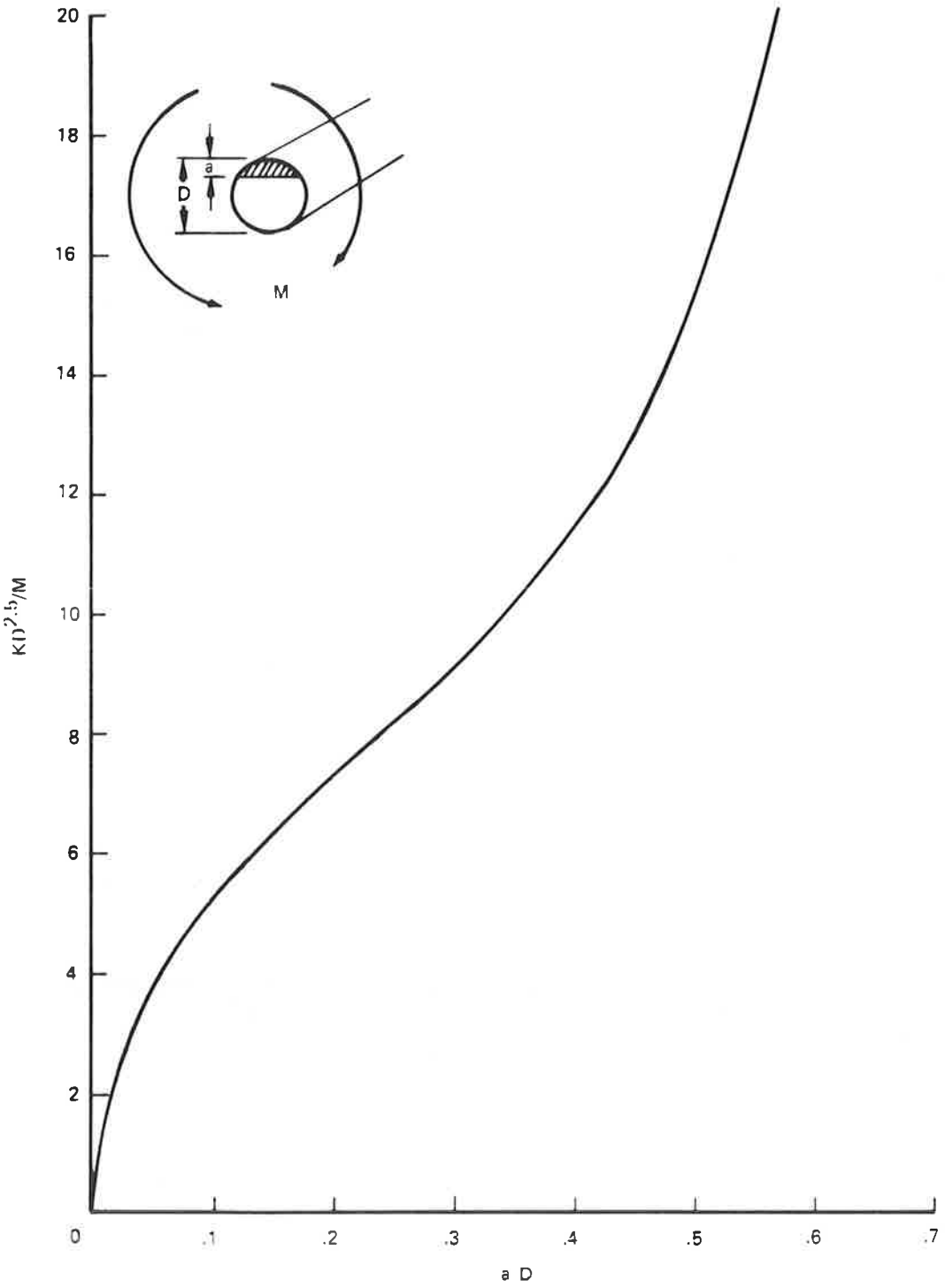

FIGURE 65.—RELATIONSHIP BETWEEN STRESS INTENSITY AND CRACK DEPTH FOR AXLE IN BENDING (AFTER CANNON AND ALLEN REF. 15)

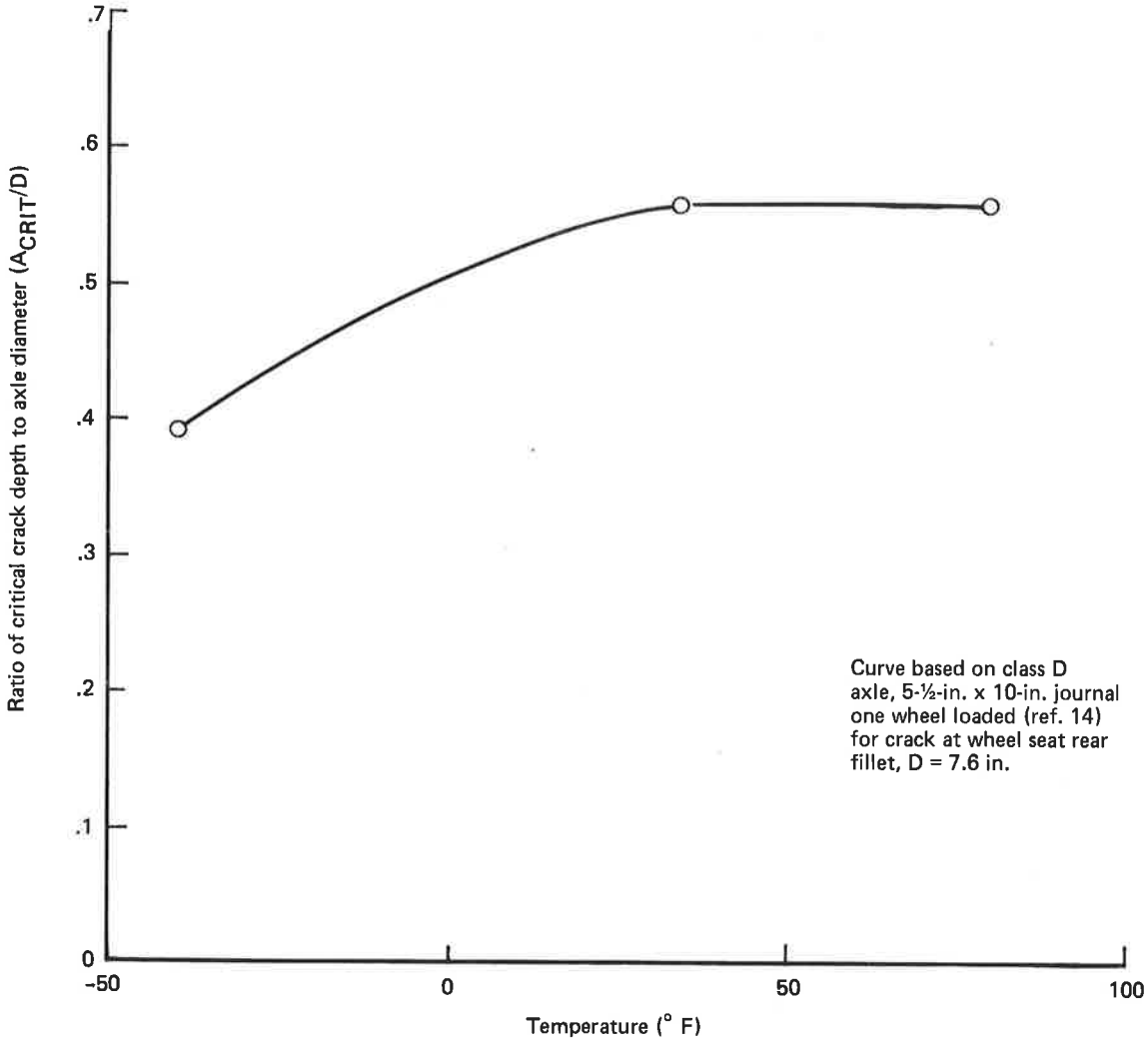

FIGURE 66.–EFFECT OF TEMPERATURE ON CRITICAL CRACK SIZE

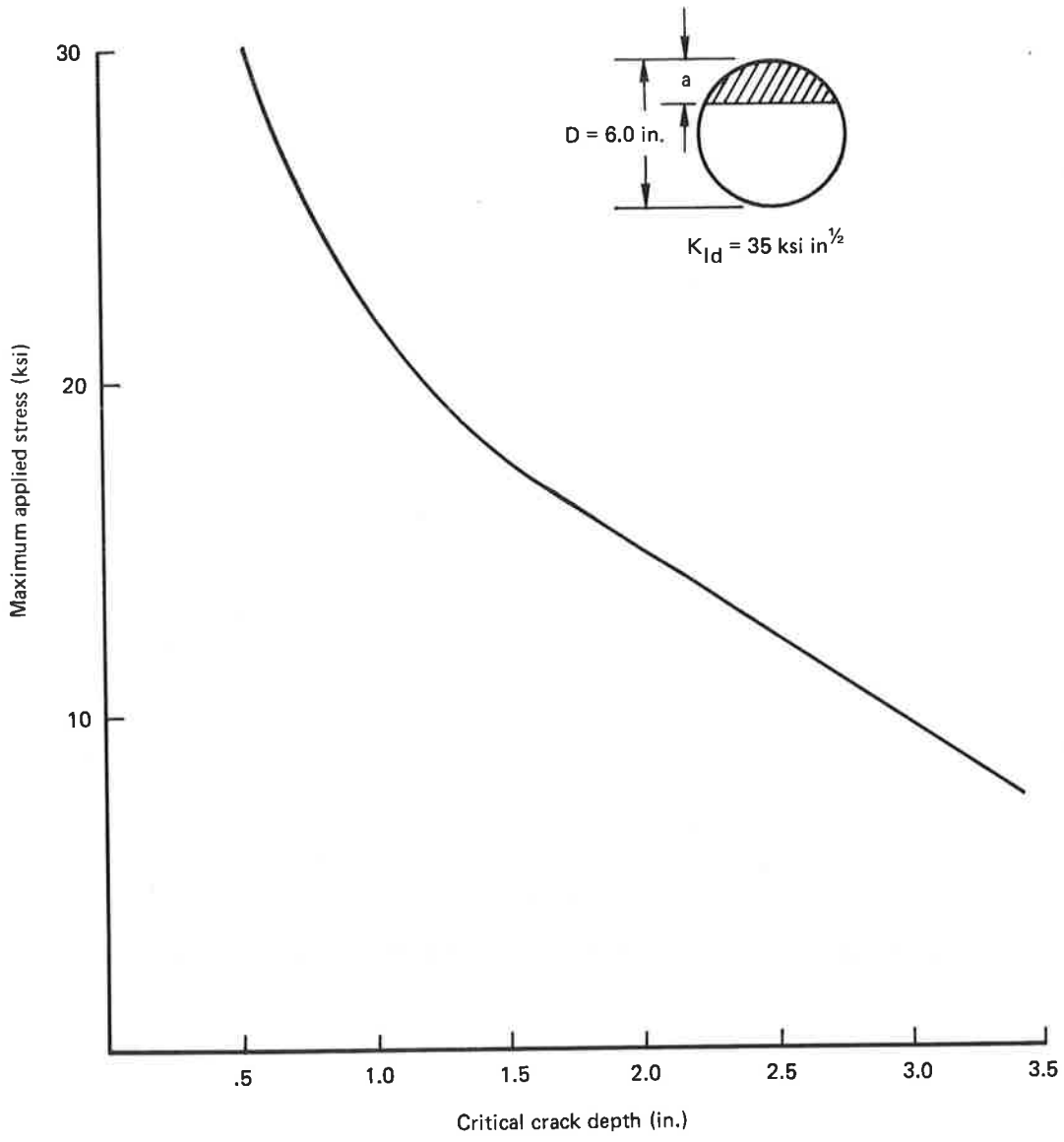

FIGURE 67.—RELATIONSHIP BETWEEN APPLIED STRESS AND CRITICAL CRACK DEPTH FOR GRADES U AND F AXLES

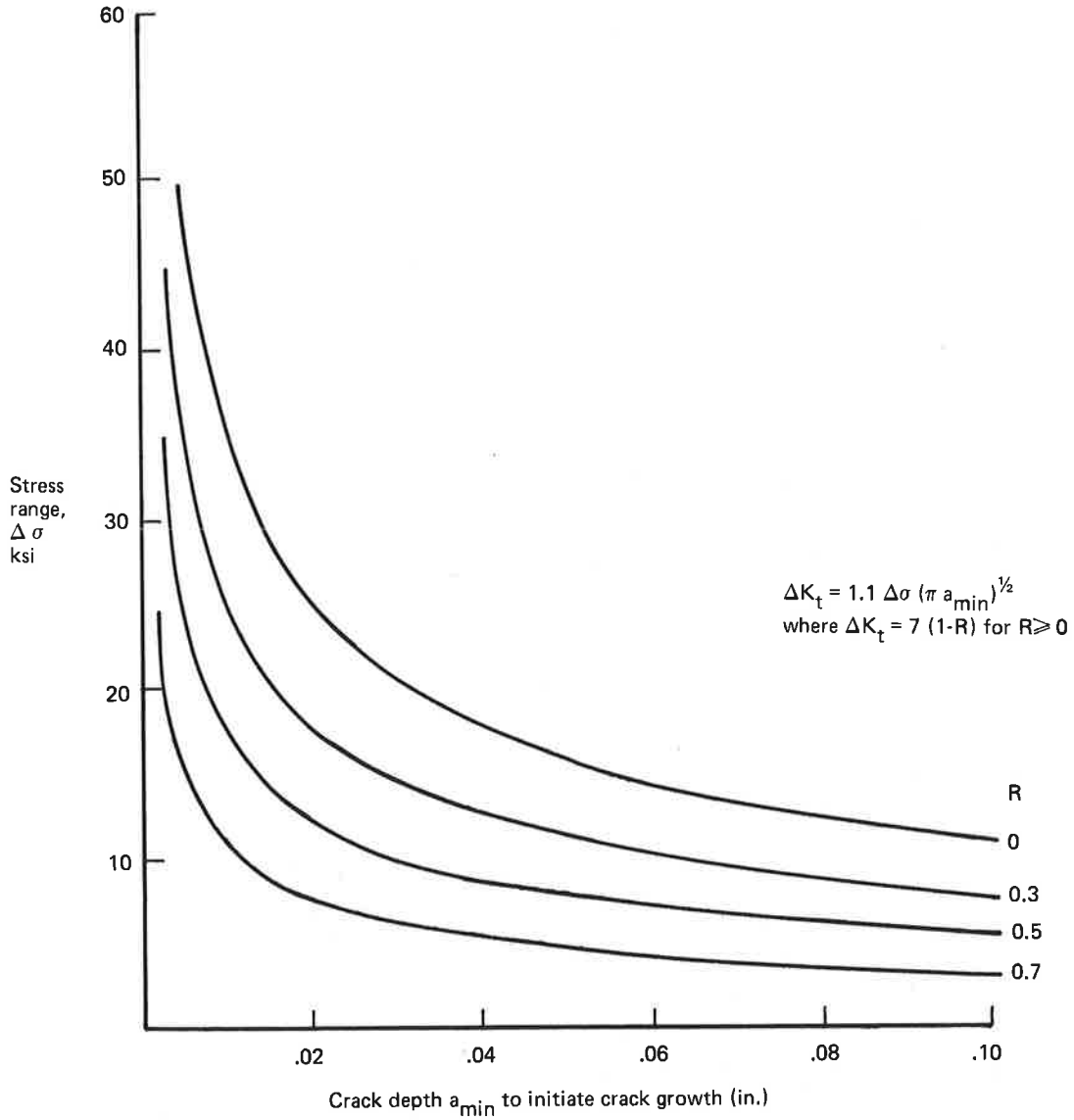

FIGURE 68.—RELATIONSHIP BETWEEN CYCLIC STRESS RANGE AND MINIMUM DEPTH OF DEFECT TO INITIATE FATIGUE CRACK GROWTH

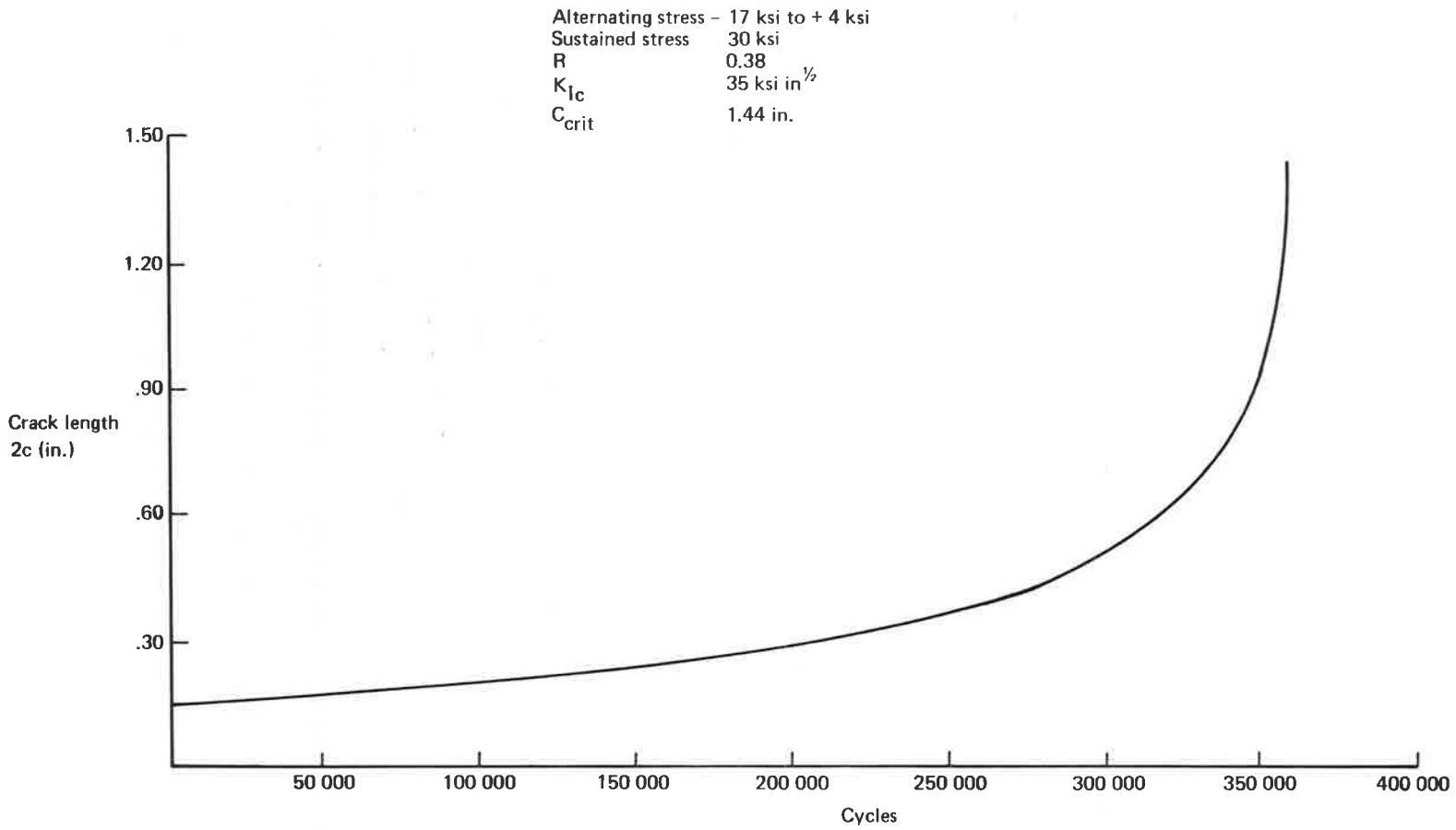

FIGURE 69.– CRACK LENGTH VERSUS CYCLES CURVE FOR CLASS U AND C WHEELS

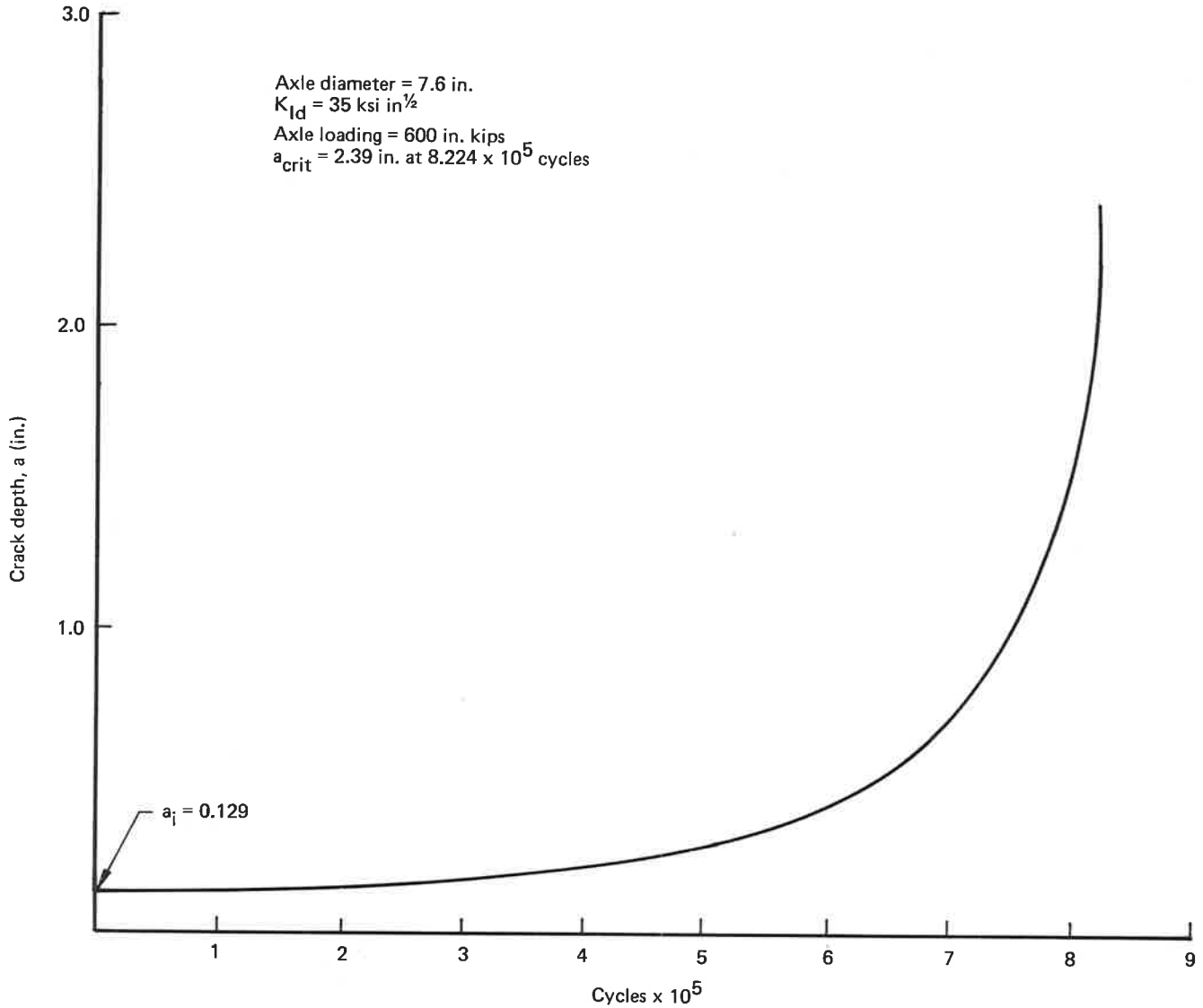

FIGURE 70.—CRACK LENGTH VERSUS CYCLES CURVE FOR CRACK INITIATING AT AXLE WHEEL SEAT CLASS D AXLE

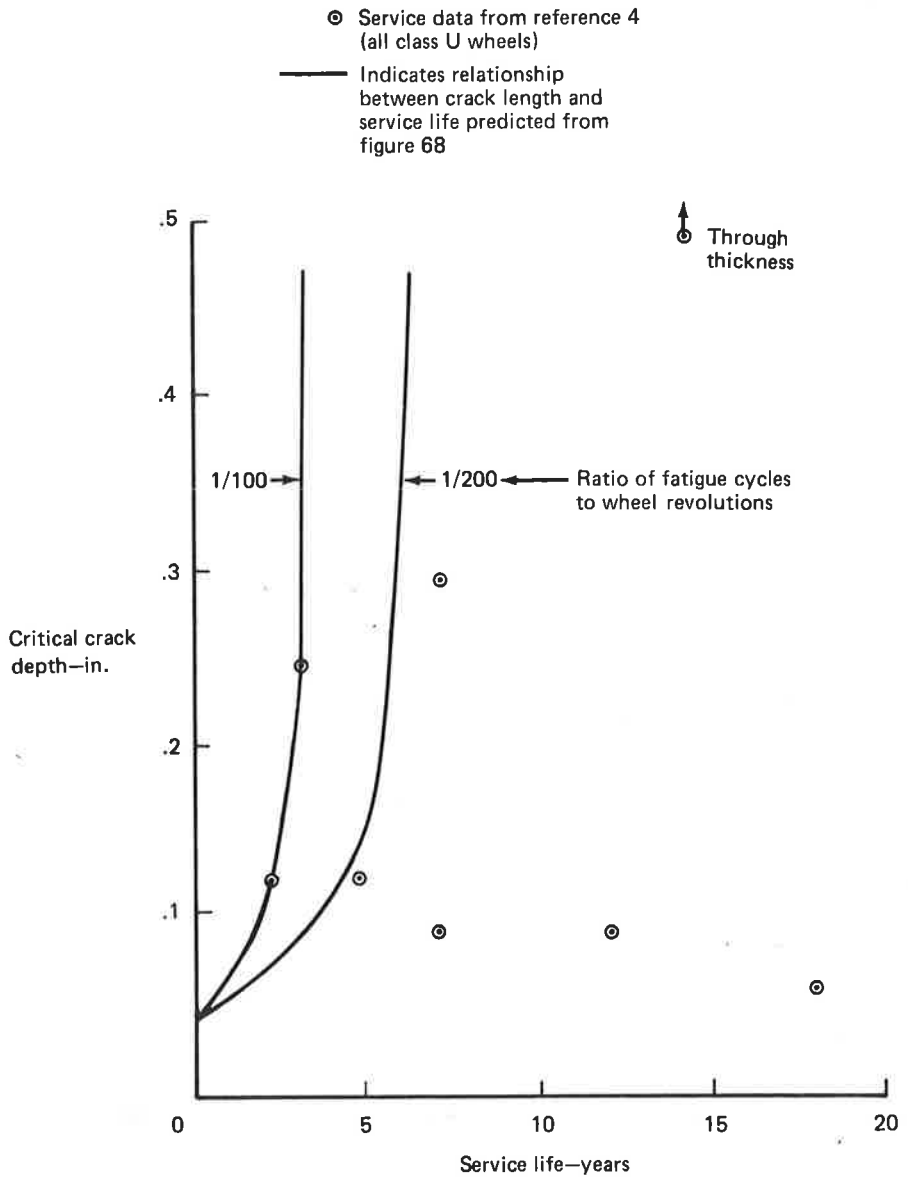

FIGURE 71.—RELATIONSHIP BETWEEN CRITICAL CRACK DEPTH AND SERVICE LIFE FOR FRONT HUB FILLET FAILURES

APPENDIX A

FATIGUE CRACK GROWTH DATA

TABLE A1.—GRADE U AXLE, SPECIMEN UUB-F1, 100% RH, RT AIR

Crack length (in.)	K_{min} (ksi $in^{1/2}$)	K_{max} (ksi $in^{1/2}$)	ΔK (ksi $in^{1/2}$)	Stress ratio, R	da (in.)	dN (in.)	da/dN	Average ΔK (ksi $in^{1/2}$)	Remarks
1.46	1.7	28.4	26.7	0.06	–	–	–		Start precrack
1.59	2.1	27.2	25.1	0.08	0.13	42 040	–		End precrack
1.59	1.7	26.6	24.9	0.06	–	–	–		Reset
1.63	2.0	26.4	24.4	0.07	0.04	12 503	3.2×10^{-6}	24.7	
1.72	2.6	25.7	23.1	0.10	0.09	28 417	3.2×10^{-6}	23.7	
1.72	1.2	16.0	14.8	0.08	–	–	–		Reset
1.72	1.6	16.3	14.7	0.10	<0.01	31 300			
1.72	1.4	20.0	18.6	0.07	–	–	–		Reset
1.76	1.8	19.4	17.6	0.09	0.04	52 805	7.6×10^{-7}	18.1	
1.80	1.7	19.0	17.3	0.09	0.04	56 060	7.1×10^{-7}	17.4	
1.87	2.1	19.0	16.9	0.11	0.07	93 702	7.5×10^{-7}	17.1	

TABLE A2.—AXLE F1, SPECIMEN FFB-F1, 100 RH, RT AIR

Crack length (in.)	K_{min} (ksi $in^{1/2}$)	K_{max} (ksi $in^{1/2}$)	ΔK (ksi $in^{1/2}$)	Stress ratio, R	da (in.)	dN (in.)	da/dN	Average ΔK (ksi $in^{1/2}$)	Remarks
1.47	1.9	27.8	25.9	0.07	–	–	–		Start precrack
1.58	2.1	28.2	26.1	0.07	0.11	30 164	–		End precrack
1.58	1.4	27.9	26.5	0.05	–	–	–		Reset
1.63	1.4	27.3	25.9	0.05	0.05	8 501	5.9×10^{-6}	26.1	
1.69	1.8	27.0	25.2	0.07	0.06	12 027	5.0×10^{-6}	25.5	
1.73	1.8	27.0	25.2	0.07	0.04	8 004	5.0×10^{-6}	25.2	
1.73	1.6	22.1	20.5	0.07	–	–	–		Reset
1.77	2.0	21.0	19.0	0.10	0.04	55 328	7.2×10^{-7}	19.7	
1.82	2.1	20.6	18.5	0.10	0.05	38 804	1.3×10^{-6}	18.7	
1.82	1.3	18.3	17.0	0.07	–	–	–		Reset
1.86	1.4	17.7	16.3	0.08	0.04	41 800	9.6×10^{-7}	16.7	
1.86	1.0	17.5	16.5	0.06	–	–	–		Reset
1.91	1.2	17.5	16.3	0.07	0.05	44 331	1.1×10^{-6}	16.4	
1.91	0.8	9.4	8.6	0.09	–	–	–		Reset
1.91	0.8	9.4	8.6	0.09	<0.01	10 936	–		
1.91	0.4	12.4	12.0	0.03	–	–	–		Reset
1.91	0.4	12.6	12.2	0.03	<0.01	57 802	–		
1.98	0.4	12.0	11.6	0.03	0.07	279 347	2.5×10^{-7}		
					0.07	337 149	2.1×10^{-7}	11.8	
1.98	0.4	7.6	7.2	0.05	–	–	–		Reset
1.98	0.4	7.6	7.2	0.05	–	–	–		Reset
1.98	0.8	7.8	7.0	0.10	<0.01	194 948			
1.98	0.6	8.0	7.4	0.08	<0.01	243 331			
1.98	0.6	7.6	7.0	0.08	<0.01	92 000			
					<0.01	530 279		7.2	No measured growth

TABLE A6.–CLASS C WHEEL CAST, SPECIMEN 23-F1, 100% RH, RT AIR

Crack length (in.)	K_{min} (ksi $in^{1/2}$)	K_{max} (ksi $in^{1/2}$)	ΔK (ksi $in^{1/2}$)	Stress ratio, R	da (in.)	dN (in.)	da/dN	Average ΔK (ksi $in^{1/2}$)	Remarks
1.49	2.0	26.8	24.8	0.07	–	–			Start precrack
1.61	2.0	26.4	24.4	0.07	0.12	32 423			End precrack
1.61	1.8	26.7	24.9	0.07	–				Reset
1.65	2.0	26.1	24.1	0.08	0.04	7 002	5.7×10^{-6}	24.5	
1.72	1.9	25.6	23.7	0.07	0.07	12 500	5.6×10^{-6}	23.9	

TABLE A7.–CLASS U WHEEL WROUGHT, SPECIMEN 33-F1 100% RH, RT AIR

Crack length (in.)	K_{min} (ksi $in^{1/2}$)	K_{max} (ksi $in^{1/2}$)	ΔK (ksi $in^{1/2}$)	Stress ratio, R	da (in.)	dN (in.)	da/dN	Average ΔK (ksi $in^{1/2}$)	Remarks
1.47	1.7	28.0	26.3	0.06	–	–	–		Start precrack
1.58	1.7	27.9	26.2	0.06	0.11	35 131	–		End precrack
1.58	1.0	27.1	26.0	0.04	–	–	–		Reset
1.63	1.3	26.5	25.3	0.05	0.05	8 003	6.2×10^{-6}	25.6	
1.63	1.3	26.5	25.3	0.05	–	–	–		
1.66	1.1	26.6	25.5	0.04	0.03	7 002	4.3×10^{-6}		
1.71	0.8	26.1	25.3	0.03	0.05	8 002	6.2×10^{-6}		
					0.08	15 004	5.3×10^{-6}	25.4	

TABLE A8.–CLASS A WHEEL WROUGHT, SPECIMEN 43-F1, 100% RH, RT AIR

Crack length (in.)	K_{min} (ksi $in^{1/2}$)	K_{max} (ksi $in^{1/2}$)	ΔK (ksi $in^{1/2}$)	Stress ratio, R	da (in.)	dN (in.)	da/dN	Average ΔK (ksi $in^{1/2}$)	Remarks
1.62	a	a	34.1	b	–				Reset
1.65			33.3		0.03	1 786			
1.67			33.6		0.02	1 045			
					0.05	2 831	1.8×10^{-5}	33.6	
1.72			32.7		0.05	4 008	1.2×10^{-5}	33.1	
1.79			31.2		0.07	4 794	1.5×10^{-5}	31.9	
1.83			29.6		0.04	4 489	8.9×10^{-6}	30.4	
1.87			29.8		0.04	4 905	8.1×10^{-6}	29.7	
1.93			28.5		0.06	4 708	1.3×10^{-5}	29.1	
1.97			28.9		0.04	4 690	8.5×10^{-6}	28.7	
2.03			28.4		0.06	6 213	9.7×10^{-6}	28.6	
2.08			27.7		0.05	6 574	7.6×10^{-6}	28.0	
2.12			27.1		0.04	7 895	5.1×10^{-6}	27.4	
2.19			26.7		0.07	9 200	7.6×10^{-6}	26.9	
2.24	a	a	26.1	b	0.05	11 023	4.5×10^{-6}	26.4	

[a]Not recorded

[b]Not recorded $R \cong 0.06$

TABLE A9.—CLASS A WHEEL, SPECIMEN 43-F2, 100% RH, RT AIR

Crack length (in.)	K_{min} (ksi $in^{1/2}$)	K_{max} (ksi $in^{1/2}$)	ΔK (ksi $in^{1/2}$)	Stress ratio, R	da (in.)	dN (in.)	da/dN	Average ΔK (ksi $in^{1/2}$)	Remarks
1.60	a	a	17.1	b	—	—	—		Reset after precrack
1.63	↓	↓	16.7	↓	0.03	11 723	2.7×10^{-6}		
1.65	↓	↓	16.5	↓	0.02	13 176	1.5×10^{-6}		
	↓	↓	↓	↓	0.05	24 899	2.0×10^{-6}	16.7	
1.65	↓	↓	12.6	↓	—	—	—		Reset
1.67	↓	↓	12.4	↓	0.02	33 397	6.0×10^{-7}		
1.69	↓	↓	12.2	↓	0.02	35 079	5.7×10^{-7}		
	↓	↓	↓	↓	0.04	68 476	5.8×10^{-7}	12.4	
1.69	↓	↓	8.0	↓	—	—	—		Reset
1.92	↓	↓	11.7	↓	—	—	—	—	Straighten crack, reset
1.92	↓	↓	11.0	↓	<0.01	76 650	$<1.3 \times 10^{-7}$		
1.94	↓	↓	10.9	↓	0.02	48 472	4.1×10^{-7}		
1.94	↓	↓	7.9	↓	—	—	—		Reset
1.97	↓	↓	7.4	↓	0.03	338 426	8.9×10^{-8}		
1.99	a	a	7.2	b	0.02	123 984	1.6×10^{-7}		
					0.05	462 410	1.1×10^{-7}	7.5	
1.99	14.1	27.1	13.0	0.52	—	—	—		Reset
2.01	14.0	26.9	12.9	0.52	0.02	10 500	1.7×10^{-6}		
2.02	13.0	26.9	13.9	0.48	0.01	10 012	1.0×10^{-6}		
2.03	13.7	26.6	12.9	0.51	0.01	5 003	2.0×10^{-6}		
2.04	13.5	26.6	13.1	0.51	0.01	10 035	1.0×10^{-6}		
					0.05	35 550	1.4×10^{-6}	13.2	
2.04	10.8	20.9	10.1	0.52	—	—	—		Reset
2.04	11.2	20.2	9.0	0.55	<0.01	10 000	—		
2.05	10.8	19.1	8.3	0.56	0.01	50 002	2.6×10^{-7}		
2.05	1.0	16.8	15.8	0.06	—	—	—		Reset
2.06	0.5	15.6	15.1	0.03	0.01	25 008	4.0×10^{-7}		
2.06	1.3	18.5	17.2	0.07	—	—	—		Reset
2.09	1.6	18.5	16.9	0.09	0.03	13 002	1.9×10^{-6}		
2.09	0.8	11.2	10.4	0.07	—	—	—		Reset
2.09	0.3	11.6	1.3	0.03	<0.01	55 004	$<1.8 \times 10^{-7}$		
2.10	0.7	11.5	10.8	0.06	0.01	100 005	5.0×10^{-8}		
2.11	0.7	10.9	10.2	0.06	0.01	50 053	2.0×10^{-7}		
2.12	0.5	10.7	10.2	0.04	0.01	50 013	2.0×10^{-7}		
					0.03	255 075	1.2×10^{-7}	10.4	
2.12	0.5	8.4	7.9	0.06	—	—	—		Reset
2.12	0.2	7.9	7.7	0.03	<0.01	115 006	$<8.7 \times 10^{-8}$		
2.14	—	—	—	—	—	—	—		Machine problems
2.14	12.6	28.6	16.0	0.44	—	—	—		Reset
2.15	12.5	28.3	15.8	0.44	0.01	5 008	2.0×10^{-6}		
2.15	15.8	29.9	14.1	0.53	—	—	—		Reset
2.16	17.0	29.2	12.2	0.58	0.01	5 005	2.0×10^{-6}		
2.16	14.7	30.5	15.8	0.48	—	—	—		Reset
2.17	14.4	30.2	15.8	0.48	0.01	5 004	2.0×10^{-6}		
2.18	14.3	30.2	15.9	0.47	0.01	5 006	2.0×10^{-6}		
2.20	14.4	30.0	15.6	0.48	0.02	5 102	3.9×10^{-6}		
2.21	14.6	30.2	15.6	0.48	0.01	5 000	2.0×10^{-6}		
					0.05	20 112	2.5×10^{-6}	15.7	

TABLE A9.–CONCLUDED

Crack length (in.)	K_{min} (ksi $in^{1/2}$)	K_{max} (ksi $in^{1/2}$)	ΔK (ksi $in^{1/2}$)	Stress ratio, R	da (in.)	dN (in.)	da/dN	Average ΔK (ksi $in^{1/2}$)	Remarks
2.21	17.5	33.3	15.8	0.52	–	–	–		Reset
2.22	17.7	33.2	15.5	0.53	0.01	5 006	2.0×10^{-6}		
2.23	17.5	33.4	15.9	0.52	0.01	5 007	2.0×10^{-6}		
2.24	17.9	33.5	15.6	0.53	0.01	5 316	1.9×10^{-6}		
2.25	17.8	33.6	15.8	0.53	0.01	5 011	2.0×10^{-6}		
					0.04	20 333	2.0×10^{-6}	15.8	
2.25	18.8	34.4	15.6	0.55	–	–	–		Reset
2.26	18.7	34.4	15.7	0.54	0.01	5 016	2.0×10^{-6}		
2.26	11.5	26.3	14.8	0.44	–	–	–		Reset
2.27	11.0	25.3	14.3	0.43	0.01	5 004			
2.27	17.2	35.5	18.3	0.48	–	–			
2.29	17.2	35.7	18.5	0.48	0.02	5 000			
2.31	16.9	35.4	18.5	0.48	0.02	5 000			
2.32	16.8	35.7	18.9	0.47	0.01	3 007			
					0.05	13 011	3.8×10^{-6}	18.5	
2.32	16.7	35.0	18.3	0.48	–	–	–		Reset
2.34	17.0	35.2	18.2	0.48	0.02	5 011	4.0×10^{-6}		
2.34	18.2	36.1	17.9	0.50	–	–	–		Reset
2.35	19.2	37.0	17.8	0.52	0.01	3 008	3.3×10^{-6}		
2.35	20.8	38.5	17.7	0.54	–	–	–		Reset
2.37	21.1	39.3	18.2	0.54	0.02	5 013	4.0×10^{-6}		
2.38	20.2	37.8	17.6	0.53	0.01	3 003	3.3×10^{-6}		
2.38	21.0	39.3	18.3	0.53	–	–	–		Reset
2.39	21.2	39.5	18.3	0.54	0.01	5 005	2.0×10^{-6}		
2.39	18.6	41.2	22.6	0.45	–	–	–		Reset
2.41	18.4	40.4	22.0	0.45	0.02	3 508	5.7×10^{-6}		
2.43	18.8	40.8	22.0	0.46	0.02	3 606	5.5×10^{-6}		
					0.04	7 114	5.6×10^{-6}	22.2	

[a]Not recorded.

[b]Not recorded $R \cong 0.06$

TABLE A10.—CLASS A WHEEL, SPECIMEN 44-F4, 3.5% NaCl AQUESUS SOLUTION

Crack length (in.)	K_{min} (ksi $in^{1/2}$)	K_{max} (ksi $in^{1/2}$)	ΔK (ksi $in^{1/2}$)	Stress ratio, R	da (in.)	dN (in.)	da/dN	Average ΔK (ksi $in^{1/2}$)	Remarks
1.47	1.1	18.4	17.3	0.06	—	—	—	—	Start precrack
1.60	1.2	18.0	16.8	0.07	0.13	138 290	—	—	End precrack
1.60	0.5	8.7	8.2	0.06	—	—	—		Reset
1.60	0.5	9.5	9.0	0.05	<0.01	105 000	$<9.5 \times 10^{-8}$		
1.60	1.0	16.4	15.4	0.06	—	—	—		Reset
1.62	1.3	16.6	15.3	0.08	0.02	30 003	6.7×10^{-7}		
1.63	1.5	16.9	15.4	0.09	0.01	30 000	3.3×10^{-7}		
1.64	1.5	16.8	15.3	0.09	0.01	30 010	3.3×10^{-7}		
1.65	1.8	16.9	15.1	0.10	0.01	71 000	1.4×10^{-7}		
					0.05	161 013	3.1×10^{-7}	15.3	
1.65	0.9	12.3	11.4	0.07	—	—	—		Reset
1.65	1.2	11.9	10.7	0.10	<0.01	138 006	$<7.2 \times 10^{-8}$		
1.65	1.2	11.7	10.5	0.10	<0.01	140 000	$<7.1 \times 10^{-8}$		
					<0.01	278 006	$<3.6 \times 10^{-8}$	10.8	
1.65	1.7	16.5	14.8	0.10	—	—	—		Reset
1.65	2.0	16.9	14.9	0.11	<0.01	105 617	9.5×10^{-8}		
1.65	1.7	27.3	25.6	0.06	—	—	—		Reset
1.66	1.7	26.9	25.2	0.06	0.01	—	—		No cycle count
1.68	2.2	26.4	24.2	0.08	0.02	7 060			
1.70	2.0	27.3	25.3	0.07	0.02	7 073			
1.73	2.3	27.8	25.5	0.08	0.03	7 005			
1.75	2.7	27.6	24.9	0.10	0.02	7 611			
					0.09	28 749	3.1×10^{-6}	25.0	
1.75	2.7	31.7	29.0	0.08	—	—	—		
1.79	3.1	31.0	27.9	0.10	0.05	7 015	7.0×10^{-6}	28.4	
1.79	2.2	30.1	27.9	0.07	—	—	—		Reset
1.82	2.8	29.7	26.9	0.09	0.03	7 003	4.3×10^{-6}		
1.82	2.4	29.7	27.3	0.08	—	—	—		Reset
1.86	2.4	29.2	26.8	0.08	0.04	7 156	5.6×10^{-6}		
1.89	2.8	29.3	26.5	0.09	0.03	7 001	4.3×10^{-6}		
					0.07	14 157	4.9×10^{-6}	26.8	
1.89	2.0	32.8	30.8	0.06	—	—	—		Reset
1.95	2.2	32.5	30.3	0.07	0.06	7 002	8.6×10^{-6}	30.5	
2.00	2.6	32.1	29.5	0.08	0.05	6 000	8.3×10^{-6}	29.9	
2.04	2.7	30.3	27.7	0.09	0.04	7 000	5.7×10^{-6}	28.6	
2.04	1.5	23.9	22.4	0.06	—	—	—		Reset
2.07	2.3	24.6	22.3	0.09	0.03	20 001	1.5×10^{-6}		
2.07	1.4	26.0	24.6	0.06	—	—	—		Reset
2.09	1.9	25.4	23.5	0.07	0.03	25 004	1.2×10^{-6}		
2.09	1.2	20.6	19.4	0.06	—	—	—		Reset
2.10	1.8	20.5	18.8	0.08	0.01	195 882	5.1×10^{-8}		

TABLE A11.—CLASS A WHEEL, SPECIMEN 45-F5, PEAK LOADED IN 100% RH, RT AIR

Crack length (in.)	K_{min} (ksi $in^{1/2}$)	K_{max} (ksi $in^{1/2}$)	ΔK (ksi $in^{1/2}$)	Stress ratio, R	da (in.)	dN (in.)	da/dN	Average ΔK (ksi $in^{1/2}$)	Remarks
1.47	1.1	18.5	17.4	0.06	—	—	—		Start precrack
1.60	1.3	16.8	15.5	0.08	0.13	168 366			
1.60	1.3	22.6	21.3	0.06	—	—	—		Reset
1.65	1.4	22.1	20.8	0.06	0.05	15 002	3.3×10^{-6}	21.1	
1.69	1.5	22.6	21.1	0.07	0.04	12 010	3.3×10^{-6}	20.9	
1.69	~0.0	34.4	34.4	~0.00	<0.01	10	—		Peak load
1.69	1.2	22.5	21.3	0.05	—	—	—		Reset
1.74	1.3	21.6	20.3	0.06	0.05	29 013	1.7×10^{-6}	20.8	
1.77	1.2	21.6	20.4	0.06	0.03	15 115	2.0×10^{-6}		
1.77	1.1	21.8	20.7	0.05	—	—	—		Reset
1.82	0.9	20.6	19.7	0.04	0.05	16 768	3.0×10^{-6}	20.2	
1.82	0.9	17.8	16.9	0.05	—	—	—		Reset
1.84	1.2	17.1	15.9	0.07	0.02	20 200			
1.86	1.4	17.5	16.1	0.08	0.02	15 000			
1.87	1.3	17.0	15.7	0.08	0.01	7 099			
					0.05	42 299	1.2×10^{-6}	16.1	
1.87	1.0	16.8	15.8	0.06	—	—	—		Reset
1.89	1.6	16.9	15.3	0.09	0.02	15 001	1.3×10^{-6}		
1.89	~0.0	23.8	23.8	~0.00	<0.01	10			Peak load
1.89	1.0	17.2	16.2	0.06	—	—	—		Reset
1.91	1.2	17.3	16.1	0.07	0.03	20 003	1.5×10^{-6}		
1.94	1.4	16.9	15.5	0.08	0.03	27 012	1.1×10^{-6}		
					0.06	47 015	1.3×10^{-6}	15.8	
1.96	1.3	17.0	15.7	0.08	0.02	11 000	1.8×10^{-6}		

TABLE A12.–CLASS C WHEEL WROUGHT, SPECIMEN 53-F1, 100% RH, RT AIR

Crack length (in.)	K_{min} (ksi $in^{1/2}$)	K_{max} (ksi $in^{1/2}$)	ΔK (ksi $in^{1/2}$)	Stress ratio, R	da (in.)	dN (in.)	da/dN	Average ΔK (ksi $in^{1/2}$)	Remarks
1.60	[a]	[a]	25.8	[b]	–	–			End precrack
1.65			26.3		0.05	5 022	1.0×10^{-5}	26.1	
1.71			25.0		0.06	7 815	7.7×10^{-6}	25.6	
1.71			18.6		–	–	–		Reset
1.76			17.8		0.05	14 060	3.6×10^{-6}	18.2	
1.82			16.9		0.06	32 168	1.9×10^{-6}	17.3	
1.88			16.4		0.06	32 112	1.9×10^{-6}	16.6	
1.88			10.4		–	–	–		Reset
1.96			9.9		0.08	~350 000	$\sim 2.3 \times 10^{-7}$	10.2	
1.97			9.4		0.01	50 016	2.0×10^{-7}		
1.97			8.9		<0.01	25 047	$<4.0 \times 10^{-7}$		
2.02			8.8		0.05	283 176	1.8×10^{-7}	8.8	
2.02			5.6		–	–	–		Reset
2.05			12.9		–	–	–		Reset
2.09			12.5		0.04	80 037	5.0×10^{-7}	12.7	
2.09			15.2		–	–	–		Reset
2.12			14.9		0.03	25 122	1.2×10^{-6}		
2.12			30.6		–				
2.17			29.2		0.05	4 016	1.2×10^{-5}	29.9	
2.17			35.2		–				
2.21			33.7		0.04	2 012	2.0×10^{-5}	34.4	
2.25			32.4		0.04	2 514	1.6×10^{-5}	33.0	
2.25			27.3		–	–	–		Reset
2.26			27.1		0.01	4 005	2.5×10^{-6}		
2.26			21.4		–	–	–		Reset
2.27			21.3		0.01	4 010	2.5×10^{-6}		
2.28	[a]	[a]	21.2	[b]	0.01	4 568	2.2×10^{-6}		

[a] Not recorded.

[b] Not recorded $R \simeq 0.06$.

TABLE A13.–CLASS U WHEEL USED, SPECIMEN 63-F1, 100% RH, RT AIR

Crack length (in.)	K_{min} (ksi $in^{1/2}$)	K_{max} (ksi $in^{1/2}$)	ΔK (ksi $in^{1/2}$)	Stress ratio, R	da (in.)	dN (in.)	da/dN	Average ΔK (ksi $in^{1/2}$)	Remarks
1.47	1.1	18.4	17.2	0.06	–	–	–		Start precrack
1.57	2.0	18.1	16.1	0.11	0.10	268 000			End precrack
1.57	0.4	7.4	7.0	0.05	–	–			Reset
1.57	1.0	7.6	6.6	0.13	<0.01	10 000	–		
1.57	0.4	7.1	6.7	0.06	<0.01	511 059	$<1.9 \times 10^{-8}$	6.7	
1.57	0.8	12.1	11.3	0.07	–	–	–		Reset
1.58	0.8	12.0	11.2	0.07	0.01	50 003	2.0×10^{-7}		
1.59	0.9	11.9	11.0	0.08	0.01	50 000	2.0×10^{-7}		
1.59	1.2	16.8	15.6	0.07	–	–	–	–	Reset
1.60	1.2	17.7	16.5	0.07	0.01	6 000	1.7×10^{-6}		
1.61	–	–	–	–	–	–	–		Machine malfunction
1.62	1.1	17.8	16.7	0.06	0.01	10 005	1.0×10^{-6}		
1.63	1.2	17.9	16.7	0.07	0.01	10 001	1.0×10^{-6}		
1.65	1.3	17.5	16.2	0.07	0.02	12 175	1.6×10^{-6}		
					0.04	32 181	1.2×10^{-6}	16.4	
1.67	–	–	–	–	–	–	–		Machine malfunction
1.67	1.6	25.4	23.8	0.06	–	–	–		Reset
1.69	1.9	25.0	23.1	0.08	0.02	1 000	2.0×10^{-5}		
1.70	1.9	25.0	23.1	0.08	0.01	1 028	9.7×10^{-6}		
1.72	–	–	–	–	–	–			
1.72	1.6	27.3	25.7	0.06	–	–			
1.74	1.9	27.2	25.3	0.07	0.02	2 202	9.0×10^{-6}		
1.75	1.8	27.1	25.3	0.07	0.01	2 002	5.0×10^{-6}		
1.75	2.3	30.5	28.2	0.08	–	–			
1.76	2.5	30.5	28.0	0.08	0.01	997	1.0×10^{-5}		
1.79	2.9	30.7	27.8	0.09	0.03	1 484	2.0×10^{-5}		
					0.04	2 481	1.6×10^{-5}	27.9	
1.79	2.2	30.8	28.6	0.07	–	–			
1.81	2.6	30.1	27.5	0.09	0.02	2 010	1.0×10^{-5}		
1.86	2.6	30.4	27.8	0.09	0.01	1 998	5.0×10^{-6}		

TABLE A14.—CLASS CE WHEEL WROUGHT, SPECIMEN 73-F1, 100% RH, RT AIR

Crack length (in.)	K_{min} (ksi $in^{1/2}$)	K_{max} (ksi $in^{1/2}$)	ΔK (ksi $in^{1/2}$)	Stress ratio, R	da (in.)	dN (in.)	da/dN	Average ΔK (ksi $in^{1/2}$)	Remarks
1.47	2.3	25.8	23.5	0.09	—	—	—		Start precrack
1.58	2.1	24.8	22.7	0.08	0.11	50 620	—		End precrack
1.58	0.8	26.1	25.3	0.03	—	—	—		Reset
1.61	2.0	26.2	24.2	0.08	0.03	8 449	3.6×10^{-6}		
1.67	1.9	25.2	23.3	0.08	0.06	12 205	4.9×10^{-6}	23.7	
1.71	2.1	24.8	22.7	0.08	0.04	9 603	4.2×10^{-6}	23.0	
1.71	1.2	15.7	14.5	0.08	—	—	—		Reset
1.79	1.5	15.2	13.7	0.10	0.08	108 450	7.4×10^{-7}	14.1	
1.79	0.2	10.1	9.9	0.02	—	—	—		Reset
1.80	0.2	10.7	10.5	0.02	0.01	137 711	7.3×10^{-8}		
1.83	0.2	10.0	9.8	0.02	0.03	89 954	3.3×10^{-7}		
					0.04	227 655	1.8×10^{-7}	10.0	
1.87	0.6	10.8	10.2	0.06	0.04	190 607	2.1×10^{-7}	10.2	
1.87	0.4	7.7	7.3	0.05	—				
1.90	0.8	8.1	7.3	0.10	0.03	413 260	7.3×10^{-8}		
1.90	0.6	7.9	7.3	0.08	<0.01	125 128	$<8.0 \times 10^{-8}$		
1.93	0.6	7.9	7.3	0.08	0.03	305 357	9.8×10^{-8}		
					0.06	843 745	7.1×10^{-8}	7.3	

TABLE A15.—CLASS SUB A WHEEL WROUGHT, SPECIMEN 84-F1, 100% RH, RT AIR

Crack length (in.)	K_{min} (ksi $in^{1/2}$)	K_{max} (ksi $in^{1/2}$)	ΔK (ksi $in^{1/2}$)	Stress ratio, R	da (in.)	dN (in.)	da/dN	Average ΔK (ksi $in^{1/2}$)	Remarks
1.47	1.6	27.3	25.7	0.06	—	—			Start precrack
1.62	3.0	29.0	26.0	0.10	0.15	38 190			End precrack
1.62	1.5	26.2	24.7	0.06	—	—			Reset
1.66	1.6	26.5	24.9	0.06	0.04	10 003	4.0×10^{-6}	24.8	
1.71	1.8	25.4	23.6	0.07	0.05	10 002	5.0×10^{-6}	24.2	

TABLE A16.—CLASS A WHEEL, SPECIMEN 44-F3, -40° F TEST

Crack length (in.)	K_{min} (ksi $in^{1/2}$)	K_{max} (ksi $in^{1/2}$)	ΔK (ksi $in^{1/2}$)	Stress ratio, R	da (in.)	dN (in.)	da/dN	Average ΔK (ksi $in^{1/2}$)	Remarks
1.48	1.1	27.3	26.2	0.04	—	—	—		Start precrack
1.58	1.8	26.6	24.8	0.07	0.10	71 107	—		End precrack
1.58	1.3	28.4	27.1	0.05	—	—	—		Reset
1.69	1.9	29.0	27.1	0.07	0.11	20 044	5.5×10^{-6}	27.1	-40° F data point
1.69	1.7	28.3	26.6	0.06	—	—	—		Reset
1.74	1.4	27.2	25.8	0.05	0.05	8 061	6.2×10^{-6}	26.2	-40° F data point

TABLE A17.–AXLE F2, SPECIMEN HHB-F2, 3.5% NaCl AQUEOUS SOLUTION

Crack length (in.)	K_{min} (ksi $in^{1/2}$)	K_{max} (ksi $in^{1/2}$)	ΔK (ksi $in^{1/2}$)	Stress ratio, R	da (in.)	dN (in.)	da/dN	Average ΔK (ksi $in^{1/2}$)	Remarks
1.48	1.9	24.8	22.9		–	–	–		Start precrack
1.58	1.8	20.8	19.0		0.10	47 800	–		End precrack
1.58	1.8	20.8	19.0		–	–	–		Reset
1.62	2.5	24.7	22.2		0.04	15 101	2.6×10^{-6}	20.6	3.5% NaCl solution
1.62	1.0	22.5	21.5		–	–	–		
1.69	1.9	24.9	23.0		0.07	54 102	1.3×10^{-6}	22.2	3.5% NaCl solution

TABLE A18.–GRADE U AXLE, SPECIMEN UUB-F2, 100% RH, RT AIR

Crack length (in.)	K_{min} (ksi $in^{1/2}$)	K_{max} (ksi $in^{1/2}$)	ΔK (ksi $in^{1/2}$)	Stress ratio, R	da (in.)	dN (in.)	da/dN	Average ΔK (ksi $in^{1/2}$)	Remarks
1.48	1.4	27.6	26.2	0.05	–	–	–		Start precrack
1.58	1.3	25.8	24.5	0.05	0.10	3 996	2.5×10^{-5}		End precrack
1.58	11.7	23.0	11.3	0.51	–	–	–		Reset
1.60	11.9	22.8	10.9	0.52	0.02	110 000	1.8×10^{-7}		Forked crack tip
1.60	11.3	27.7	16.4	0.41	–	–	–		Reset
1.65	11.6	27.6	16.0	0.42	0.05	27 001	1.85×10^{-6}	16.2	
1.65	10.3	25.8	15.5	0.40		–	–	–	Reset
1.70	10.6	25.5	14.9	0.42	0.05	51 100	9.8×10^{-7}	15.2	
1.75	11.6	25.9	14.3	0.45	0.05	46 008	1.1×10^{-6}	14.6	

APPENDIX B

REPORT OF INVENTIONS

Under this contract, baseline data were developed to characterize the fatigue and fracture properties of railroad wheels and axles. These data were not previously in existence and are necessary in order to measure any subsequent improvements in wheel and axle technology.

Evaluation of steels with carbon contents in the range 0.35 to 0.77 weight percent showed carbon to be a principal factor controlling K_{Ic}.

Fatigue properties were determined to be similar for comparable conditions of testing.

This work indicated that using presently available NDI techniques, flaws could only reliably be detected in Classes A and Sub A wheels and Grade U and F axles.

It is not believed that any inventions or patentable items resulted from this basic research program.

138 copies